Palaeozoic stromatoporoid diagenesis: a synthesis

Stephen Kershaw[1,2*] Axel Munnecke[3], Emilia Jarochowska[4], Graham Young[5]

[1]Department of Life Sciences, Brunel University, Kingston Lane, Uxbridge, UB8 3PH, UK
[2]Department Earth Sciences Department, The Natural History Museum, Cromwell Road, London, SW7 5BD, UK
[3, 4]GeoZentrum Nordbayern, Friedrich-Alexander University Erlangen-Nuremberg (FAU), Fachgruppe Paläoumwelt, Loewenichstrasse 28, D-91054 Erlangen, Germany; axel.munnecke@fau.de; emilia.jarochowska@fau.de
[5]Manitoba Museum, 190 Rupert Avenue, Winnipeg, Manitoba R3B ON2, Canada; gyoung@manitobamuseum.ca

*Corresponding author: Stephen.kershaw@brunel.ac.uk

Abstract

Palaeozoic stromatoporoids, throughout their 100 million+ year history (Middle Ordovician to Late Devonian and rare Carboniferous), are better preserved than originally-aragonite molluscs, but less well-preserved than low magnesium-calcite brachiopods, bryozoans, trilobites and corals. However, the original mineralogy of stromatoporoids remains unresolved, and details of their diagenesis are patchy. This study of approximately 2000 stromatoporoids and the literature recognises three diagenetic stages, applicable throughout their geological history. Timing of processes may vary in and between stages; some components are not always present. **Stage 1**, on or just below sediment surface, comprising: micrite filling of upper gallery space after death, then filling of any remaining space by non-ferroan then ferroan calcite in decreasing oxygen of pore-waters; partial lithification of associated sediment from which stromatoporoids may be exhumed and redeposited, evidence of general early lithification of middle Palaeozoic shallow-marine carbonates; microdolomite formation, with the Mg interpreted to have been derived from original high-Mg calcite (HMC) mineralogy (likely overlaps Stage 2). **Stage 2**, short distance below sediment surface, comprising: fabric-retentive recrystallisation (FRR) of stromatoporoid skeletons forming fabric-retentive irregular calcite (FRIC), mostly orientated normal to growth layers, best seen in cross-polarised light. FRIC stops at stromatoporoid margins in contact with sediment and bioclasts. FRIC geometry varies, indicating some taxonomic control. Evidence that FRIC formed early in diagenetic history includes syntaxial continuation of FRIC into some sub-stromatoporoid cavities (Type 1 cement), although others were pre-occupied by early cement fills (Type 2 cement) formed before FRR, preventing syntaxial continuation of FRIC into cavities. Likely contemporaneous with FRIC formation, stromatoporoids in argillaceous micrites drew carbonate from adjacent sediment during reorganisation of argillaceous micrite into limestone-marl rhythms that are also early diagenetic. **Stage 3**, largely shallow burial, comprising: dissolution and silicification, but these may have occurred earlier in stromatoporoid diagenetic histories (more data required); burial pressure dissolution forming stylolites.
(300 words)

Keywords: stromatoporoids; hypercalcified sponges; taphonomy; tabulates

Introduction and aims

Stromatoporoids are hypercalcified sponges that first became important in shallow-marine reefal systems in the Middle Ordovician (Wilson 1975), continuing as dominant reef components until Late Devonian time. They are generally recognised to have become extinct at the end of the Devonian Period (Stearn 2015a), although rare Carboniferous records are evidence of their survival into the Late Palaeozoic (Wood et al. 1989; Kershaw and Sendino 2020), see Fig. 1. Stromatoporoids resurged in the Mesozoic Era but those are not considered in this study.

Because they are highly abundant in middle Palaeozoic strata, stromatoporoids have attracted interest in assessments of reef system development (e.g., Copper 2002; Webby 2002), but also in the debate about the hypothesis of calcite-aragonite seas (Stanley 2006; Stanley and Hardie 1998). Most stromatoporoid work deals with their growth processes and taxonomy (e.g., Kershaw et al. 2018; Webby and Kershaw 2015); but there is no comprehensive study of Palaeozoic stromatoporoid diagenesis through their geological history. Thus, this study has two aims: 1) to assess evidence of diagenetic change in Palaeozoic stromatoporoids, with a view to identifying their original mineralogy, and 2) to survey processes of stromatoporoid diagenesis throughout their individual and geological histories, to identify trends and variations in diagenetic processes and products. The outcome of this work may inform views of marine carbonate diagenesis, and the relationship between stromatoporoids and ideas concerning calcite-aragonite seas.

Materials and methods

Most information on stromatoporoid diagenesis comes from thin-sections. The traditional study of stromatoporoids has focused on taxonomy, for which thin-sections need to be thicker than the normal 30 µm because of the common poor preservation of stromatoporoids. At 30 µm thickness, stromatoporoid structure is faint and poorly defined; thus 50-80 µm is normally used for stromatoporoid taxonomy. Unfortunately, such sections are normally too thick for detailed diagenetic study because the birefringence of calcite in cross-polarised light cannot be utilised at those thicknesses. In addition, the narrow focal range in higher-power objective lenses means that much of the view is out of focus, obfuscating clear imaging of details. To mitigate these problems, for this study a range of thin-sections was prepared of 15 - 30 µm thickness. Many sections were finished by hand on lapping plates at 1200 grade, using silicon carbide powders, inducing a wedge-shape profile of the rock slice, so that the structure can be examined at different thicknesses. In view of pervasive recrystallisation, sections thinner than around 15 µm make the skeletal structure indiscernible; the skeleton appears as a faint speckle in the calcite crystals of which stromatoporoids are composed. In this study, several hundred new thin-sections were prepared, and some existing thin-sections were modified by further grinding to make them thinner and wedge-shaped. Many older thin-sections are capped with a glass coverslip or are museum samples, so that thinning is not possible. Overall, approximately 2000 thin-sections from Ordovician to Carboniferous specimens were examined from authors' collections and registered collections (Natural History Museum, London, UK; Sedgwick Museum of Earth Sciences, Cambridge, UK; and the British Geological Survey, Keyworth, UK). A total of 23 stromatoporoid taxa are illustrated in this study (Fig. 1), including images in this script and a supplemental (Kershaw et al. 2021). However, many more were examined, but are not included in the figures; those illustrated in this study are considered sufficient to represent the range of stromatoporoid structures for the analysis.

For uncapped thin-sections, selected examples were stained using a combined stain of alizarin red S and potassium ferricyanide (ARS-KFeCN). ARS stains calcite pink-red; KFeCN stains ferroan calcite blue; ferroan cements indicate precipitation in the absence of oxygen. ARS-KFeCN stain allows discrimination between calcite and dolomite, both ferroan and non-ferroan. Some samples were examined using cathodoluminescence and UV fluorescence at Kingston University, UK. Key scanning electron microscope (SEM) secondary electron images by Stearn (2015b) are reproduced with permission, as well as a selection of new SEM images made at GeoZentrum Nordbayern in Erlangen, Germany. Submersion of polished stromatoporoid fragments in 0.1 normal HCl for ca. 30 seconds, caused gentle etching of the surface to avoid formation of deep pits, allowing for better comparison between stromatoporoids, cements, micrite and other fossils in the same samples. Etched samples were then sputter-coated with gold and examined using a Tescan Vega\\XMU SEM with a tungsten filament electron source. Photos were taken using the Secondary Electron detector at 10 kV acceleration voltage. Literature reports of carbon and oxygen isotopes, and some geochemical results, are also used here in comparison with the textural features obtained by the above methods. See also the supplemental file (Kershaw et al. 2021, Table 1).

Background Literature summary

Stearn (2015b) provided a comprehensive account of research into stromatoporoid microstructure and diagenesis, drawing attention to an appreciation of diagenesis in stromatoporoid studies going back to the 19th Century. Since Stearn's review remains current, only key points are repeated here. It is well known that aragonitic molluscs are more poorly preserved than stromatoporoids, whereas stable-mineral low-Mg calcite (LMC) shells such as brachiopods, bryozoans, corals and trilobites are generally better preserved. Stromatoporoid taxonomy uses variations of arrangements of skeletal elements and microstructural features within those elements, summarised by Stearn (2015b). Regardless of the variety of construction, even the best-preserved samples show some alteration (Kershaw 2013); in the worst cases, structure is completely lost by diagenetic change. Stromatoporoids have inclusion-rich skeletons; the inclusions were formerly referred to as specks by Stearn (1989), later recognised as fluid inclusions by Stearn (2015b).

Preservation differences between stromatoporoids and other groups occurring in the same rocks have driven the debate about stromatoporoid mineralogy, leading to interpretations that their original mineralogy was aragonite and/or high-Mg calcite (HMC). Studies based largely on thin-sections (e.g., Riding 1974; Stearn 1972; 1975; Smosna 1984) pointed to stromatoporoids as having original skeletons of aragonite. Trabelsi (1989) considered that Silurian and Devonian forms were aragonite, and Semeniuk (1971) interpreted labechiids as being originally aragonitic. Smosna (1984) recognised that stromatoporoids are recrystallised to irregular bladed calcite crystals orientated normal to the growth layers, considered in the current study as the most important feature of Palaeozoic stromatoporoid diagenesis. Smosna (1984) also drew attention to abundant inclusions in the recrystallised skeleton and assumed they were organic matter, a point strengthened by Clark (2005) in work on a range of modern and fossil hypercalcified sponges and corals. SEM study by Wendt (1984) interpreted some stromatoporoid microstructures as reflecting an original calcite mineralogy, but others aragonite. Stearn and Mah (1987) investigated a range of altered microstructures in stromatoporoids and further explored the idea that stromatoporoids were aragonitic. In the 1990s, investigations drew attention to raised levels of Sr in some stromatoporoids, particularly in Ordovician stromatoporoids. Tobin and Walker (1998) interpreted stromatoporoids in the Middle Ordovician Chazy group as aragonitic, based on higher Sr levels compared to calcitic fossils. Labechiids were considered aragonitic by Mallamo (1995), reported also by Mallamo and Stearn (1991); their work proposed that Ordovician stromatoporoids were aragonitic, but that Silurian and Devonian cases were calcitic. Rush and Chafetz (1991) and Yoo and Lee (1993) recognised abundant microdolomite inclusions in stromatoporoids; these were interpreted as evidence that stromatoporoids were high-Mg calcite originally, further explored in this study.

Kershaw (1994; 2013) examined stromatoporoids from a textural viewpoint, using thin-sections in PPL, XPL and CL, highlighting the difference between altered structures in PPL and XPL versus potentially original structures in CL views that luminesce yellow and orange. We note that Casella et al. (2017), in work on modern brachiopods, showed that modern shells luminesce with a blue colour, whereas yellow and orange colours represent alteration in their material. Those results contrast work by Barbin (1992) and Barbin et al. (1991) who illustrated a range of modern shells (marine and non-marine bivalves, nautiloids, several foraminifera taxa and calcified red algae) showing a large variety of CL response, including blue, green, yellow and orange CL in unaltered shells. In view of this variation in CL response in modern shell carbonate, there is some uncertainty about whether CL responses in stromatoporoid skeletons reflect original or partly altered structures, but the CL differs from adjacent sediment and cement, contrasts that are used in this study to interpret diagenesis in stromatoporoids. There is general recognition that stromatoporoid diagenesis was an early process (e.g., Smosna 1984; Nothdurft et al. 2004). Detailed and comprehensive investigation is required, which this study attempts.

Key features of stromatoporoid diagenesis

Extensive examination of stromatoporoids from Ordovician to Carboniferous successions reveals a consistent set of features reflecting processes that are here interpreted to have affected stromatoporoids throughout their history. First we describe basic features of stromatoporoid diagenesis and then make comparisons.

Basic diagenetic features of stromatoporoids

The range of stromatoporoid diagenesis is shown in Figs. 2 - 11. The most obvious features of stromatoporoid diagenesis are seen in thin-section using a combination of plane- and cross-polarised light (henceforth PPL and XPL) (Fig. 2a-f). All stromatoporoids examined in thin-section in this study and in our literature survey display overprinting of the skeleton and gallery cements (see Rush and Chafetz 1991; Smosna 1994) involving fabric-retentive recrystallisation (henceforth FRR). FRR occurs in some associated fossils, notably syringoporid tabulates and some halysitids, and was observed by the authors in other groups (e.g., some partly altered Silurian brachiopods and a Jurassic mollusc) during the research for this study. However, in stromatoporoids, the form of FRR is apparently unique. The neomorphism results in fabric-retentive irregular calcite (henceforth FRIC), seen in vertical sections as bladed cement crystals orientated normal to the growth layers, thus following the curvature of stromatoporoid laminae in vertical sections (Fig. 2c, d). In transverse sections, FRIC crystals are equant (Fig. 2e, f); in three dimensions their form is mostly club-shaped. Thin-section and SEM images show the crystal boundaries of FRIC passing from the skeleton into gallery space (e.g., Fig. 2i). However, Fig. 2j shows a rare case (in fact the only one found in this study), figured by Stearn (2015b, page 536) of an apparently well-preserved fibrous skeletal structure where gallery cement terminates against the stromatoporoid skeleton and does not pass through it.

In plane-polarised light (PPL), using ARS-KFeCN combined staining, stromatoporoid skeletons are in almost all cases preserved as non-ferroan cement; ferroan cement is rare. The gallery spaces are commonly filled or partly filled with early cement that is non-ferroan, but final filling of galleries also commonly contains ferroan calcite (Fig. 2g, h, k & l). The same sequence of cements is observed in other fossils containing voids, particularly rugose corals and tabulates in the same thin-sections as stromatoporoids.

Cathodoluminescence (CL) is a valuable tool in stromatoporoid study because of contrasts in CL response between the stromatoporoid skeleton, gallery cements and associated pore-filling cements. In limestones generally, a well-established CL response (Scoffin 1987) shows a normally consistent sequence of three types of cement zones from non- to bright- to dull-luminescent cements interpreted to follow the process of burial from a) oxygenated (non-luminescent) to b) anoxic sub-surface zones, where bright cement indicates bacterial sulphate-reduction (BSR, removes Fe as pyrite, leaving Mn as luminescent activator), to c) dull cement zones, indicating cementation below the BSR zone (Fe2+ incorporated into calcite cement to quench the CL response). This sequence is found in cements associated with stromatoporoid samples studied here (Fig. 3) and matches ARS-KFeCN-stained zones (Fig. 3e). However, CL response of stromatoporoid skeletal carbonate is a fine speckled mixture of bright and dull luminescence (Figs. 3c & d; 4e), in some cases with non-luminescent areas (Figs. 8 & 10) contrasting with the gallery cements. When compared with cross-polarised light (XPL) views (Figs. 3 & 4) CL reveals zoning in gallery cement adjacent to the skeletal tissue, interpreted here to have existed prior to FRR (fabric-retentive recrystallisation) because FRIC (fabric-retentive irregular calcite) overprints CL cement zones when viewed in XPL. Thus, CL of stromatoporoid skeletons may show the original, or perhaps modified original, stromatoporoid texture. Fig. 3c (lower right corner) shows the three types of CL cement zones but other parts of Fig. 3c show the relationship between CL and sediment that occupied the upper few gallery layers after death; sediment is commonly more brightly luminescent than the stromatoporoid skeleton. Fig. 3d shows a variation of CL zoning in another part of the same thin-section. Fig. 4 shows another taxon from the same location and facies as Fig. 3, with a more fibrous FRIC texture that was disturbed by a growth interruption surface; the CL view (Fig. 4e) reveals the three CL zone types in gallery spaces. Figs. 2, 3 and 4 are from middle Silurian-age facies, and Fig. 5 shows representative examples of Ordovician and Devonian stromatoporoids. Together with a rare Viséan (Early Carboniferous) example that also shows FRIC (not illustrated, see Kershaw and Sendino 2020) these cases demonstrate that FRIC occurs throughout Palaeozoic stromatoporoid history. Finally, a small selection of stromatoporoids studied using UV fluorescence (see supplemental file, Kershaw et al. 2021, Fig. S1) shows differences between skeleton and gallery space consistent with stained sections and CL images.

Comparison between stromatoporoids and other organisms

Figs. 6-9 illustrate differences between stromatoporoids and associated fossils in PPL, XPL, CL and SEM. These all show that stromatoporoids are better preserved than originally aragonitic molluscs but less well-preserved than low Mg-calcitic fossils such as brachiopods, bryozoans or ostracods, see also Kershaw (2013) for more examples. Differences of preservation between stromatoporoids and chaetetids are illustrated by Balthasar et al. (2020) who showed that chaetetids are better preserved than stromatoporoids because crystal boundaries of the cement fills do not pass through chaetetid walls (also see supplemental file, Kershaw et al. 2021).

Comparison between stromatoporoid taxa

Figures in this paper and the supplemental file include examples from Ordovician, Silurian and Devonian rocks, and cover the range of skeletal architecture, that is quite variable across the stromatoporoid taxa. Fabric-retentive recrystallisation (FRR) resulted in overprinting diagenetic cement (FRIC - fabric-retentive irregular calcite) in all stromatoporoid thin-sections studied, but there is also a taxonomic influence on the exact appearance of FRIC. In general terms, those taxa with prominent laminae (e.g., *Cystostroma*, Fig. 5) and pillars (e.g., *Petridiostroma,* Figs. 2, 3, 10) show that the FRIC has more equant-shaped crystals in comparison to the more elongate FRIC crystals of other taxa that themselves have significant differences in skeletal structure (compare *Actinostroma* [Fig. 5], *Plectostroma* [Fig. 10], *Eostromatopora* [Figs. 4,6] and *Densastroma* [Fig. 7]), which in all cases have elongate FRIC normal to the growth layers. Stromatoporoid microstructure also plays a part in the geometry of FRIC crystals. Taxa with the type of microstructure called compact tend to have blocky FRIC (e.g., *Cystrostroma* and *Petridiostroma,* Figs. 2, 3 & 5). *Lophiostroma* (Fig. 10), composed of a solid skeleton and questioned as a stromatoporoid, has blocky FRIC that follows the wavy growth layering and partly overlaps it. In *Labechia*, the elongate FRIC crystals cut across the thick pillars and thin dissepiments (see Fig. 21, and Kershaw and Sendino 2020, figs. 9, 10). In *Stachyodes*, that comprises prominent vertical rods (pachysteles), the FRIC crystals are in the same orientation as the rods (Kershaw et al. 2021, Figs. 16-18).

Differences in FRIC between three taxa in Figs. 2, 3 and 4 are further explored in Fig. 10, which shows variations amongst stromatoporoid taxa that encrust one another, from one biostrome in the Hemse Group (Ludlow) of Gotland. Not only do these examples demonstrate consistent differences between taxa in the results of FRR in their FRIC within the same locality and facies, but in adjacent stromatoporoids the precise style of FRIC does not cross from one taxon into the next (Fig. 10), indicating a strong taxonomic control on the diagenetic product. Stearn (2015b, page 540) described variations in recrystallised fabric in stromatoporoids related to their original microstructures. Fig. 11 shows an unusual example from the Klinteberg Formation (Wenlock) of Gotland (Frykman 1989) where microstructure of the type called cellular in stromatoporoid terminology (unrelated to biological cells, see Stearn 2015b, p530), is apparently represented in the CL image, contrasting the FRIC overprint seen in XPL. The origin of stromatoporoid cellular microstructure is unknown although is much debated in the literature (Stearn 2015b, Stearn and Mah 1987). Jackson et al. (2010) showed that the living calcified sponge *Astrosclera willeyana* forms its spherulitic-constructed skeleton using degraded bacteria; the superficial similarity to the cellular microstructure in Palaeozoic stromatoporoids opens the possibility of such a process in some stromatoporoid taxa, originally raised by Stearn (1975) and this may be explored in future studies.

Fig. 11c also shows that intergrown syringoporid tabulate tubes are partly altered by diagenesis, found in all thin-sections that contain such intergrowths in this study, in contrast to the well-preserved structure of other tabulates, and thus demonstrates differences between syringoporids and other tabulate taxa in their resistance to diagenetic change.

Stromatoporoid diagenetic sequence

Stromatoporoid diagenetic processes may be divided into three broad time divisions, Stages 1, 2 and 3 (Fig.12). Stages 1 and 2 occurred very early in the diagenetic history, with Stage 3 later. Each stage contains various processes, described below in their approximate time sequence. Events may have occurred in a different order within and between stages, and not all events are necessarily present in each specimen.

Stage 1

This took place on or just below the seafloor and comprises early cementation and some early dissolution and bioerosion (See Figs. 13 - 20).

Stage 1a: Stromatoporoid living tissues likely occupied only the top few laminae, by comparison with modern hypercalcified sponges (Stearn and Pickett 1994). Prior to cement growth, upper layers of stromatoporoid skeletons accumulated micrite in galleries after death (Figs. 13 and 14); this is evidence that cementation of upper galleries did not occur immediately after death, in contrast to modern calcified sponges that show filling of space directly below the living layer while the sponge is alive (Fig. 13b). Such filling is best seen in bored specimens, mostly on upper surfaces, by presumed domichnial taxa such as *Trypanites* (Fig. 13a, c, d, f). After death of the borer, boreholes were filled with fine-grained sediment; some examples show depth of boring to at least 10 mm below the stromatoporoid surface. Some stromatoporoid specimens were overturned after death (or were perhaps killed by overturning and smothering of soft tissue on their upper surfaces) and these may uncommonly show *Trypanites* borings on their bases; one such example is shown in Fig. 13e, revealing filling of gallery space. In addition to gallery space, some stromatoporoid taxa have porous skeletal elements (microgalleries) and fine-grained sediment may penetrate that porosity (e.g., Fig. 14). Finally, one specimen from the Klinteberg Formation, Wenlock of Gotland (Fig. 15) shows loss of part of the stromatoporoid skeleton, which may have been caused by dissolution, followed by filling of the space thus created, with bioclasts, prior to burial. Material from the same unit as this sample (not illustrated), indicates that subaerial processes affected these limestones, in which dissolution may be expected in view of the of the unstable original mineralogy of the stromatoporoid. This rare case illustrates preferential loss of stromatoporoid skeleton in contrast to the intergrown rugose corals and syringoporid tabulates, emphasising the greater susceptibility of stromatoporoids to diagenetic alteration. Smosna (1984, p. 1004) hypothesised that stromatoporoid recrystallisation occurred in the meteoric phreatic environment in a Lower Devonian reef in Virginia, USA, also indicated in work by Semeniuk (1971) on the alteration of several fossils, including a stromatoporoid, from the Ordovician of New South Wales, Australia, discussed later.

Stage 1b: Most gallery space was filled by first generation non-ferroan carbonate cement represented as red-stained calcite (Fig. 2). Second generation ferroan cement likely also formed in this early stage, presumably in anoxic locations in galleries out of contact with surrounding seawater, corresponding to dull cathodoluminescent (CL) zones (Figs. 2 and 3). Some ferroan cement may have been precipitated while the stromatoporoid was still exposed on the seafloor, with its interior out of contact with the surface. Stromatoporoid taxa vary in the density of their skeletal elements, but no evidence was found that more open skeletons developed more, or less, ferroan cement than stromatoporoids with more closely spaced elements. Upper Ordovician examples in Manitoba (Fig. 16) show gallery cement bioeroded by tangential borers, that is evidence of cementation while stromatoporoids lay on the seafloor (discussed later). Similar features are present in Middle Ordovician stromatoporoids from the Chazy Group in Vermont (see supplemental file in Kershaw et al. 2021, Fig. S13), but such tangential borers have not been described from the lower portions of skeletons of Silurian or Devonian stromatoporoids, so current evidence does not allow confirmation of whether gallery cementation on or just below the seafloor was widespread in stromatoporoids.

Stage 1c. Stromatoporoids and corals are commonly out of growth position, with delicate marginal areas of skeleton preserved intact (Kershaw et al. 2018, figs. 1 and 4), contrasting other samples where marginal flanges are sharply broken, explained only if the preserved delicate margins were bound into protective sediment. Fig. 7a shows evidence of partial lithification, on or just below the seafloor, where a stromatoporoid grew on an irregular topographic high, interpreted as partly lithified eroded wackestone-packstone that formed a solid base for growth. In wackestone-packstone sediment below the stromatoporoid in that sample, Fig. 7b shows a lithoclast. Wright and Cherns (2016) proposed that widespread lithification of sediment just below the seafloor occurred in the Middle Ordovician as a partial driver of the Great Ordovician Biodiversification Event (GOBE), see also Christ et al. (2015); Munnecke and Samtleben (1996) also showed evidence of early subsurface lithification from the Silurian of Gotland. Evidence from stromatoporoids illustrated in this study is that such early lithification was a control on growth and diagenesis throughout their geological history (see also Kershaw et al. 2018).

Stage 1d. Sub-stromatoporoid primary cavities became cement-filled (Fig. 17); such cement may be either ferroan or non-ferroan, or a mixture, identified by ARS-KFeCN staining, with varying CL response. In the case of Fig. 17, the cavity cement is not continuous with FRIC of the stromatoporoid, evidence that the cavity filled with cement prior to development of FRIC (a Stage 2 feature, see below). Scoffin (1972) interpreted some cavities below reef-builders in the Wenlock of England as formed by dissolution of the calcareous skeleton, creating secondary cavities. However, features in Figs. 19 & 20 allow for an interpretation that sediment was also dissolved beneath reef builders. Alternatively, these cavities could have formed by washing out of unconsolidated material during storms, or by sag of fine sediment below the protective rigid sheets of metazoan reef-building skeletons. Nevertheless, irregular contact between micritic sediment and sparite in Fig. 19g-I may be best explained by dissolution of the sediment. Scoffin (1972) also reported hybrid sub-skeletal cavities that formed initially as primary cavities, and thus are geopetals, but were developed by dissolution of the skeletons. Fig. 21 shows features that could be explained by sediment dissolution, developing a primary geopetal cavity, to form such a hybrid cavity.

Stage 1e. Tiny (ca 10-20 µm) rhombohedral crystals (rhombs) that do not stain with ARS-KFeCN are common in stromatoporoids, concentrated in stromatoporoid skeletal elements, but less common in gallery spaces (Fig. 18). Such rhombs have been described as microdolomite by numerous authors (e.g., Lohman and Meyers

1977). Optical features point to a dolomite composition for these tiny crystals in stromatoporoids, but this mineralogy awaits confirmation (e.g., by XRD). If confirmed, microdolomite is evidence of a high-Mg calcite (HMC) original mineralogy (Lohman and Meyers 1977; Rush and Chafetz 1991); more details of this are given below. Microdolomite formation is interpreted as taking place in the later part of Stage 1, because it is overprinted by later events, but it may overlap with Stage 2.

Stage 2

Stage 2 processes are interpreted to have occurred a short distance below the sediment surface, and they may overlap, in location and possibly timing, with Stage 1.

Stage 2a. Fabric-retentive recrystallisation (FRR) produced fabric-retentive irregular calcite (FRIC) cement cutting across earlier ARS-KFeCN-stained cement zones and CL zones (Figs. 2-5). FRIC is thus an *in-situ* replacement that seems not to have disrupted locations of geochemical components, because staining and CL zones must reflect chemical composition of the stromatoporoid. FRIC stops at stromatoporoid margins in contact with sediment and bioclasts (Fig. 6 and Kershaw 2013). In contrast, cases where cement is in contact with stromatoporoid margins (mostly sub-stromatoporoid cement-filled cavities) reveal two types of arrangement of cements, described below:

Type 1 cements: show syntaxial continuation of FRIC into many sub-stromatoporoid cavities, due to either cement of the same carbonate mineral as the stromatoporoid, recrystallised in optical continuity, or cavities that were empty when the stromatoporoids recrystallised (Figs. 19-21). Type 1 cements occur in cavities that commonly include primary geopetals, but may represent secondary cavities due to sediment removal, that left a highly irregular sediment surface beneath the stromatoporoid. In some cases, remnant sediment adheres to the stromatoporoid base (Fig. 19c & d). As noted above, the cause of sediment removal is not clear, but possibilities are storm action, early sediment dissolution (Fig. 19g-l) or settling prior to lithification. Here it is stressed that syntaxial growth of FRIC into space next to stromatoporoids is an extension of the stromatoporoid recrystallisation process and is not present in other adjacent skeletal components. Good examples of this difference can be observed in crinoids, which show syntaxial overgrowths that are extensions of crinoid crystallographic axes and not recrystallisation of the crinoid.

Type 2 cements: These show no syntaxial continuation of FRIC into the cavities, which are interpreted to have been pre-occupied by cement fills before FRR occurred. Thus, the FRIC abuts cement on the cavity margin; Fig. 17 is a good example. Fig. 22 is an unusual example where both Types 1 and 2 cements are present in different cavities about 20 mm apart, within the same specimen. Type 1 and 2 cements are considered further in the Discussion.

Another feature found in some stromatoporoid samples is apparently early fracturing of the skeleton. Cavities thus created were open at the time of FRIC formation (Fig. 23). For Fig. 23a-f the fractures are interpreted to have occurred on the seabed, and rapid cementation of surrounding sediment can explain why such fractures were not closed by compaction before the FRIC cement grew. Fig. 23g is a rare example which appears to be a curved boring close to the upper surface of the stromatoporoid that was not filled with sediment, and so developed a cement fill when FRIC formation occurred. Borings in stromatoporoids are normally straight (as in *Trypanites*); curved borings have been found in only a few specimens in this study.

Stage 2b. External to stromatoporoids are early diagenetic processes in micritic sediments that led to reorganisation of sedimentary components to produce limestone-marl alternations (Munnecke and Samtleben 1996; Nohl et al. 2019). Stromatoporoids that occur in such sediments are normally easily extracted whole from the rock mass; in some cases, they fall out of coastal cliffs by weathering. Examples are seen in the Upper Visby Formation (early Wenlock, Gotland) (Fig. 24), the Much Wenlock Limestone Formation (late Wenlock, UK) and marly sediments of the Hemse Group (Ludlow, Gotland). It is interpreted that stromatoporoids in marly micrite drew carbonate from adjacent sediment during reorganisation of clay-bearing micrite into limestone-marl rhythms, so that fabric-retentive processes in stromatoporoids were coeval with general diagenesis in the sediment. Overall, the stromatoporoid early diagenetic changes of Stages 1 and 2 are viewed as part of a system of carbonate reorganisation in shallow-marine burial settings.

Stage 3

Stage 3 processes reflect later events, which presumably took place at levels in the sediment below Stage 2, but in some cases they may still have been close to the sediment surface.

Stage 3a. Dissolution of stromatoporoid skeletons and filling of the cavities with cement seems to be uncommon, but Fig. 25 shows an example of differential dissolution where stromatoporoid skeleton was lost but intergrown syringoporid tubes were not.

Stage 3b. Silicification of stromatoporoids is uncommon, and normally it has only partly altered the skeleton. In rare cases, silicification has formed blebs cutting across the skeleton indiscriminately, but in most Ordovician, Silurian and Devonian stromatoporoids studied here, silicification occurred along laminae in narrow zones, where fluids must have passed through the stromatoporoid skeleton, leaving most of it unaffected. Figs. 26 and 27 illustrate the range of silicification features; the skeleton behaved differently from the gallery cements during the process of silicification; thus this is further evidence of fabric-retentive processes in stromatoporoids (discussed later).

Stage 3c. Although later dissolution and silicification events are placed in Stage 3, they may have occurred earlier (the number of available samples is limited). Two additional samples show the problem of determining the timing of stromatoporoid diagenetic processes: a) Fig. 28 shows the interior of a stromatoporoid that was further modified after FRIC formation, but it is unclear whether this occurred in Stage 2 or Stage 3; and b) pyrite framboids, that must form in anoxic conditions, are present in some stromatoporoids (Fig. 29a, b), and their relationship with the timing of FRIC is uncertain. Pyrite formation is placed in Stage 3 but it is acknowledged that this may have also occurred in Stage 1 during the development of bright CL cement commonly interpreted to be due to sequestering of Fe as pyrite, and thus not incorporated into the calcite (Scoffin 1987). Finally, pressure dissolution associated with chemical compaction is common at stromatoporoid margins and certainly formed during later burial (Fig. 29c, d). Stromatoporoids examined from strata affected by pressure dissolution normally show no difference in the nature of their diagenesis from those in strata that lack pressure dissolution effects. This observation indicates that stromatoporoid diagenesis was complete prior to pressure dissolution, although some cases of later modification of the stromatoporoids (e.g., Fig. 28) may have been due to mobilised carbonate-rich fluids during burial.

Further change in stromatoporoids associated with larger-scale processes later in the history of the rocks are not developed in this study. Three examples are: a) the tectonic degradation of Devonian limestones in some localities in South Devon, England, associated with the Variscan Orogeny (author observations); b) well-known pervasive dolomitisation of Devonian carbonates in Alberta, Canada, and c) geochronometric dating of Silurian limestones on Gotland, using stromatoporoids as samples Russell (1995). In this latter case, Russell (1995) revealed the expected Silurian dates in most samples, but some material gave Carboniferous ages reflecting later recrystallisation. Unfortunately, Russell (1995) did not illustrate the stromatoporoids dated, so it has not been possible to assess any possible diagenetic differences from our material. However, Russell's (1995) work demonstrates that even the well-preserved Silurian strata of Gotland, rich in stromatoporoids, contains evidence of later change.

Discussion

Stromatoporoid original mineralogy

Despite effort by numerous researchers cited in the literature summary, and additional study of new material in this project, the original mineralogy of stromatoporoids remains elusive. The following three points are relevant.

1) Rhombohedral crystals generally agreed to be microdolomite inclusions, commonly viewed as indicating a former HMC mineralogy, do not occur consistently in stromatoporoids. Some specimens have abundant rhombs in skeletal tissue compared to adjacent gallery space, seemingly a powerful indicator of HMC (Rush and Chafetz 1991; Yoo and Lee 1993), but are absent in many other stromatoporoids (e.g., see Stearn and Mah 1987). Some cases show interpreted microdolomite in adjacent micritic sediment and even nearby Tabulata fossils (Fig. 18); however, it can be noted that if some stromatoporoids were aragonitic and others calcitic (e.g., Mallamo 1995; Wendt 1984), this is not reflected in the preservation of the skeletons, which show the same FRR (fabric-retentive recrystallisation) preservation, evidence for a single original mineral composition in stromatoporoids (explored further in point 2 below). Furthermore, it remains possible that diagenesis involved removal of Mg from stromatoporoids, in pore waters, such that microdolomite inclusions did not form.
2) Many stromatoporoids examined in this study were collected from shallow-marine, argillaceous shelf carbonates, lithologically developed as limestone-marl alternations. Limestones in such sequences were lithified early, i.e., they imported $CaCO_3$, whereas the marl released $CaCO_3$ and was subsequently compacted (Bathurst, 1971; Ricken, 1986). According to Munnecke and Samtleben (1996) only the aragonitic constituents (both of the aragonitic portion of the mud as well as larger aragonitic bioclasts) were selectively dissolved from marls during early marine burial diagenesis. Such locally-sourced dissolved calcium carbonate provided the carbonate cement for lithification of adjacent limestone. This model was confirmed by petrographic studies by Nohl et al. (2019), who proved through thin-section studies that in these limestone-marl alternations, aragonitic bioclasts were selectively dissolved in the marls, whereas components that consist primarily of HMC or LMC show no dissolution phenomena. In the limestones, primarily aragonitic

bioclasts are completely replaced by blocky calcite, but in contrast, adjacent stromatoporoids in such sequences do not exhibit any dissolution (e.g., Fig. 7). Furthermore, our field observations of stromatoporoids in limestone-marl alternations show that stromatoporoids are preserved in both the marl and limestone layers and individual specimens commonly cross boundaries between those layers, with no difference in preservation (e.g., Fig. 24). Such lines of evidence support the hypothesis that stromatoporoids primarily had a calcitic mineralogy.

3) As far as we aware, this study is the first to identify two arrangements of sub-stromatoporoid cavity-filling cements, part of Stage 2 diagenetic features: Type 1 cement in syntaxial continuation of stromatoporoid FRIC (fabric-retentive irregular calcite); and Type 2 cement that terminates at the base of the stromatoporoid, not syntaxial with FRIC. However, within Type 1 there are two further possible cases: either a cavity was empty before FRR occurred, or it was occupied by the same mineral type cement as the stromatoporoid skeleton and was recrystallised to LMC as part of the FRIC process. We have not identified clear criteria to discriminate these two subcases in Type 1 cement, but Fig. 21 shows evidence of prior cavity filling because the non-ferroan to ferroan cement sequence in the cavity is the same as in the stromatoporoid gallery space in that sample, both these voids being syntaxial within the same crystals of FRIC (Fig. 21d). Other cases, such as in Figs. 19 and 20, may have had empty cavities, filled by cement syntaxial to growth of FRIC, but this is not verified. The features of Fig. 21 contrast those in Fig. 17: in the latter, cavity cement terminates against the stromatoporoid (thus Type 2) and the cavity cement sequence identified in both XPL and CL is different from the gallery cement sequence. Thus, it is possible that sub-stromatoporoid cavities may have been cemented at different times in different specimens; the example in Fig. 22, where both Types 1 and 2 occur 20 mm apart in different cavities in the same specimen, may be due to differential timing of cement fills. It is also possible that the calcium carbonate mineral was different. If stromatoporoids were originally HMC, then recrystallisation that resulted in syntaxial growth of FRIC into gallery cements implies that the gallery cement was also HMC (Fig. 21); but if some sub-skeletal cements were aragonite, then this may explain why FRIC is not syntaxial in those cases: calcite and aragonite have different crystallographic structure. In samples observed in CL, both the CL zoning and XPL views of gallery cements show bladed crystals in CL, characteristic of HMC (e.g., Fig. 17), but not acicular cements characteristic of aragonite (see Tucker and Wright 1990, fig. 7.3). In their description of modern reef carbonates, Tucker and Wright (1990, Chapter 7) explained that both aragonite and HMC form in modern reefs. It is postulated here that if stromatoporoids grew HMC skeletons and gallery fills but in some cases had aragonite sub-stromatoporoid cavity cements, then when FRR took place, FRIC (as LMC) would have been able to overprint the gallery cements but not enter sub-stromatoporoid cavities (unless they were empty or filled with HMC). Thus, in the case of Fig. 17, where FRIC does not pass into the geopetal cavity, this may have been pre-occupied with aragonite cement that was later replaced by calcite.

These arguments broadly favour an interpretation that stromatoporoids were originally composed of HMC rather than aragonite. Such a deduction has value in wider-scale application of knowledge of carbonate mineralogy. Stanley and Hardie (1998) proposed that if stromatoporoids were calcitic, they would have been compatible with the calcite-sea episodes of the hypothetical concept of fluctuations of calcite-aragonite seas. However, the problem with microdolomite discussed above means that stromatoporoid original mineralogy remains unproven.

Insights into biomineralization models from extant sponges

This section provides essential information on modern hypercalcified sponges to assist assessment of stromatoporoid diagenesis. Hypercalcified sponges vary widely in mineralogy and chemistry of their skeletons even between closely related taxa, but dominant mineralogies are either calcite or aragonite, whereas HMC and mixtures of two mineralogies are less common (Kopp et al., 2011; Gilis et al., 2011; Smith et al., 2013).

Modern sponges show a range of anatomical and cytological adaptations to formation of a mineralized skeleton with precisely controlled properties, presumed the result of millions of years of evolution. Noting that calcareous sponges are polyphyletic and their skeleton formation processes involve bacterial endosymbionts, a compilation of studies on their biomineralization indicates that they show three distinguishing characteristics of biominerals as defined by Perez-Huerta et al. (2018) and Gilis et al. (2013): **1)** skeletons show a hierarchical structure (Kopp et al. 2011) comprising larger crystal domains corresponding to crystals visible under SEM after etching; such crystals commonly appear as fibres, organised into bundles (e.g. Gilis et al. 2013). **2)** these crystals in many species have a composite nanogranular-organic structure (Sethmann et al. 2006; Kopp et al. 2011; Gilis et al. 2011; 2013). **3)** biological control over crystallographic orientations has been documented in spicules of Calcaronea and Calcinea sponge groups (Rossi et al. 2016) and in the massive skeletons of calcareous Demospongiae (Gilis et al. 2013); in both of these the growth of skeletal units (fibre bundles or spicules) followed specific crystal directions with a strictly limited range of variation in crystal orientations, wherein the angles between adjacent crystals (called misorientations) are small. Päßler et al. (2018) proposed that a small range of misorientations is a potential criterion to recognize significant biological control over biomineralization, expected in metazoans, in contrast to microbial structures which have a wide range of misorientations and are thus under less biological control. Consequently, the fibrous nature of most hypercalcified sponge skeletons may indicate a narrow range of crystal misorientations consistent with their metazoan status. The presence of such a control is supported by observations of the organic molecules participating in skeleton secretion. In various groups, a matrix of acidic macromolecules, predominantly glycoproteins, inhibits crystal growth on selected faces, thus permitting crystal elongation only in specific directions (Reitner et al. 2001; Sethmann et al. 2006; Gilis et al. 2011; 2012). Gilis et al. (2011) demonstrated in the modern Mediterranean hypercalcified sponge, *Petrobiona massiliana*, the presence of organised bundles of crystal fibres that are orientated vertically within the skeleton. Such vertical orientation of crystal elements in modern sponges is potentially significant in understanding the FRIC cements of stromatoporoids (see below).

Biological control over biomineral formation bestows the skeleton with specific properties, such as reduced brittleness and the ability to hinder crack propagation (Sethmann and Wörheide 2008). These advantageous properties are obtained through crystal growth on non-classical pathways, not the classical simple monomeric crystal growth (see De Yoreo et al. 2015). In living organisms, non-classical pathways commonly involve amorphous precursors (Weiner and Addadi 2011; Wolf et al. 2016; Perez-Huerta et al. 2018), which are notoriously difficult to study, but they have been documented in a range of phyla, including corals and a range of phylogenetically-distant calcareous sponges (Aizenberg et al. 2003; Gilis et al. 2011). What makes the mechanism of biomineralization in sponges stand out from other phyla is the proposed involvement of endosymbiotic bacteria (Garate et al. 2017). The hypercalcified sponge *Astrosclera* (considered to be the best representative of stromatoporoid fossils amongst living sponges) exhibits a number of adaptations to skeleton formation at the cellular level (Reitner et al. 2001). These adaptations include: a) formation of specialized large vesicle cells, and b) a multi-step pathway of skeleton accretion, involving intra- and extra-cellular transport. Seeding of the crystals takes place on bacterial membranes and exopolymers obtained from bacteria which had been farmed and then degraded by the sponge (Jackson et al. 2010). The phylogenetic and physiological diversity of sponge bacterial endosymbionts might be behind the diversity of biomineralization mechanisms. This diversity manifests itself even within single species. For example, in the only known living hypercalcified demosponge that employs Mg-calcite, *Acanthochaetetes wellsi*, the skeleton is formed through four different mechanisms in separate anatomical areas (Reitner and Gautret 1996).

If any, or perhaps more than one, of the processes seen in modern calcified sponges existed in Palaeozoic stromatoporoids (and chaetetids, which were co-existing hypercalcified sponges) then they may explain the organised FRR structure of FRIC, which is a diagenetic alteration product of presumed prior-ordered mineralisation. Evidence from electron backscatter diffraction methodology on stromatoporoids and a chaetetid (Balthasar et al. 2020) supports the interpretation that FRR preserved remnants of an original fibrous structure. Fig. 2j is a rare example of well-preserved fibrous structure in stromatoporoids, consistent with this interpretation. However, we noted earlier the taxonomically-related variation of FRIC in stromatoporoids; discussion by Stearn (2015b, page 540) drew attention to the type of stromatoporoid microstructure called compact, which Stearn theorised to be due to randomly-oriented microcrystals that constructed the skeleton. Indeed, as noted earlier, stromatoporoids with compact microstructure show a more blocky appearance of FRIC (Figs. 2, 3 & 5), evidence for taxonomic influence on the process of diagenesis and the form of FRIC, which may thus reflect variation in original construction of the skeleton.

Finally, the consistent distinction of the stromatoporoid skeleton from cements in gallery space revealed in unstained, stained and silicified examples in thin-sections, plus SEM, CL and UV fluorescence, could be explained by preserved organic matter in the skeleton that governed the diagenetic process. Although there is little work on organic matter in stromatoporoid skeletons, Clark (2005) discovered its common occurrence in a range of fossil taxa including Palaeozoic calcified sponges, with chaetetid and stromatoporoid examples. The few samples examined here under UV fluorescence (several stromatoporoid taxa, see supplemental file in Kershaw et al., 2021, Fig. S1) show bright fluorescence in skeletal material whereas gallery cement does not fluoresce, which might be caused by chromatic groups in the organic matter that reacted to electromagnetic radiation. Although we have not studied Mesozoic sponges, Mastandrea and Russo (1995) identified an aggrading type of alteration in Triassic sponges interpreted to have been controlled by organic matter. Differences in shape and size of FRIC cement in different taxa, even encrusting one another within one thin-section (Fig. 10), may relate to complex interaction between skeletal elements and enclosed organic matter. However, in all cases, the FRR overprinting by irregular bladed calcite did not disturb staining and CL patterns, evidence of fine-scale recrystallisation.

Beyond sponges, such interactions between aligned skeletal elements and organic matter occur in other groups. For example, Hoffmann et al. (2016) presented analysis of Jurassic and Cretaceous belemnite rostra that comprise aligned crystal elements with notable microporosity between the elements. This material is interpreted to have been filled with organic matter, then cemented during early diagenesis with non-biogenic carbonate. Their results have parallels with stromatoporoids; although the belemnites show excellent preservation, they too are overprinted with a diagenetic fabric.

Ordovician stromatoporoids of Manitoba, Canada: a special case?

The timing of initial diagenetic change is not revealed in most stromatoporoids, but important information comes from Ordovician stromatoporoids from Canada, discussed here separately because of their unusual setting. Stromatoporoids in carbonates of the decorative Tyndall Stone, in the Selkirk Member, Red River Formation, Katian (Upper Ordovician) may be a special diagenetic case because they occur in a limestone affected by differential dolomitization (Fig. 16). Wackestones in which the stromatoporoids are found are strongly mottled, with two sizes of mottle (larger are up to 30 mm diameter, smaller are 7-10 mm diameter). The interior of mottles is composed of dolomite but the surrounding rock is not. There are two principal views of this rock. Kendall (1977) considered the large mottles to represent largely horizontal burrows of the ichnogenus *Thalassinoides*, with the smaller burrows occurring within. Burrows acted as conduits for the input of dolomitising fluids in this model. In contrast, Gingras et al. (2004) recognised smaller burrows as conduits for the input of dolomitising fluids, but interpreted the larger mottles to be diagenetic, not burrows.

Stromatoporoids and corals grew as individuals on what was presumably a level seafloor; they did not accumulate in reefs or layers. Thus, each stromatoporoid and coral is an isolated growth, except where numerous overgrown and intergrown corals and stromatoporoids occur due to successive recolonisation of hard surfaces (Young et al. 2008). Of great interest are the tangential bioerosion features recognised in this study, which contain evidence of cutting through gallery cement (Fig. 16f, g), indicating that lower parts of the stromatoporoid gallery fills were cemented in early diagenesis while they were still on the seafloor. Borings have an overall range of 1-15 mm diameter but are mostly 2-5 mm; they are filled with laminated bound sediment fills with a central cavity (Fig. 16e, f); the animal may have excavated the stromatoporoid then created a sediment lining in which to live. Tangential burrow fills are shown in Fig. 16c, d to be largely, but not entirely, dolomitised. Stromatoporoids cut by the borings are partly affected by the dolomite, in the marginal areas and edges of burrows, shown by staining. A wider aspect of the features described here is that evidence of cementation in the lower part of a stromatoporoid, while its upper surface was presumably still alive, indicates that the growth process of individual stromatoporoids may have included a hybrid of organic (calcified tissue growth) and inorganic processes (gallery calcite fills), as proposed by Riding and Virgone (2020).

Minute rhombohedral crystals (interpreted as microdolomite) were found in the stromatoporoids and tabulates of the Selkirk Member, in skeleton walls and cavities, although it is not clear whether the microdolomite is present because of dolomitisation, or was a component of the diagenesis regardless of the dolomitisation of the mottled sediment. Nevertheless, the microstructure of Tabulata fossils in this facies is well-preserved; stromatoporoids display FRR and well-developed FRIC, rare in tabulates, the same relationship as seen in Silurian and Devonian co-existing stromatoporoids and tabulates. It is postulated here that the smaller burrows (= mottles) in these Selkirk Member carbonates may have been made by the same organisms as the borers in the stromatoporoids, changing their behaviour in a hard skeletal substrate compared to unlithified sediment. Otherwise the borers were specialised to live in stromatoporoids, and thus would have lived in “islands” on the seafloor presented by stromatoporoid skeletons, which parsimoniously is less likely. Dolomitisation of the sediment fills of borings unfortunately does not help to discriminate between the hypotheses of Kendall (1977) and Gingras et al. (2004). In contrast to stromatoporoids and tabulates, receptaculitids found in the same deposit vary in preservation. Observations by the authors show that some receptaculitids are completely dolomitised; others are preserved as calcite. Since they are recrystallised, receptaculitids were presumably originally aragonite, and, in comparison with stromatoporoids, provide circumstantial evidence that stromatoporoids were protected from alteration, and may have been composed of HMC. Finally, the borers in these Ordovician samples are somewhat different from those in the Silurian cases studied here (see Fig. 13e), where there is no evidence in our samples of such early cementation of the gallery space. Nevertheless, a boring in an early Silurian stromatoporoid illustrated by Tapanila and Holmer (2006, fig. 3) shows sediment which barely invaded the stromatoporoid gallery; this can be explained by early cementation of the gallery space in that sample. More data are required to determine whether early gallery cementation was common or not.

Silicification

The question as to the timing of silicification, indicated by uncertain placing of silicification into Stage 3 (Fig. 12) was also addressed by Henderson (1984) who viewed the process as a later diagenetic event, based on a single sample from the Middle Devonian of Australia in which silicification preferentially affected the skeleton rather than gallery cement. Henderson also noted that replacement of the skeleton calcite was by quartz rich in inclusions, in contrast to inclusion-free quartz in the gallery space, thus preserving the contrast between inclusion distributions of skeleton and gallery. We concur with Henderson’s view that fabric-retentive silicification occurred through molecule-by-molecule replacement. Clarke’s (1998, p. 36) study of the Devonian Slave Point Formation in Canada recorded silicification in an *Amphipora* stromatoporoid and *Thamnopora* tabulate, also interpreted to have been late in diagenetic history, cross-cutting late-stage fractures filled with calcite. In Fig. 27c of this study, silicification cuts across the FRIC. Henderson also recorded silicification that occurred in close proximity to pressure dissolution seams that provide conduits for silica-rich fluids to pass into stromatoporoids, supporting the view of a late-stage timing. In the current study, the few silicified stromatoporoids show either fractures in the skeletons (e.g., Fig. 26f, g) or occur in deposits substantially affected by pressure dissolution, consistent with Henderson’s view of access of silicifying fluids. Such fluids then clearly used stromatoporoid growth layering as conduits into the interior of skeletons, possibly via growth interruption surfaces or by tangential fracturing under compaction. Nevertheless, it remains possible that silicification took place earlier in cases lacking verification of timing, such that the FRR process forming FRIC may have occurred around the already-formed silicified structure. The contrast between Henderson's work and our new information indicates that a larger sample set may be needed to resolve the full pattern of silicification processes and their relationship with fabric-retentive processes. Overall, the key outcome of this range of studies is that the stromatoporoid skeleton behaved differently from the gallery cements during silicification, reflecting the fabric-retentive character of stromatoporoids during diagenesis. Stromatoporoids may be subject to other mineralisation, as shown by one example presented by Kano and Lee (1997) of fluorite replacing part of the skeleton of an Ordovician stromatoporoid from Korea, which also contains dolomitisation and silicification textures.

Isotopic composition

Only a few geochemical studies of stromatoporoids have been made, with a few stromatoporoid samples included in studies largely focused on brachiopods because of the greater stability of brachiopod shells. Examples are: Voice et al. (2018) from the lower Silurian of the Michigan Basin, USA; Frykman (1986) from the late Wenlock of Gotland, Sweden; Clarke (1998) from the Middle Devonian of Alberta, Canada; Corlett and Jones (2011) from the Middle Devonian of the Mackenzie Basin, Northwest Territories, Canada. None of these studies provided the isotopic values other than on plots; therefore we digitised them to identify commonalities (Table 1 in Kershaw et al. 2021), the results are compiled in Fig. 30.

Each of these studies recorded a different range of $\delta^{13}C_{carb}$ and $\delta^{18}O_{carb}$ values. Average carbon isotope values in stromatoporoids were close to those of associated brachiopod shells and matrix, ranging from 1.1‰ in stromatoporoids and 1.2‰ in matrix (Clarke, 1998) to 3.1‰ in stromatoporoids and 2.9‰ in matrix (Frykman, 1986). In contrast, average oxygen isotope values were consistently lighter in stromatoporoids than in associated brachiopods and matrix, but heavier than in the cements: values range from -5.5‰ in stromatoporoids and -4.8‰ in brachiopods (Voice et al., 2018) to -8.4‰ in stromatoporoids, -6.5‰ in associated brachiopods and -12.9‰ in blocky cement (Clarke, 1998). We interpret this systematic difference as an indication that $\delta^{18}O_{carb}$ values reflect the recrystallised, secondary mineralogy of stromatoporoids. However, it is noted here that macroscopic techniques of sampling, as employed in these studies, are not sufficient to avoid contamination from gallery cement when sampling stromatoporoid skeletal structure. Therefore $\delta^{18}O_{carb}$ values lighter than those in associated brachiopods and matrix are most likely a product of an unknown proportion of admixed cement, and further analyses are necessary to resolve the isotopic composition of stromatoporoid skeletons. On the other hand, stromatoporoids seem to record $\delta^{13}C_{carb}$ close to equilibrium with the seawater of the time. This is similar to their purported closest living relative *Astrosclera willeyana*, which shows virtually no vital effects and precipitates its aragonitic skeleton in equilibrium with ambient seawater (Asami et al. 2020). Previously-reported negligible vital effects in extant hypercalcified sponges are evidence that precipitation of their skeletal tissues took place in isotopic equilibrium with seawater (Sim-Smith et al. 2017), irrespective of evidence of a biological control on calcareous skeleton formation discussed above.

Other geochemical data in stromatoporoids relevant to diagenesis

To complete this discussion of diagenetic change in stromatoporoids, rare-earth element (REE) data from stromatoporoids are included in some studies and applied to help understand their diagenesis. In Devonian limestones from the Canning Basin, Western Australia (Nothdurft et al. 2004) and the Northwest Territories of Canada (Corlett and Jones 2011, fig. 11), data from stromatoporoids record REE signatures similar to seawater. REE results may indicate early marine diagenesis in these examples. However, given that stromatoporoids are composed of skeletal elements and gallery cements combined on a microscopic scale, results from such analyses are likely to be time-averaged including skeletal signatures and diagenetic results. Nevertheless, because of early FRR identified in this paper, with potential import of carbonate into stromatoporoid skeletons (note Fig. 24) perhaps it is not surprising that stromatoporoids give a seawater signature for REE.

Conclusions

This study of diagenesis of Middle Ordovician to Carboniferous stromatoporoids reveals the following outcomes:

1. Evidence from thin-sections in plane-polarised and cross-polarised light, ARS-KFeCN staining, cathodoluminescence, UV fluorescence and SEM, as well as some published results of carbon and oxygen isotopes, REE, and numerous literature descriptions of sedimentology and diagenesis relating to stromatoporoids, is drawn together in this study. The range of information indicates that the majority of the diagenetic changes in Palaeozoic stromatoporoids consistently occurred early in the history of the limestones in which they occur.
2. Three stages of diagenesis are recognised with Stages 1 and 2 overlapping, starting on the seafloor and almost fully complete within shallow burial zones.
3. Stromatoporoids are commonly found disorientated and encased in micrite, where delicate margins of the stromatoporoids are preserved undamaged, evidence of early seafloor lithification prevalent throughout middle Palaeozoic shallow-marine carbonates.
4. In thin-section study, all stromatoporoids are affected by an apparently unique form of fabric-retentive recrystallisation (FRR) leading to overprinting of the skeleton and gallery cements by large fabric-retentive irregular calcite (FRIC) crystals arranged normal to the skeletal laminae. FRIC shows variation in structure related to stromatoporoid taxa, which influenced their diagenesis. FRIC is interpreted to have developed early in very shallow burial settings and is associated with early formation of limestone-marl rhythms. The FRR process may have been controlled by organic proteins in the skeletal tissue and may be a remnant of an original fibrous skeletal structure, commonly seen in modern hypercalcified sponges, but more detailed investigations are needed.
5. Many stromatoporoids contain 10-20 μm rhombohedral crystals in their skeletal structure, which remain unstained with alizarin red S and are attributed to microdolomite. These are less abundant in gallery space, but rhombs also occur in some cases in associated sub-stromatoporoid cavities, micritic sediments and even adjacent tabulates, so the interpretation that stromatoporoids were originally high-Mg calcite (HMC) based on microdolomite is not fully robust. Nevertheless, cement crystals revealed by

CL in cavities within and adjacent to stromatoporoids are bladed and equant, very different from the acicular crystal shapes of aragonite. Stromatoporoids are always better preserved than aragonitic molluscs but less well-preserved than calcitic shells such as brachiopods. Stromatoporoids are also preserved in carbonate sequences of alternating limestones and marls, in contrast to aragonitic shells. These features are consistent with an interpreted HMC mineralogy, supporting earlier views that stromatoporoids are compatible with the calcite phases of aragonite-calcite sea fluctuations.

6. This study of Palaeozoic stromatoporoid diagenesis is informed by the literature on modern calcified sponges, skeletons of which are constructed from fibrous calcium carbonate crystals that may reflect the formation of fabric-retentive diagenetic structures in stromatoporoids.

Acknowledgments

SK thanks: Ulla Kapp (Canada) for donation of Ordovician samples from the Goodsell Quarry, Vermont; the late Bruno Mistiaen for donation of some Devonian samples, in 1987, from France and Spain; Kingston University, Surrey, England, for facilities to obtain cathodoluminescence and UV light images, funded by the Nuffield Foundation; Anne-Christine Da Silva (Liege, Belgium) for assistance with UK Silurian stromatoporoids; Matt Riley (Sedgwick Museum of Earth Sciences, Cambridge, UK) for facilitating permission to image sample A7384 for Fig. 26; Consuelo Sendino and Richard Turney (Natural History Museum, London, UK) for helping with access to the stromatoporoid collection; Paul Shepherd, Simon Harris and Louise Neep (British Geological Survey, Keyworth, UK) for access to Carboniferous stromatoporoid samples; Institute of Paleontology, University of Kansas for permission to reproduce figures 344-1 and 345-1 from Stearn (2015b), used in Fig. 2. GY thanks Edward Dobrzanski and Janis Klapecki (Manitoba Museum, Winnipeg) for assistance with collecting and preparing stromatoporoids from Garson, Manitoba. EJ was supported by the Deutsche Forschungsgemeinschaft (grant no JA 2718/3-1). Birgit Leipner Mata (GeoZentrum Erlangen) quickly prepared thin sections required for the revised version of this manuscript which is gratefully acknowledged. We thank Pawel Wolniewicz, an anonymous referee and Facies editor Maurice Tucker for helpful review comments on the manuscript that have improved the final result.

References

Aizenberg J, Weiner S, Addadi L (2003) Coexistence of amorphous and crystalline calcium carbonate in skeletal tissues. Connective Tissue Research 44: 20-25. DOI: 10.1080/03008200390152034

Asami R, Kinjo A, Ohshiro D, Naruse T, Mizuyama M, Uemura R, Shinjo R, Ise Y, Fujita Y, Sakamaki T (2020) Evaluation of geochemical records as a paleoenvironmental proxy in the hypercalcified demosponge *Astrosclera willeyana*. Progress in Earth and Planetary Science 7:15. https://doi.org/10.1186/s40645-020-00329-z

Balthasar U, Kershaw S, Da Silva A-C, Seuss B, Cusack M, Eichenseer K, Chung P (2020) Palaeozoic stromatoporoids and chaetetids analysed using Electron Backscatter Diffraction (EBSD); implications for original mineralogy and microstructure. Facies 67: 8

Barbin V, Ramseyer K, Debenay JP, Schein E, Roux M, Decrouez D (1991) Cathodoluminescence of Recent biogenic carbonates: an environmental and ontogenetic fingerprint. Geological Magazine 128: 19-26

Barbin V (1992) Fluctuation in shell composition in *Nautilus* (Cephalopoda, Mollusca): evidence from cathodoluminescence. Lethaia 25: 391-400

Bathurst RGC (1971) Carbonate Sediments and their Diagenesis: Amsterdam, Elsevier, Developments in Sedimentology 12, 620 p

Bolton TE (1988) Stromatoporoidea from the Ordovician rocks of central and eastern Canada. Contributions to Canadian Palaeontology, Geological Survey of Canada, Bulletin 379: 17-45

Christ N, Immenhauser A, Wood RA, Darwich K, Niedermayr A (2015) Petrography and environmental controls on the formation of Phanerozoic marine carbonate hardgroounds. Earth Science Reviews 15: 176-226

Clark GR (2005) Organic matrix in the Porifera and Cnidaria: Deja vu through a temporal microscope. Geological Society of America, Abstracts with Programs 37: 366

Clarke JD (1998) Petrology, geochemistry and diagenesis of the Middle Devonian Slave Point Formation, Hamburg Field, northwestern Alberta. Unpublished MSc thesis, University of Windsor, Ontario. Electronic Theses and Dissertations. 3076. https://scholar.uwindsor.ca/etd/3076

Copper P (2002) Silurian and Devonian reefs: 80 million years of global greenhouse between two ice ages. Pp.181–238. In Kiessling, W., Flügel, E., Golonka, J. (eds). *Phanerozoic Reef Patterns*, SEPM Special Publication No. 72

DeCarlo TM, Ren H, Farfan GA (2018) The origin and role of organic matrix in coral calcification: insights from comparing coral skeleton and abiogenic aragonite. Frontiers in Marine Science 5: 170, doi: 10.3389/fmars.2018.00170

De Yoreo JJ, Gilbert PUPA, Sommerdijk NAJM, Penn RL, Whitelam S, Joester D, Zhang H, Rimer JD, Navrotsky A, Banfield JF, Wallace AF, Michel FM, Meldrum FC, Cölfen H, Dove, PM (2015) Crystallization by particle attachment in synthetic, biogenic, and geologic environments. Science 349, aaa6760 (2015). DOI: 10.1126/science.aaa6760

Frykman P (1986) Diagenesis of Silurian bioherms in the Klinteberg Formation, Gotland, Sweden. Pp399-423, In Schroeder, J.H., Purser, B.H. (eds.) Reef Diagenesis. Springer-Verlag, Berlin, Heidelberg

Garate L, Sureda J, Agell G, Uriz MJ (2017) Endosymbiotic calcifying bacteria across sponge species and oceans. Scientific Reports 7: 43674, DOI: 10.1038/srep43674

Germer J, Mann K, Wörheide G, Jackson DJ (2015) The skeleton forming proteome of an early branching metazoan: a molecular survey of the biomineralization components employed by the coralline sponge *Vaceletia* sp. PLOS One 10(11): e0140100. doi:10.1371/journal.pone.0140100

Gilis M, Grauby O, Willenz P, Dubois P, Legras L, Heresanu V, Baronnet A (2011) Multi-scale mineralogical characterization of the hypercalcified sponge *Petrobiona massiliana* (Calcarea, Calcaronea). Journal of Structural Biology 176: 315–329. doi:10.1016/j.jsb.2011.08.008

Gilis M, Grauby O, Willenz P, Dubois P, Heresanu V, Baronnet A (2013) Biomineralization in living hypercalcified demosponges: Toward a shared mechanism? Journal of Structural Biology 183: 441–454. DOI: 10.1016/j.jsb.2013.05.018

Gingras MK, Pemberton SG, Muelenbachs K, Machel H (2004) Conceptual models for burrow-related, selective dolomitization with textural and isotopic evidence from the Tyndall Stone, Canada. Geobiology 2: 21-30

Henderson RA (1984) Diagenetic growth of euhedral megaquartz in the skeleton of a stromatoporoid. Journal of Sedimentary Petrology 54: 1138-1146

Hoffmann R, Richter DK, Neuser RD, Jöns N, Linzmeier BJ, Lemanis RE, Fusseis F, Xiao X, Immenhauser A (2016) Evidence for a composite organic-inorganic fabric of belemnite rostra: implications for palaeoceanography and palaeoecology. Sedimentary Geology 341: 203-215

Jackson DJ, Thiel V, Wörheide G (2010) An evolutionary fast-track to biocalcification. Geobiology 8: 191-196

Kano A, Lee D-J (1997) Fluorite cement in Ordovician stromatoporoid skeletons. *Boletín de la Real Sociedad Española de Historia Natural (Section Geologicas)* 91: 67-76

Kendall AC (1977) Origin of dolomite mottling in Ordovician limestones from Saskatchewan and Manitoba. Bulletin of Canadian Petroleum Geology 25: 480-504.

Kershaw S (1990) Stromatoporoid palaeobiology and taphonomy in a Silurian biostrome, Gotland, Sweden. Palaeontology 33: 681-705

Kershaw S (1994) Classification and geological significance of biostromes. Facies, 31: 81-92

Kershaw S (2013) Palaeozoic stromatoporoid futures: a discussion of their taxonomy, mineralogy and applications in palaeoecology and palaeoenvironmental analysis. Journal of Palaeogeography 2: 163-182

Kershaw S, Munnecke A, Jarochowska E (2018) Understanding Palaeozoic stromatoporoid growth. Earth Science Reviews 187: 53-76

Kershaw S, Munnecke A, Jarochowska E, Young G (2020) Isotopes in stromatoporoids. figshare. Dataset. https://doi.org/10.6084/m9.figshare.13182908.v1

Kershaw S, Sendino C (2020) *Labechia carbonaria* Smith 1932 in the Early Carboniferous of England; affinity, palaeogeographic position and implications for the geological history of stromatoporoid-type sponges. Journal of Palaeogeography 9, https://doi.org/10.1186/s42501-020-00077-7

Kershaw S, Wood R, Guo L (2006) Stromatoporoid response to muddy substrates in Silurian limestones. GFF 128:131–138

Kopp C, Meibom A, Beyssac O, Stolarski J, Djediat S, Szlachetko J, Domart-Coulon I (2011) Calcareous sponge biomineralization: ultrastructural and compositional heterogeneity of spicules in *Leuconia johnstoni*. Journal of Structural Biology 173: 99-109

Lee J-H, Riding R (2018) Marine oxygenation, lithistid sponges, and the early history of Paleozoic skeletal reefs. Earth Science Reviews, 181: 98-121

Lohman KC, Meyers WJ (1977) Microdolomite inclusions in cloudy prismatic calcites: a proposed criterion for former high-Magnesium calcites. Journal of Sedimentary Petrology 47: 1078-1088

Mallamo MP (1995) Paleoceanography of the Upper Devonian Fairholme Carbonate complex, Kananaskis-Banff area, Alberta. Ph.D. thesis. McGill University. Montreal, Quebec. 433 p

Mallamo MP, Stearn CW (1991) Skeletal mineralogy of Ordovician stromatoporoids: New geochemical evidence for an aragonite skeleton. Geological Society of America, Abstracts with Programs 23: 164

Mastandrea A, Russo F (1995) Microstructure and diagenesis of calcified demosponges from the Upper Triassic of the Northeastern Dolomites (Italy). Journal of Paleontology 69: 416-431

Munnecke A, Samtleben C (1996) The formation of micritic limestones and the development of limestone-marl alternations in the Silurian of Gotland, Sweden. Facies 34: 159-176

Neuweiler F, Burdige DJ (2005) The modern calcifying sponge *Spheciospongia vesparium* (Lamarck, 1815), Great Bahama Bank: implications for ancient sponge mud-mounds. Sedimentary Geology 175: 89-98

Nohl T, Jarochowska E, Munnecke A (2019) Revealing the genesis of limestone-marl alternations: a taphonomic approach. Palaios 34: 15-31

Nothdurft LD, Webb GE, Kamber BS (2004) Rare earth element geochemistry of Late Devonian reefal carbonates, Canning Basin, Western Australia: confirmation of a seawater REE proxy in ancient limestones. Geochimica et Cosmochimica Acta 68: 263-283

Päßler J-F, Jarochowska E, Bestmann M, Munnecke A (2018) Distinguishing biologically controlled calcareous biomineralization in fossil organisms using electron backscatter diffraction (EBSD). Frontiers in Earth Science 6: doi:10.3389/feart.2018.00016

Pérez-Huerta A, Coronado I, Hegna TA (2018) Understanding biomineralization in the fossil record. Earth-Science Reviews 179: 95-122

Reitner J, Gautret P (1996) Skeletal formation in the modern but ultraconservative chaetetid sponge *Spirastrella (Acanthochaetetes) wellsi* (Demospongiae, Porifera). Facies 34: 193-208

Reitner J, Wörheide G, Lange R, Schumann-Kindel G (2001) Coralline demosponges – a geobiological portrait. Bulletin of Tohoku University Museum, 1: 219-235

Ricken W (1986) Diagenetic Bedding: A Model for Limestone-Marl Alternations: Lecture Notes in Earth Sciences, v. 6, Berlin, Springer Verlag, 210p

Riding R (1974) Stromatoporoid diagenesis: outline of alteration effects. Geological Magazine 111: 143-148

Riding RE (1981) Composition, structure and environmental setting of Silurian bioherms and biostromes in Northern Europe. 41-83. In Toomey, D.F. (ed). European Fossil Reef Models. SEPM Special Publications 30: 546p

Riding R, Virgone A (2020) Hybrid carbonates: *in situ* abiotic, microbial and skeletal co-precipitates. Earth Science Reviews 208, https://doi.org/10.1016/j.earscirev.2020.103300.

Rossi AL, Ribeiro B, Lemos M, Werckmann J, Borojevic R, Fromont J, Klautau M Farina M (2016) Crystallographic orientation and concentric layers in spicules of calcareous sponges. Journal of structural biology 196: 164-172

Rush PF, Chafetz HS (1991) Skeletal mineralogy of Devonian stromatoporoids. Journal of Sedimentary Petrology, 61: 364–369

Russell J (1995) Direct Pb/Pb dating of Silurian macrofossils from Gotland, Sweden. P. 175-200 In: Dunay, R.E. & Hailwood, E.A. (eds), *Non-biostratigraphical Methods of Dating and Correlation.* Geological Society Special Publication No. 89. London

Scoffin TP (1972) Cavities in the reefs of the Wenlock Limestone (Mid-Silurian) of Shropshire, England. Geologisches Rundschau 61: 565–578

Scoffin TP (1987) An Introduction to Carbonate Sediments and Rocks. Blackie, Glasgow and London. 274p.

Semeniuk V (1971) Subaerial leaching in the limestones of the Bowan Park Group (Ordovician) of central western New South Wales: Journal of Sedimentary Petrology 41: 939–950

Sethmann I, Wörheide G (2008) Structure and composition of calcareous sponge spicules: a review and comparison to structurally related biominerals. Micron 39: 209-228

Sethmann I, Hinrichs R, Wörheide G, Putnis A (2006) Nano-cluster composite structure of calcitic sponge spicules—a case study of basic characteristics of biominerals. Journal of Inorganic Biochemistry 100: 88-96

Sim-Smith C, Ellwood M, Kelly M (2017) Sponges as proxies for past climate events. Chapter 3 in Carballo, J.L., Bell, J.J. (eds.), *Climate Change, Ocean Acidification and Sponges*, DOI 10.1007/978-3-319-59008-0_3. Springer International Publishing AG 2017 49

Smith A, Berman J, Key MM Winter DJ (2013) Not all sponges will thrive in a high-CO_2 ocean: Review of the mineralogy of calcifying sponges. Palaeogeography, Palaeoclimatology, Palaeoecology 392: 463-472

Smosna R (1984) Diagenesis of a stromatoporoid patch reef. Journal of Sedimentary Petrology, 54: 1000–1011

Stanley SM (2006) Influence of seawater chemistry on biomineralization throughout Phanerozoic time: palaeontological and experimental evidence. Palaeogeography, Palaeoclimatology, Palaeoecology 232: 214-236

Stanley SM, Hardie LA (1998) Secular oscillations in the carbonate mineralogy of reef-building and sediment-producing organisms driven by tectonically forced shifts in seawater chemistry. Palaeogeography Palaeoclimatology Palaeoecology 144: 3-19

Stearn CW (1972) The relationship of the stromatoporoids to the sclerosponges. Lethaia 5: 369-388

Stearn CW (1975) The stromatoporoid animal. Lethaia 8: 89-100

Stearn CW (1989) Specks in the microstructure of Paleozoic stromatoporoids. Memoirs of the Association of Australasian Palaeontologists 8: 143-148

Stearn CW (2015a) Extinction patterns of the Paleozoic Stromatoporoidea. p599-612 in Selden, P.A. (ed). Treatise on Invertebrate Paleontology. Part E (Revised), Porifera, vol 4-5. The University of Kansas Paleontological Institute, Lawrence, Kansas, liii +1223p., 665 fig. 42 tables

Stearn CW (2015b) Microstructure and Mineralogy of Paleozoic Stromatoporoidea. p.521-542 in Selden, P.A. (ed). Treatise on Invertebrate Paleontology. Part E (Revised), Porifera, vol 4-5. The University of Kansas Paleontological Institute, Lawrence, Kansas, liii +1223p., 665 fig. 42 tables

Stearn CW (2015c) Diversity trends of the Paleozoic Stromatoporoidea. p.593- 597 in Selden, P.A. (ed). Treatise on Invertebrate Paleontology. Part E (Revised), Porifera, vol 4-5. The University of Kansas Paleontological Institute, Lawrence, Kansas, liii +1223p., 665 fig. 42 tables

Stearn CW (2015d) Stromatporellida, Stromatoporida, Syringostromatida, Amphiporida, and genera with uncertain affinities; systematic descriptions. p. 781–836 in Selden, P.A. (ed). Treatise on Invertebrate Paleontology. Part E (Revised), Porifera, vol 4-5. The University of Kansas Paleontological Institute, Lawrence, Kansas, liii +1223p., 665 fig. 42 tables

Stearn CW, Mah AJ (1987) Skeletal microstructure of Paleozoic stromatoporoids and its mineralogical implications. Palaios 2: 76–84

Stearn CW, Pickett JW (1994) The stromatoporoid animal revisited: building the skeleton. Lethaia 27: 1-10

Tapanila L, Holmer LE (2006) Endosymbiosis in Ordovician-Silurian corals and stromatoporoids: a new lingulid and its trace from eastern Canada. Journal of Paleontology 80: 750-759

Tobin KJ, Walker KR (1998) Diagenetic calcite from the Chazyan Group (Vermont): an example of aragonite alteration in a greenhouse ocean. Sedimentary Geology 121: 277-288

Trablesi A (1989) Internal structural elements and mineralogy of Paleozoic stromatoporoids. Geological Society of America, Abstracts with Programs 21: A160-161

Tucker ME, Wright VP (1990) Carbonate Sedimentology. Blackwell Scientific Publications, Oxford, London, 482p

Voice PJ, Harrison WB III, Grammer GM (2018) A reevaluation of the Burnt Bluff Group (Llandovery, Silurian, Michigan Basin) from Subsurface and Outcrop Data: Development of a Time-Transgressive Depositional Model. P. 55-79.in Grammer, G. M., Harrison, W. B., III, and Barnes, D. A. (eds.), Geological Society of America Special Publication 531, Geological Society of America, Boulder, CO

Webby BD (2002) Patterns of Ordovician reef development. P. 129-180 in Kiessling, W., Flügel, E., Golonka, J. (eds). *Phanerozoic Reef Patterns*, SEPM Special Publication No. 72

Webby BD, Kershaw S (2015) External morphology of the Paleozoic stromatoporoids: shapes and growth habits. P.419-486 in Selden, P.A (Ed.), Treatise on Invertebrate Paleontology. Part E (Revised), Porifera. vol. 4-5 The University of Kansas (liii +1223p., 665 fig. 42 tables)

Weiner S (2008) Biomineralization: a structural perspective. Journal of Structural Biology 163: 229-234

Weiner S, Addadi L (2011) Crystallization pathways in biomineralization. Annual Review of Materials Research 41: 21-40

West RR, Vacelet J, Wood RA, Willenz P, Hartman WD (2015) Hypercalcified extant and fossil chaetetid-type and post-Devonian Stromatoporoid-type Demospongiae: Systematic descriptions. p. 209-292 in Selden, P.A (Ed.), Treatise on Invertebrate Paleontology. Part E (Revised), Porifera. vol. 4-5 The University of Kansas (liii +1223p., 665 fig. 42 tables)

Wilson JL (1975) Carbonate Facies in Geologic History. Springer-Verlag, New York, Heidelberg, Berlin. 471p

Wolf SE, Böhm CF, Harris J, Demmert B, Jacob DE, Mondeshki M, Ruiz-Agudo E, Rodríguez-Navarro C (2016) Nonclassical crystallization in vivo et in vitro (I): Process-structure- property relationships of nanogranular biominerals. Journal of Structural Biology 196: 244–259

Wright VP, Cherns L (2016) How far did feedback between biodiversity and early diagenesis affect the nature of early Palaeozoic sea floors? Palaeontology 59: 753-765.

Yoo CM, Lee YI (1993) Original mineralogy of stromatoporoids. Carbonates and Evaporites 8: 224-229

Young GA, Elias RJ, Wong S, Dobrzanski EP (2008) Upper Ordovician Rocks and Fossils in Southern Manitoba. Canadian Paleontology Conference, Field Trip Guidebook No. 13, CPC-2008 Winnipeg, The Manitoba Museum, 19-21 September 2008, 97p

FIGURES

Fig. 1

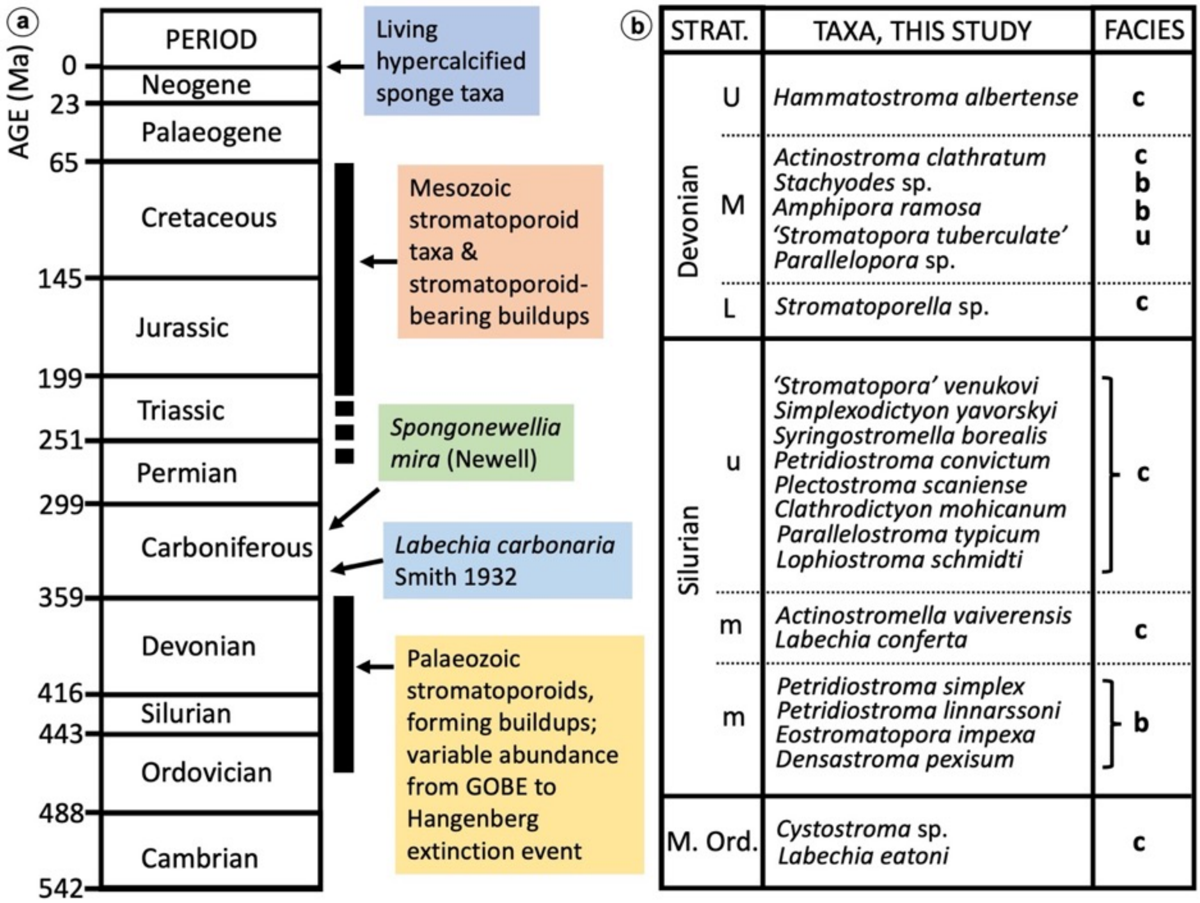

Fig. 1 **a** Simple stratigraphic chart of stromatoporoid geological history, emphasising that the major period of their history was the middle Palaeozoic Era, from Middle Ordovician to end-Devonian time, with sporadic occurrence in the Carboniferous System. Later reappearance in Jurassic and Cretaceous Systems ended by the latest Cretaceous, with no records in the Paleogene and Neogene although there are several living representatives. Detailed range charts of Ordovician to Devonian stromatoporoids are provided by Stearn (2015c). For *Labechia carbonaria* see Kershaw and Sendino (2020); for *Spongonewellia mira* see West et al. (2015, p. 273-4); **b** List of stromatoporoid taxa illustrated in this study, and their approximate stratigraphic positions; 23 taxa across the range of stromatoporoid structure, range of stratigraphic occurrence, and facies are included. Taxa grouped by a bracket were collected from the same unit. Facies are summarised as: c = a constructional deposit, broadly equating to reefal facies, noting that this also includes in-place biostromal units; b = bedded limestones; u = unknown. Note that additional taxa were examined but not illustrated.

Fig. 2

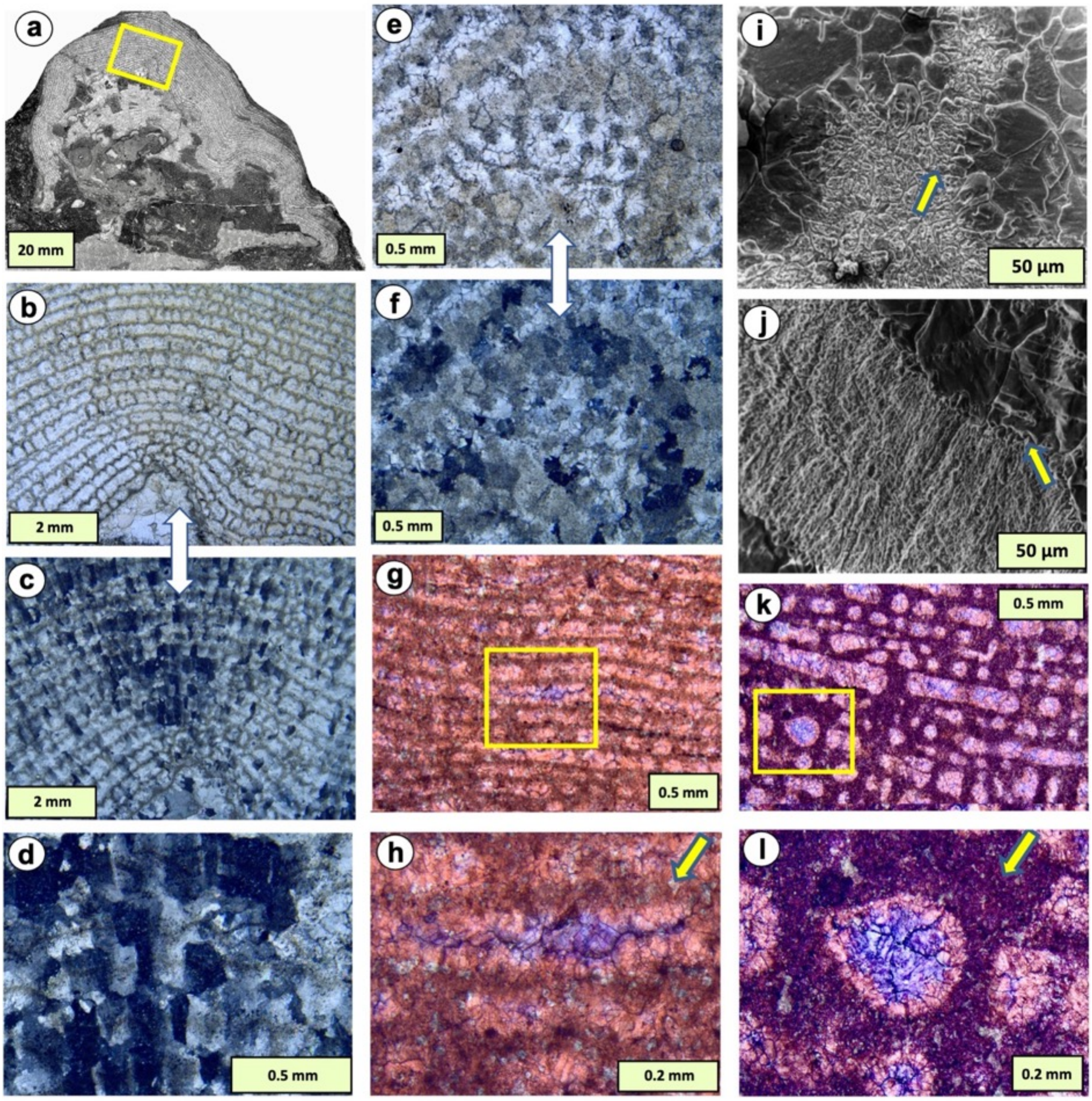

Fig. 2 Key characters of stromatoporoid structure and diagenesis, using typical examples. **a** Whole small stromatoporoid encrusting a favositid tabulate and sediment, that formed a minor topographic feature on the sea-bed. *Petridiostroma simplex*, Upper Visby Formation, Wenlock (Silurian), Gotland, Sweden; **b, c** Enlargement of yellow box in **a**, vertical (VS) section, in plane-polarised light (PPL)

(**b**), and cross-polarised light (XPL) (**c**) showing the laminae and pillars of which this taxon is constructed**. c** shows overprinting of the structure by fabric-retentive recrystallisation (FRR) comprising irregular diagenetic calcite crystals (fabric-retentive irregular calcite, FRIC), that are arranged normal to the stromatoporoid layers, producing a radial effect in an area of the skeleton that is curved; **d** Enlargement of the central part of **c**, showing detail of the FRIC; stromatoporoid skeleton is the speckled darker areas contrasting clear areas of gallery cement, FRIC cement passes through skeleton and galleries; **e, f** TS in PPL and XPL respectively showing the approximate equant cross-section of the overprinting FRIC. **g, h** VS views in PPL of *Petridiostroma linnarssoni*, Kneippbyn locality, Upper Visby Formation, Wenlock (Silurian), Gotland, Sweden, stained with combined alizarin red S and potassium ferricyanide stain solution. They show typical staining patterns: the skeleton is red-stained. In the gallery space, early diagenetic cement is red-stained (non-ferroan calcite), which in many cases fills the gallery space. Later cement is blue-stained (ferroan calcite); **i** Scanning electron microscope (SEM) secondary electron view of stromatoporoid skeleton and gallery cement in *Actinostroma clathratum* (Devonian), showing the overprinting effect of FRIC in crystal boundaries that pass through the skeleton into the gallery cements (yellow arrow); **j** SEM view of stromatoporoid skeleton and gallery cement in *Hammatostroma albertense* (Devonian), contrasting **i** because the gallery cement abuts against the stromatoporoid skeleton (yellow arrow) and does not pass through it; this is a rare example of preservation of a fibrous skeletal structure not overprinted by FRR effects. **i** and **j** are reproduced from Stearn (2015b, figures 344-1 and 345-1) with permission from the Paleontological Institute, University of Kansas; **k, l** VS views in PPL of *Stromatoporella* sp., Emsian (Devonian), Spain, sample donated by Bruno Mistiaen, showing a similar pattern to **e** and **f,** emphasising the common sequence of staining in stromatoporoids. Both samples in **h** and **l** show tiny unstained rhombohedral crystals attributed to microdolomite (arrows), discussed in the text. In **g-h, k, l** FRIC is not visible in these PPL views, but later figures illustrate the relationship between staining and FRIC.

Fig. 3

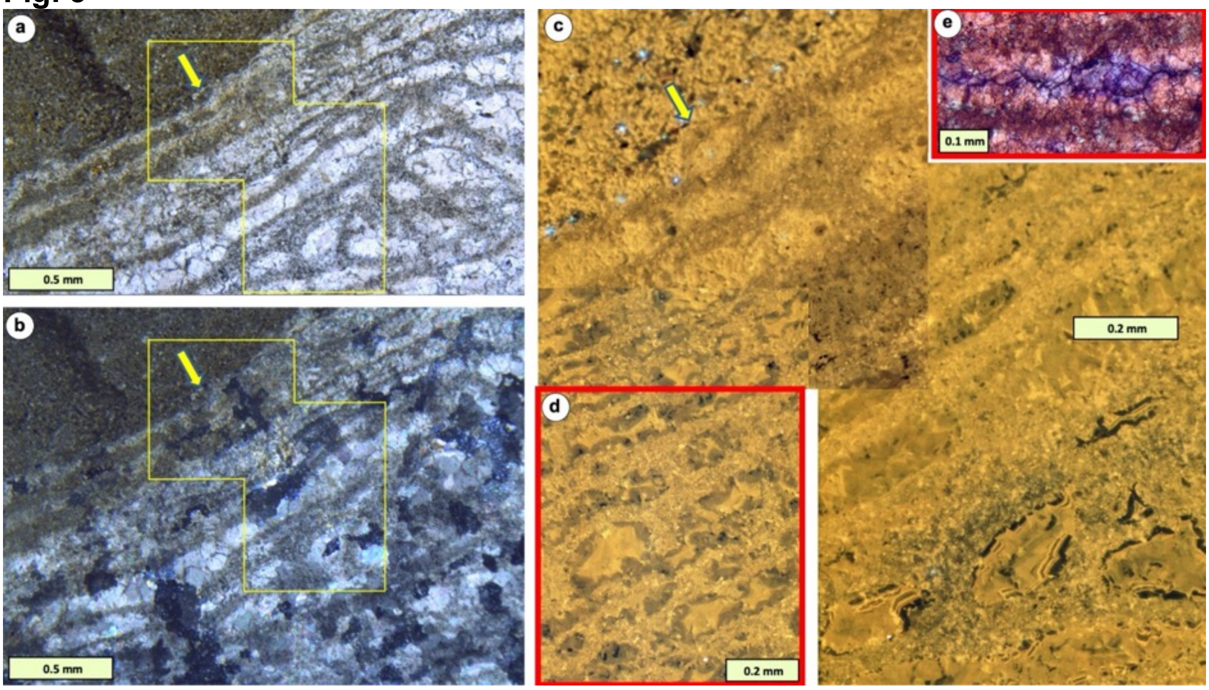

Fig. 3 Vertical thin-section views of a typical stromatoporoid overlain by micrite. **a, b** PPL and XPL views (yellow arrow shows matched points). Galleries of the upper two laminae are filled with micrite sediment that does not penetrate lower into the skeleton, discussed in the text. Note the fabric-retentive irregular calcite (FRIC) cement of the stromatoporoid terminates at the contact with sediment (**b**); **c** Cathodoluminescence (CL) view of the yellow polygonal box in **a** and **b**, with yellow arrow marking the same matched point in **a** and **b**. Upper part of skeleton displays dull luminescence in contrast to brighter luminescence in the sediment. Below, the gallery space is filled with zoned cement, that begins with non-luminescent cement, followed by a very thin bright zone, then dull cement filling the remaining space; **d** CL sequence in another part of the same thin-section, showing variation in CL zoning, in this case the entire gallery space is filled with two zones of dull cement; **e** Part of Fig. **2f**, showing comparison of a stained area of thin-section cut parallel to **a-d** from the same sample. The dull CL cement in **c** and **d** corresponds to blue-stained ferroan calcite, evidence of formation in anoxic conditions. The relationship between FRR, CL and staining is discussed in the text. *Petridiostroma linnarssoni*. Upper Visby Formation, Wenlock (Silurian), Kneippbyn locality, Gotland, Sweden, stained with combined ARS-KFeCN stain.

Fig. 4

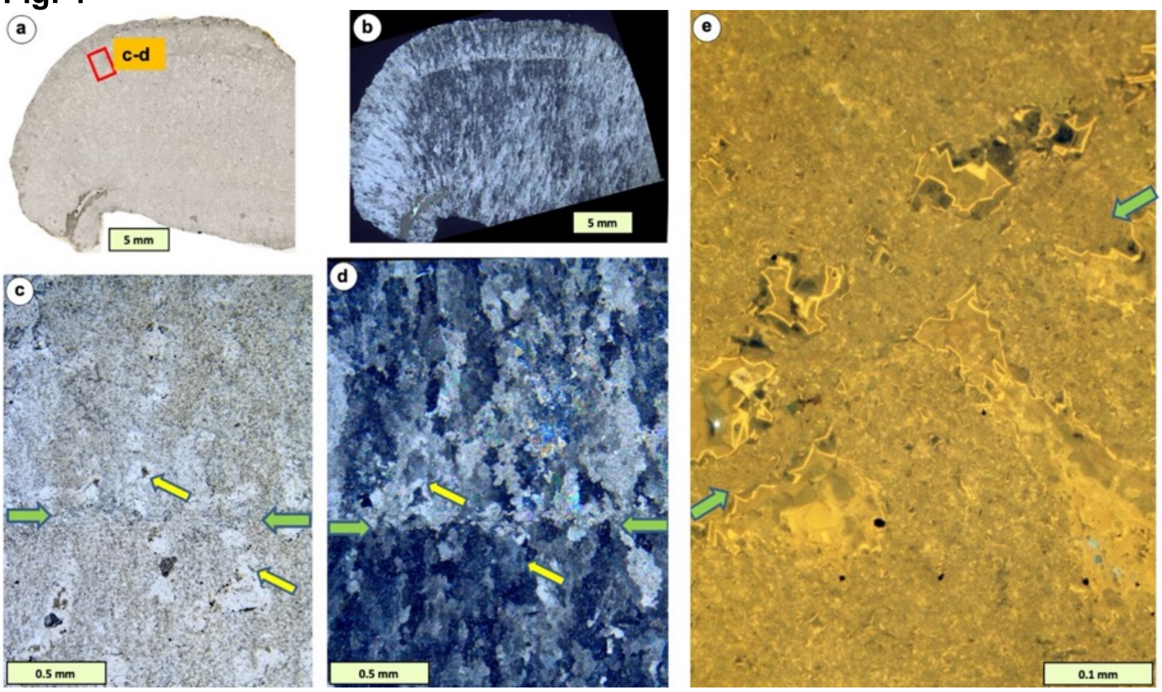

Fig. 4 Details of stromatoporoid structure and overprinting diagenetic calcite in *Eostromatopora impexa*, a taxon different from those in Figs. **2g, h** & **3** from the same locality and facies. **a, b** VS PPL and XPL views respectively of a thin-section, thinner than normal to emphasise overprinting calcite normal to growth layers. A growth interruption surface in the upper part is picked out by change in the diagenetic overprint; **c, d** Detail of **a** and **b** (from red box in **a**) showing that the skeleton (dense areas in **c**) and gallery spaces (clear areas in **c**) are overprinted by diagenetic calcite. Yellow arrows show matched points and also label gallery spaces; green arrows show horizon of the growth interruption surface seen in **b**; **e** Cathodoluminescence (CL) view of an area close to **c** and **d** (rotated about 20

degrees anticlockwise from horizontal), showing the gallery cement is zoned, indicating prior cement that is later overprinted in diagenesis. Green arrows show the level of the growth interruption surface as in **b**, **c** and **d**. See text for discussion. Upper Visby Formation, Wenlock (Silurian), Kneippbyn locality, Gotland, Sweden.

Fig. 5

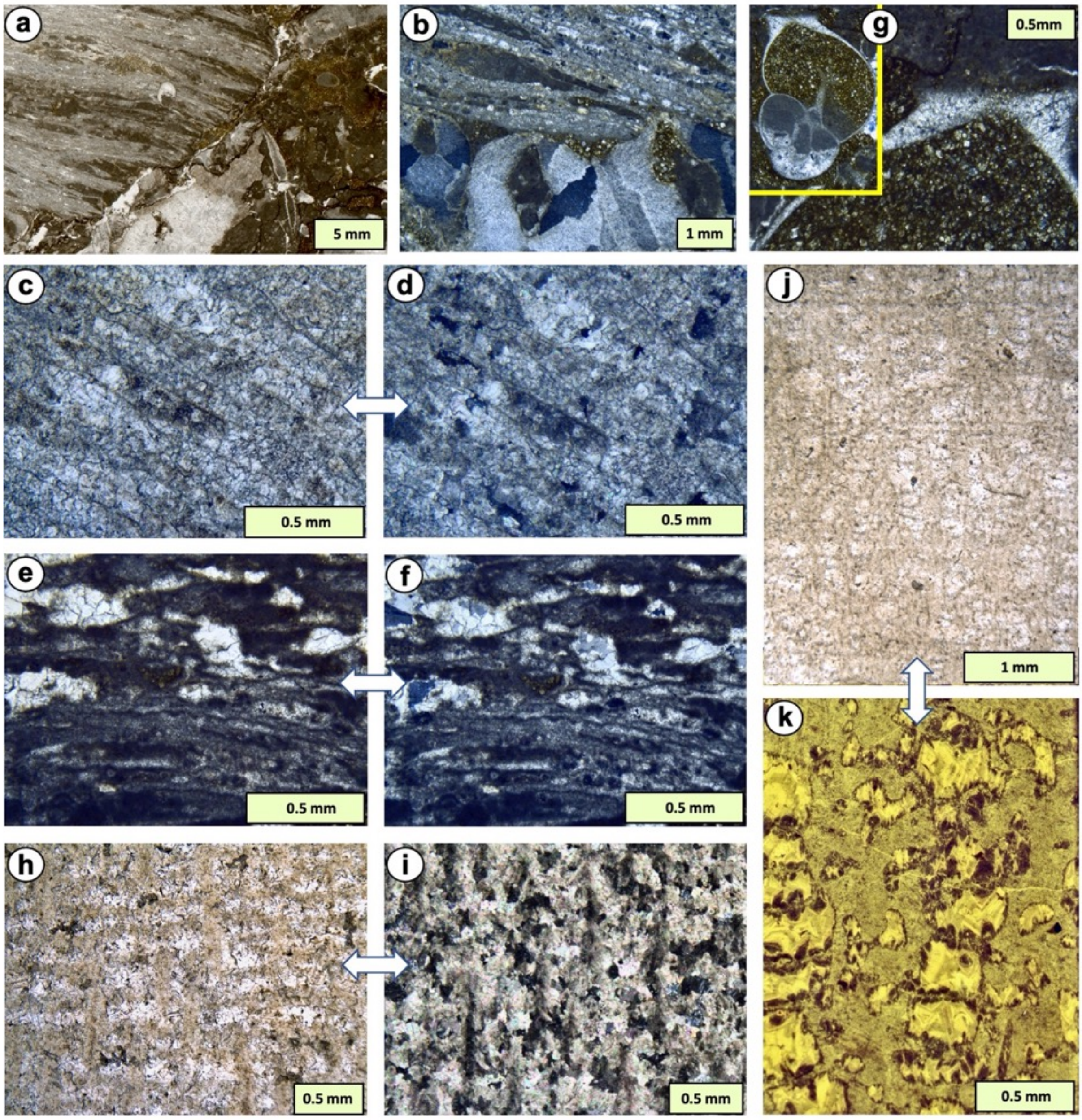

Fig. 5 Examples of Ordovician and Devonian stromatoporoids in PPL and XPL, in comparison with the Silurian examples in Figs. **2-4**. **a, b** VS sections in PPL and XPL respectively of middle Ordovician *Cystostroma*, middle Chazy Group, Darriwilian (Middle Ordovician), Goodsell Quarry, Isle La Motte, Vermont, USA, showing the poorly preserved layered stromatoporoid skeleton adjacent to a crinoid holdfast (**b**); see text for discussion; **c, d** VS PPL and XPL enlargements respectively of **a, b**,

showing the overprinted diagenetic calcite cutting across the stromatoporoid skeletal elements; **e, f** Another part of the same thin-section as in **a-d**, showing variable alteration of the skeleton, in PPL (**e**) and XPL (**f**); **g** Recrystallised gastropod in the section shown in **a-f**, to show comparison with stromatoporoid preservation; **h, i** VS PPL (**h**) and XPL (**i**) paired views respectively of *Actinostroma clathratum*, Middle Devonian, France, showing the common normal-orientated overprinting diagenetic FRIC cement; **j, k** VS PPL (**j**) and CL (**k**) views (not paired) of a sample of *Parallelopora,* Middle Devonian, France, showing the gallery space is occupied by zoned cement, as in the Silurian examples illustrated in other figures. Samples in **a-g** donated by Ulla Kapp; and **h-k** donated by Bruno Mistiaen.

Fig. 6

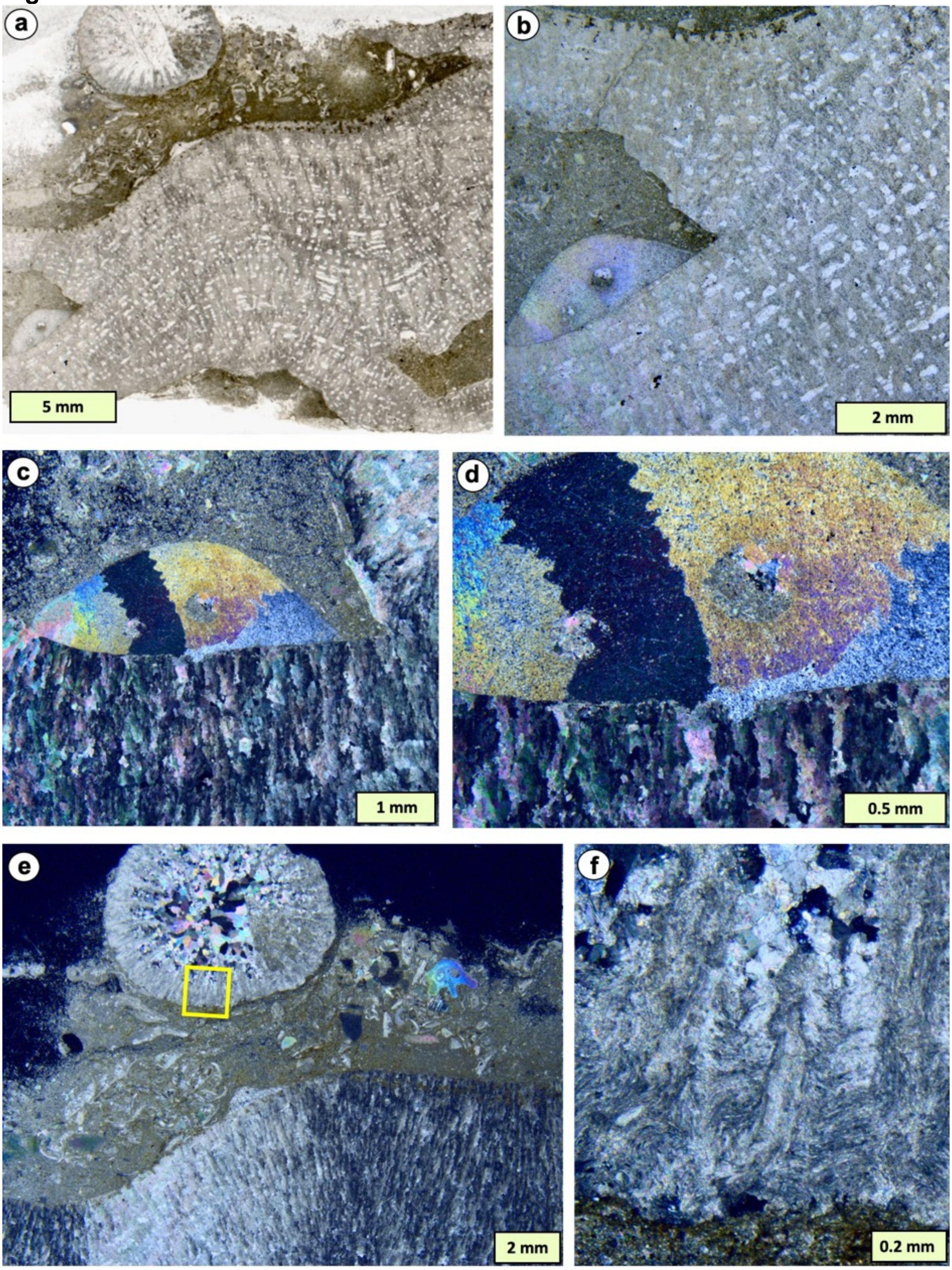

Fig. 6 Comparisons between stromatoporoid skeleton and associated fossils. **a** VS PPL thin-section of *Eostromatopora impexa*, with an encrusting crinoid holdfast (lower left), a rugose coral bioclast (upper left) in a wackestone fabric; **b** Enlarged view in PPL of lower left part of **a**, showing stromatoporoid structure of horizontal and vertical elements and the even-density crinoid holdfast. The upper part of the stromatoporoid was partly invaded by micrite sediment, discussed in the text; **c**

detail in d. Similar view as **b**, in XPL, rotated to emphasise the extinction of diagenetic calcite crystals comprising the stromatoporoid skeleton, normal to the growth layers. The fabric-retentive recrystallisation (FRR) of the stromatoporoid terminates sharply against the lower edge of the encrusting crinoid holdfast, so that alteration of the stromatoporoid does not pass into the crinoid, even though one crystal of the crinoid is in extinction and thus in crystallographic alignment with many crystals in the stromatoporoid, discussed in the text; **e** Enlargement of **a** in XPL showing the normal-oriented FRR crystals in the stromatoporoid terminate in contact with overlying wackestone; **f** Enlargement of yellow box in **e**, illustrating well-preserved lamellar rugose coral structure in XPL, contrasting the stromatoporoid in **c-e**. Much Wenlock Limestone Formation, Wenlock (Silurian), Lea South Quarry, Much Wenlock, Shropshire, UK.

Fig. 7

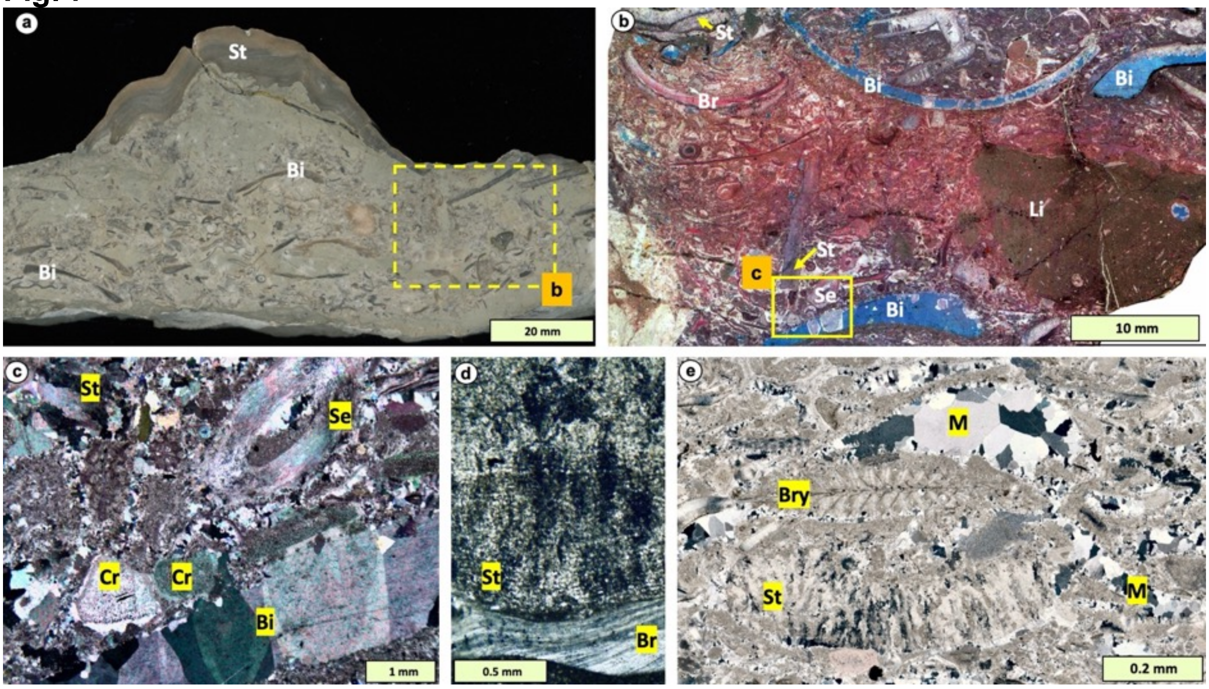

Fig. 7 a-d. Vertical sections of stromatoporoid taxon *Densastroma pexisum,* micritic sediment and associated bioclasts, to show contrasts of preservation. **a** Stromatoporoid (St) grew on a topographic high of eroded micrite that must have been partly lithified before the stromatoporoid grew. Bivalves (Bi) are visible in the wackestone-packstone below; **b** Stained acetate peel in VS of sediment from the part of **a** below the stromatoporoid [**b** is from a section parallel to the face imaged in **a**, its approximate position represented by the yellow dashed box (rather than a solid box) in **a**]. Included are: lower margin of stromatoporoid in **a** (upper left corner, St), another stromatoporoid fragment (centre left), three bivalves (Bi), recrystallised as ferroan calcite, a brachiopod (Br) preserved presumably unaltered as non-ferroan calcite and a serpulid tube (Se). A lithoclast (Li) indicates contemporaneous partial lithification of sediment on or just below the sea floor, followed by erosion; **c** Enlargement in XPL of the area of a thin-section equivalent to the box in **b**, showing a stromatoporoid fragment (St), serpulid (Se), crinoids (Cr) and altered bivalve (Bi); **d** Enlargement of another sample of *D. pexisum* (St) that encrusted an atrypid brachiopod (Br) emphasising the contrast in preservation, reflecting different original mineralogy. Both samples from the same facies. **a-c**: Ireviken 3 locality; **d**: Högklint locality; Upper Visby Formation, Wenlock (Silurian), Gotland, Sweden; **e** Vertical section of grainstone containing bioclasts of stromatoporoid (St), bryozoan (Bry) and originally aragonitic mollusc (M), demonstrating full recrystallisation of the mollusc compared to the fabric-retentive recrystallisation of the adjacent stromatoporoid, and well-preserved original LMC of the bryozoan. Haganäs locality, Slite Formation, lower Wenlock (Silurian), Gotland, Sweden.

Fig. 8

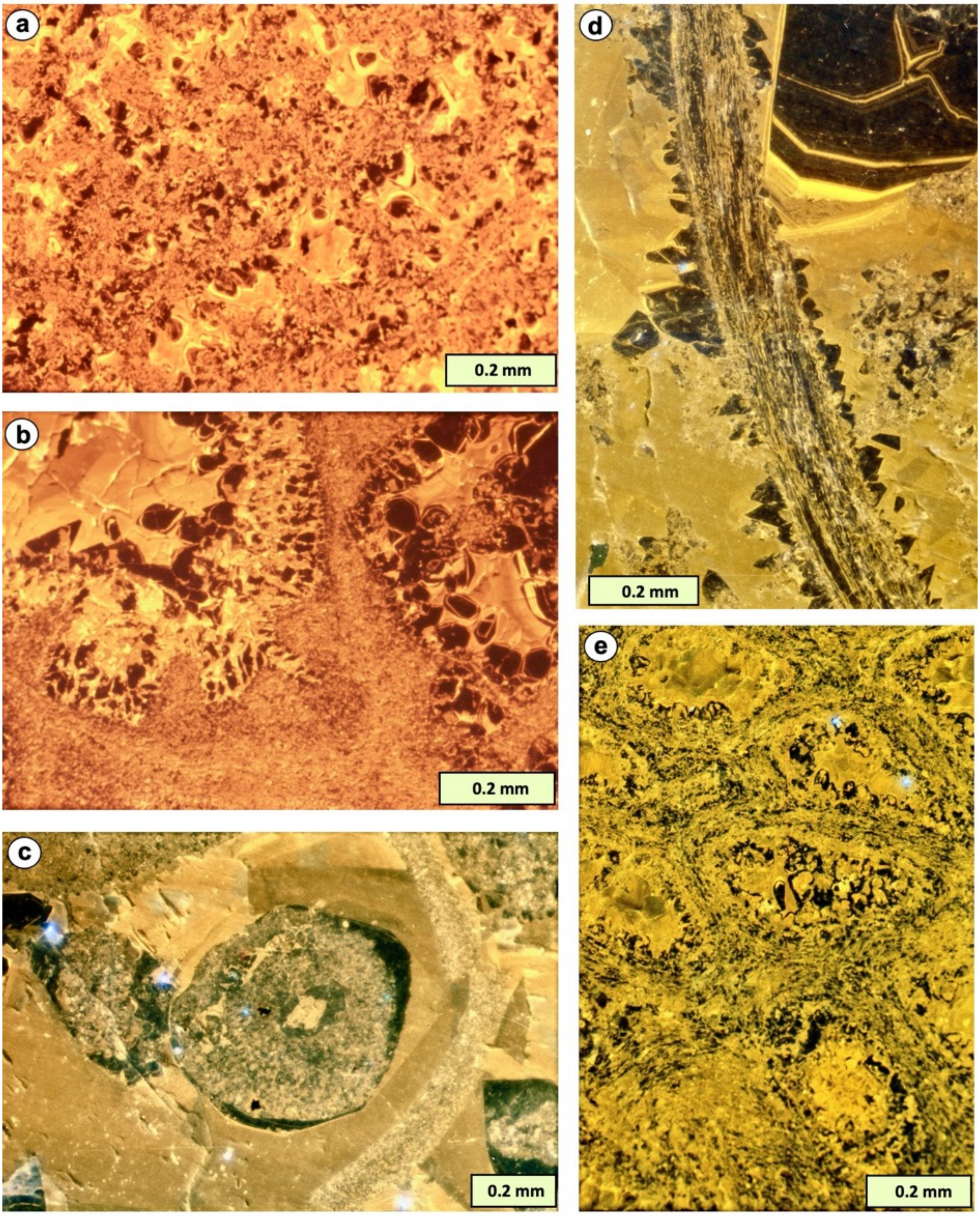

Fig. 8 Comparisons between stromatoporoids and other fossils in cathodoluminescence (CL) from one locality and facies. **a** Vertical thin-section of stromatoporoid *Clathrodictyon mohicanum* showing speckled appearance of the skeleton in CL in contrast to the zoned cements in the gallery cement; **b** Septa and part of outer wall of a rugose coral, and zoned cements in the calyx; **c** Crinoid ossicle with non-luminescent first-generation cement followed by dull cement filling most of

the remaining space. Lower area and upper right show other bioclasts, unidentified; **d** section through a brachiopod shell, centre left, with slightly altered fibrous structure, and zoned cements filling the surrounding void; **e** TS of a bryozoan, showing its well-preserved laminar wall structure. Hemse Group, Ludlow (Silurian), Kuppen biostrome locality, Gotland, Sweden.

Fig. 9

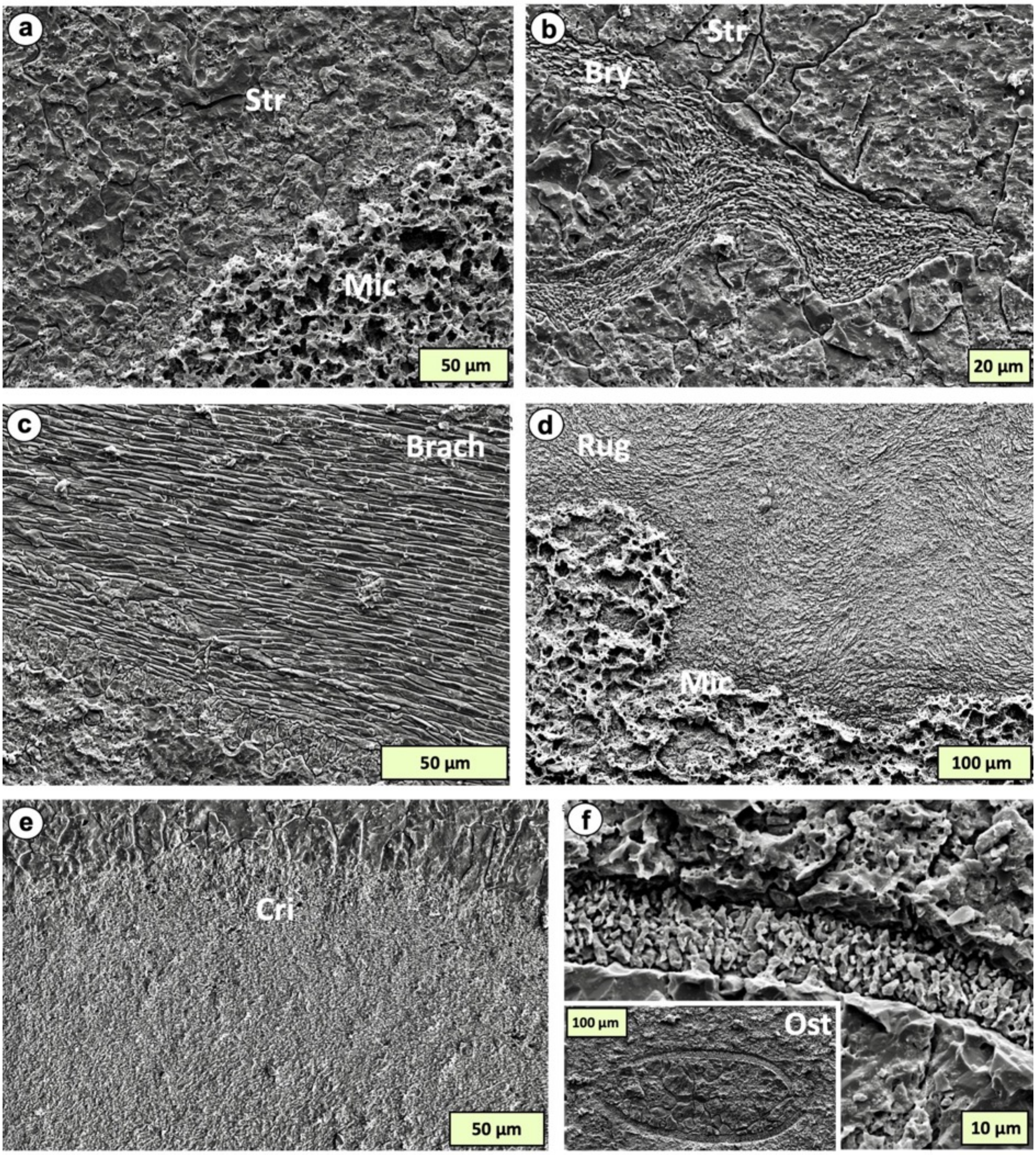

Fig. 9 Comparisons between Silurian stromatoporoids and other fossils under scanning electron microscope (SEM), using secondary electrons. **a** Basal part of stromatoporoid *Densastroma pexisum* (Str), in contact with underlying argillaceous micritic sediment (Mic); the fine-scale stromatoporoid skeletal structure characteristic of this taxon is not discernible in this gently-etched sample, but shows marked

contrast with the well-preserved skeletons of other fossils illustrated in **b-f; b** From another stromatoporoid, *Labechia conferta*, showing a downward-pointing basal encrusting bryozoan (Bry) on the base of the stromatoporoid (Str), an example of stromatoporoid growth to form a primary cavity. **a** from Much Wenlock Limestone Formation (MWLF), Wenlock (Silurian), Penny Hill Quarry, Abberley Hills, Worcestershire, UK; **b** from MWLF, Lea South Quarry, Wenlock Edge, Shropshire, UK; **c** Brachiopod in cross-section, showing its very well-preserved laminated structure. Upper Visby Formation, Wenlock (Silurian), Häftingsklint locality, Gotland, Sweden; **d** Rugose coral, showing well-preserved curved laminar structure, in contact with argillaceous micrite sediment in the lower part of the photo; **e** Edge of a crinoid ossicle (Cri) against sparite showing partial overlap of sparite crystals with the crinoid stereom, indicating partial alteration of the crinoid, consistent with its high-magnesium calcite composition. Högklint Formation, Wenlock (Silurian), Gutevägen locality, Gotland, Sweden; **f** Ostracod shell (Ost), with a fine crystalline structure, contrasting the coarse sparite of the stromatoporoid in **a**. **d** and **f** from Udevere Beds, Paadla Stage, lower Ludlow (Silurian), Katri biostrome site, western Estonia.

Fig. 10

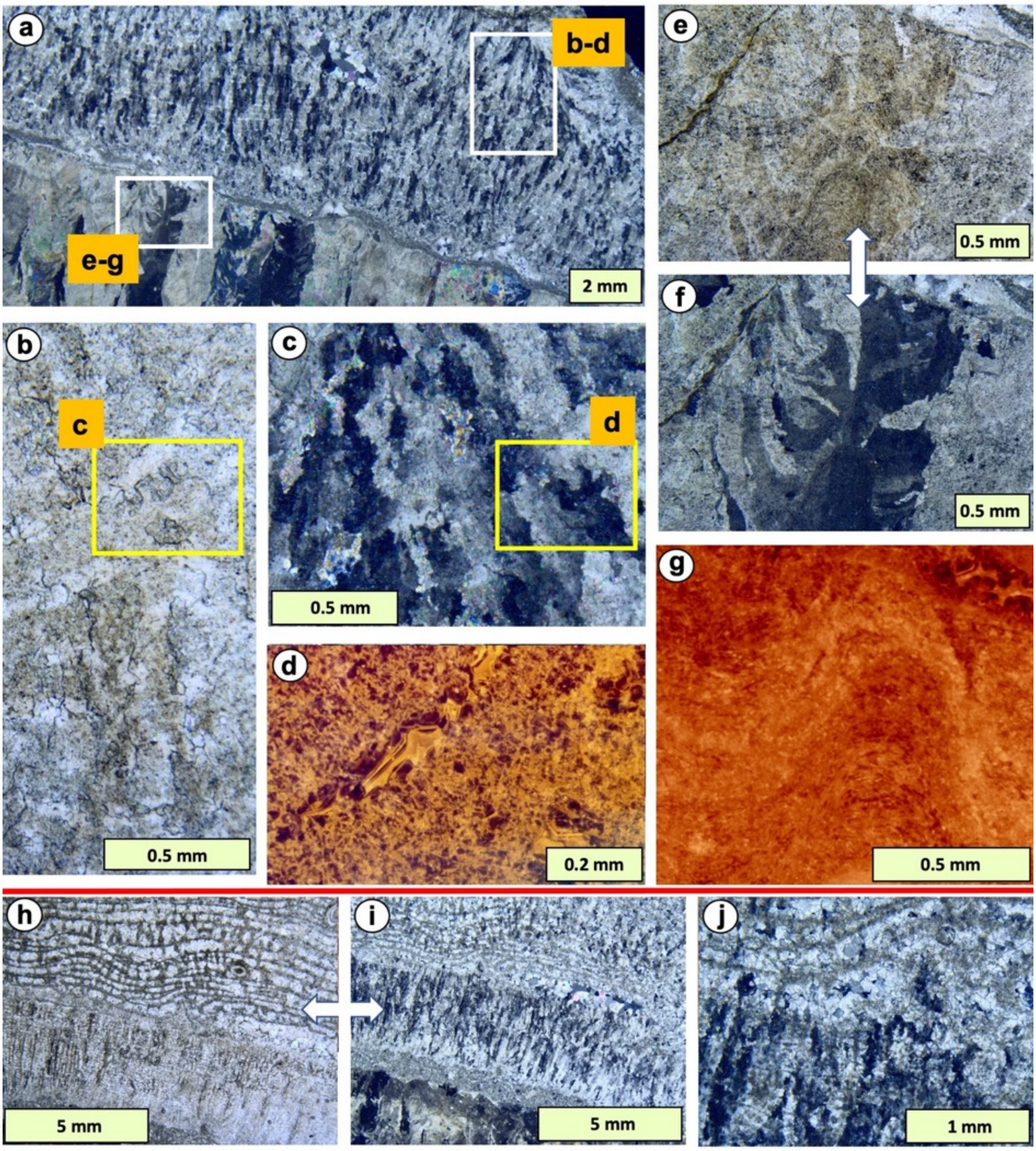

Fig. 10 Vertical thin-section views of four stromatoporoid taxa in two samples (**a-g**, **h-j**) from the same locality and facies, to show differences in diagenetic fabric compared with their skeletal structure**.** **a** General view of one sample showing *Parallelostroma typicum* encrusting *Lophiostroma schmidti*; **b, c, d** PPL, XPL and CL views respectively of *P. typicum* showing its FRR texture in XPL and speckled appearance in CL; **e, f, g** PPL, XPL and CL views respectively of *L. schmidti*

showing its FRR texture in XPL and layered crystalline composition in CL; **h, i** Three stromatoporoids in PPL and XPL respectively, from bottom to top: *L. schmidti, Plectostroma scaniense,* and *Petridiostroma convictum*; **j** *P. scaniense and P. convictum* in XPL, detailing profound difference in FRR texture, and also the sharp change in FRR texture from one taxon to the other, indicating the diagenetic fabric was conservative within each taxon and did not extend into the other. Hemse Group, Ludlow (Silurian), Kuppen biostrome locality, Gotland, Sweden.

Fig. 11

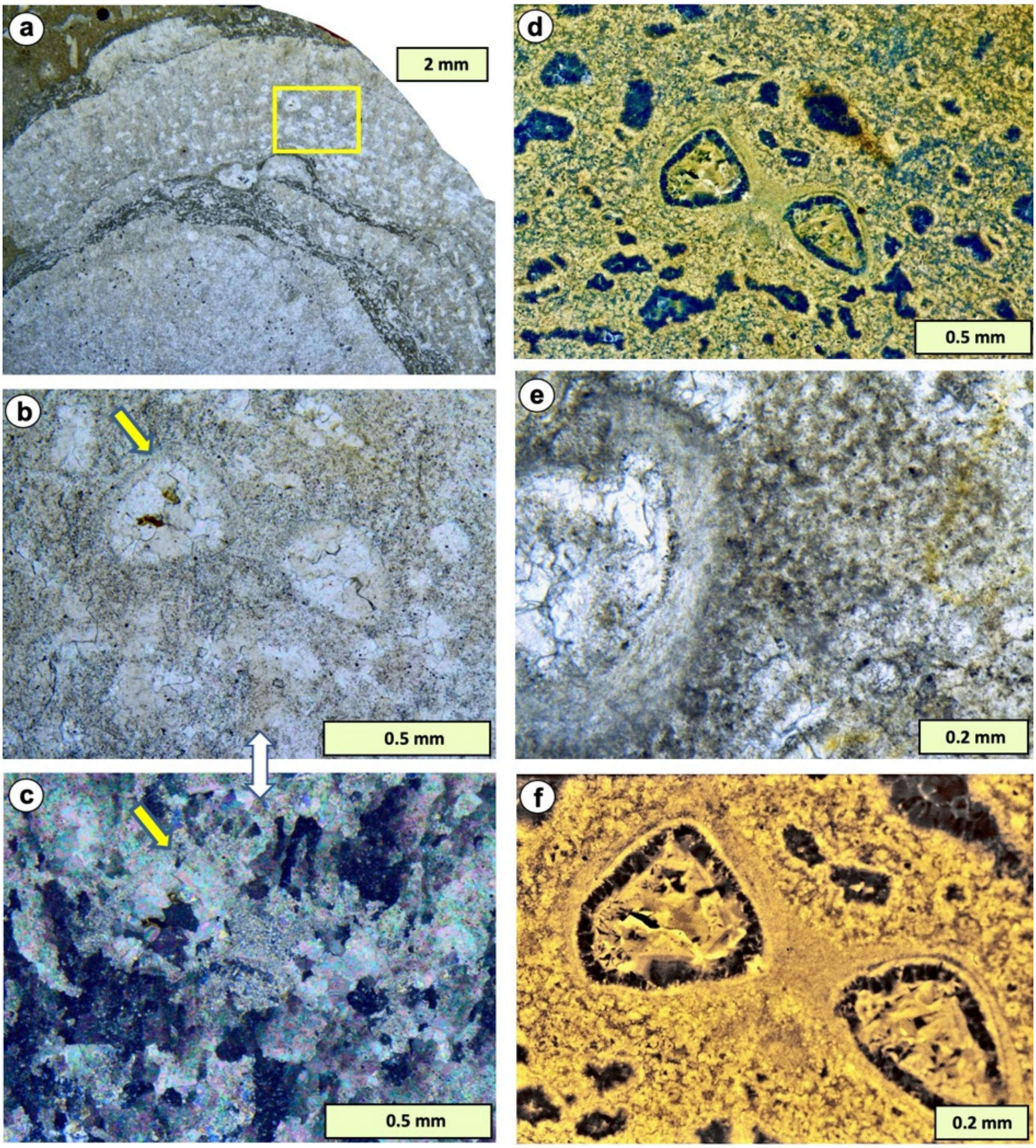

Fig. 11 Stromatoporoid with cellular type microstructure and intergrown syringoporid tabulate, in PPL, XPL and CL. **a** VS view in PPL showing overall growth of the stromatoporoid; **b, c** PPL and XPL views respectively of enlargement of yellow box in **a** showing detail of intergrowth syringoporid tabulate in stromatoporoid skeleton**. c** shows syringoporid is partly recrystallised in XPL; yellow arrows in **b** and **c** mark matched points; **d** CL view including the area of **b** and **c**, showing laminated

syringoporid, and highlights cellular microstructure of the stromatoporoid, that is only poorly visible in the thinner-than-normal thin section views in **a** and **b**; **e** Enlarged view of syringoporid and cellular stromatoporoid microstructure in PPL; **f** Enlargement of **d** in CL, comparable to **e**, of syringoporid and cellular stromatoporoid microstructure. Lowermost Klinteberg Formation, Wenlock (Silurian), Gothemshammar locality, Gotland, Sweden.

Fig. 12

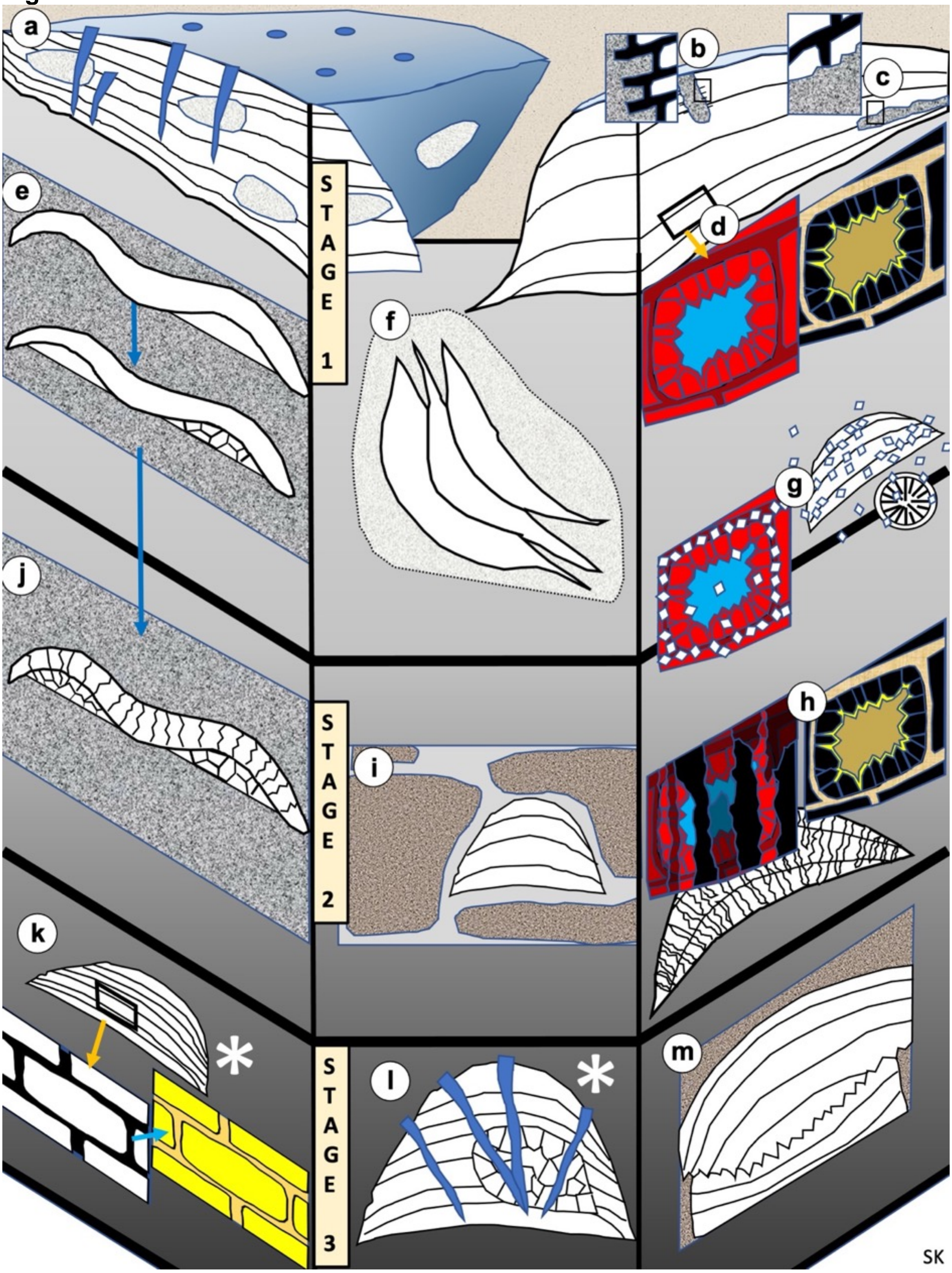

Fig. 12 Conceptual sequence of stromatoporoid diagenesis, drawing together the evidence and ideas presented in this study. The model proposes diagenetic events occurred in three stages, noting that there is overlap between stages. See text for discussion. **STAGE 1: a** Stromatoporoid subject to loss (ellipsoidal areas, probably by dissolution) prior to recrystallisation contrasting better-preserved intergrown

rugose corals (dark blue); **b** Stromatoporoid top surface bioeroded shortly after death, and micritic sediment entered the gallery space indicating it was not immediately cemented after death; **c** In some cases, borings in lower part of the skeleton cut already-formed gallery cement, indicating rapid cementing of galleries while the stromatoporoid was on the sea floor; but in other cases gallery spaces remained open; **d** Three generations of cement, shown by stained ARS-KFeCN (red denotes non-ferroan calcite, blue denotes ferroan calcite) and matched CL zoning; **e** primary and secondary sub-stromatoporoid cavities, showing differential filling; **f** Early partial lithification of sediment enclosing stromatoporoid, either on or just below the seafloor, followed by exhumation by erosion, leaving a disorientated stromatoporoid with undamaged margins; **g** Formation of microdolomite may have occurred in early diagenesis and overlaps Stage 2. **STAGE 2: h** Fabric-retentive recrystallisation process (FRR) led to overprinting of original stromatoporoid skeleton and gallery cement with fabric-retentive irregular calcite (FRIC); FRIC is not visible in CL, the latter is therefore interpreted to reflect the original or partly altered structure of the stromatoporoid and gallery cements; **i** Clay-bearing micritic sediment in which stromatoporoids are buried differentiate into limestone-marl rhythms that leave the stromatoporoids surrounded by unconsolidated sediment, related to FRR (see **h**); **j** Sub-stromatoporoid cavities are filled with cements that are either syntaxial (left, Type 1 cement) or non-syntaxial (right, Type 2 cement) with the overlying stromatoporoid. **STAGE 3: k** Differential silicification of skeleton and gallery space; left-hand diagram is the unsilicified stromatoporoid skeleton and gallery cement; right-hand diagram shows different shades of yellow to differentiate silicification of skeleton and gallery cement; **l** Interpreted late-stage dissolution of stromatoporoid skeletons, but not corals (blue); **m** Late-stage pressure dissolution in burial. In **k** and **l**, * indicates change may have occurred in an earlier stage.

Fig. 13

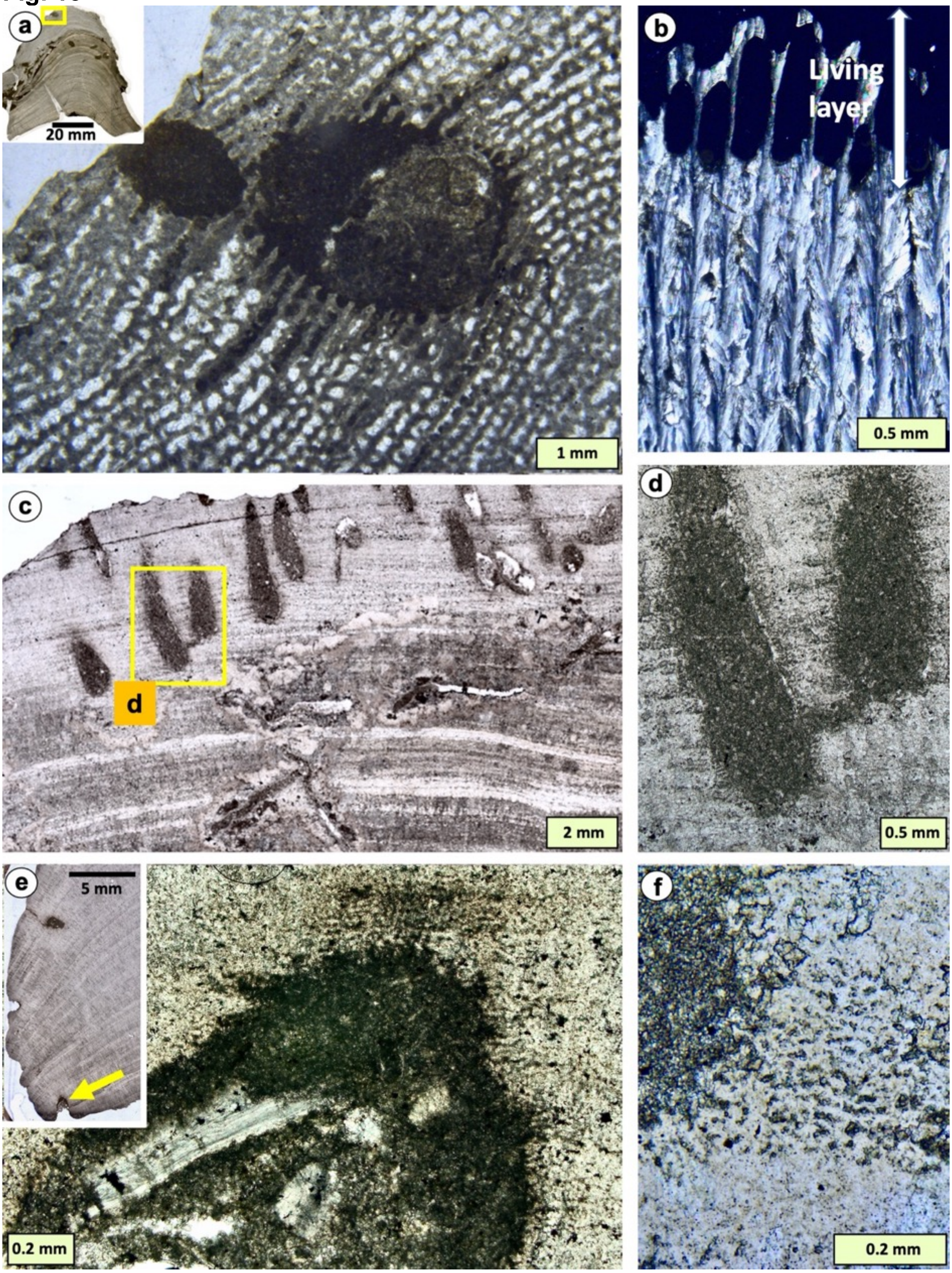

Fig. 13 a. *Trypanites* borings in the upper surface of stromatoporoid *Petridiostroma simplex* (upper stromatoporoid in the inset photo) from the Upper Visby Formation, Wenlock (Silurian), Gotland, Sweden, showing sediment infiltration into the gallery space, demonstrating that cementation of the galleries did not start immediately after death; **b** Vertical thin-section in XPL of modern *Ceratoporella* calcified sponge showing the living layer (represented by black-coloured spaces) and cement fill directly below, demonstrating early cementation of space in the skeleton; **c-d** *Trypanites* borings in the upper surface of stromatoporoid *Densastroma pexisum* with sediment infiltration into empty space within the fine-scale skeletal network that characterizes this taxon; **e** *Trypanites* boring in the partly eroded basal part of another sample of *D. pexisum*, demonstrating the early-formed part of the skeleton remained empty for some time after death of the stromatoporoid. Note that Fig. S3D in the supplemental file (Kershaw et al. 2021) is a hand-specimen of this sample before it was sectioned; **f** Another sample of *D. pexisum* showing detail of sediment invasion near the upper surface of an upright stromatoporoid, where dark micrite penetrated the horizontally-linked space in the skeleton.

Fig. 14

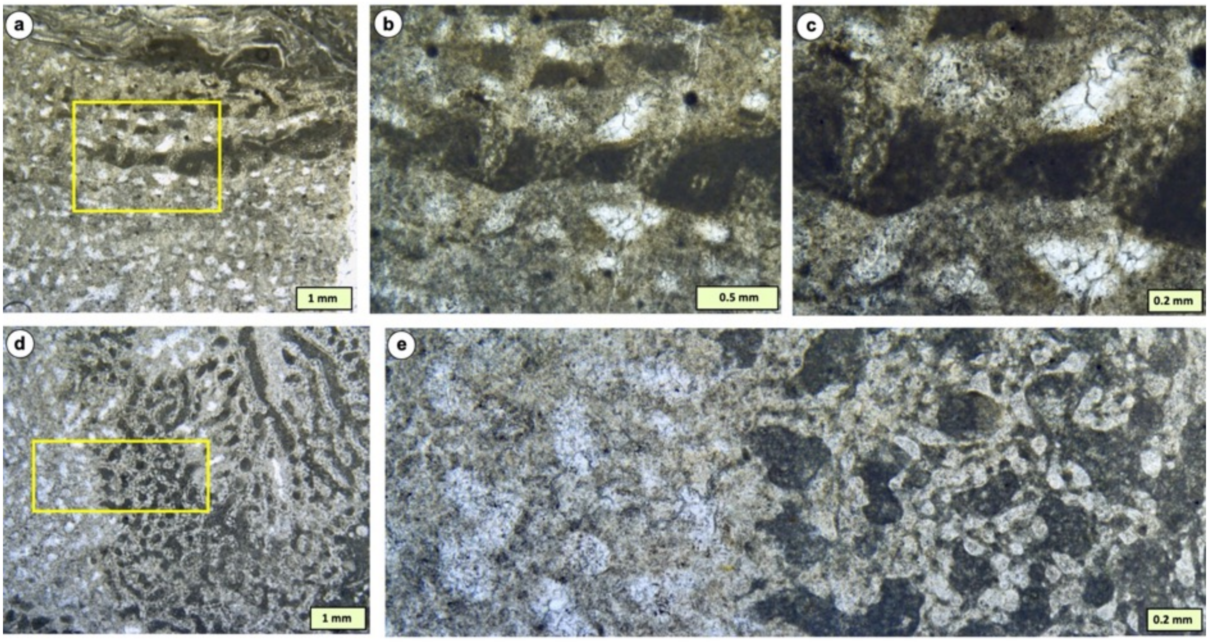

Fig. 14 VS thin-sections in PPL, showing sediment infiltration into the upper part of a specimen of *Syringostromella borealis* prior to cementation. **a-c.** Vertical section showing sediment entered the gallery space and also invaded the tiny intraskeletal spaces (microgalleries) in the stromatoporoid skeleton network. **e and e.** Transverse section showing sediment infiltrated into only part of the stromatoporoid structure. Hemse Group, Ludlow (Silurian), Kuppen biostrome locality, Gotland, Sweden.

Fig. 15

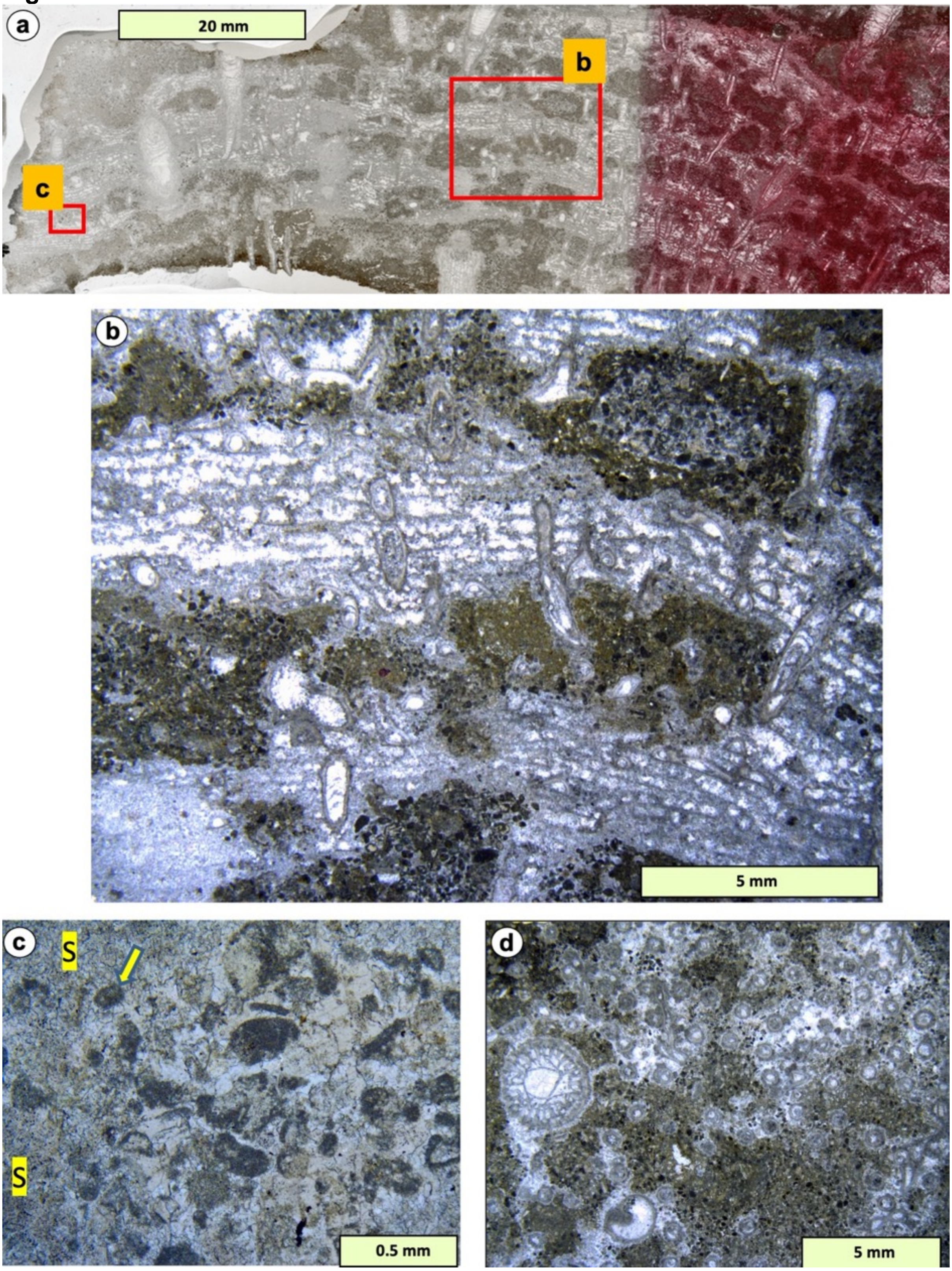

Fig. 15 *Petridiostroma convictum*, showing evidence of very early dissolution and filling of cavities with sedimentary particles. Limestone strata in equivalent nearby facies show evidence of subaerial fabrics (gravitational cements, not illustrated here), so this stromatoporoid is interpreted to have been exposed above sea level after death and partly dissolved, then cavities filled with marine sedimentary particles

as sea level rose again. **a** Vertical section of sample showing prominent intergrown rugose corals and syringoporid tabulates. Dark areas are sediment fills, identifying the locations of stromatoporoid skeleton loss. Red staining by ARS-KFeCN demonstrates that processes did not involve ferroan calcite, evidence of early change before burial; **b, c** Details of preserved skeletal structures and filled cavities, **c** showing the edge of a cavity with a recrystallised stromatoporoid structure (S); yellow arrow highlights a peloid at the edge of the cavity; **d** Transverse section showing preservation of rugose corals and syringoporid tabulates, more resistant to diagenesis than the stromatoporoid. Klinteberg Formation, Wenlock (Silurian), Fjäle 1 locality, Gotland Sweden,

Fig. 16

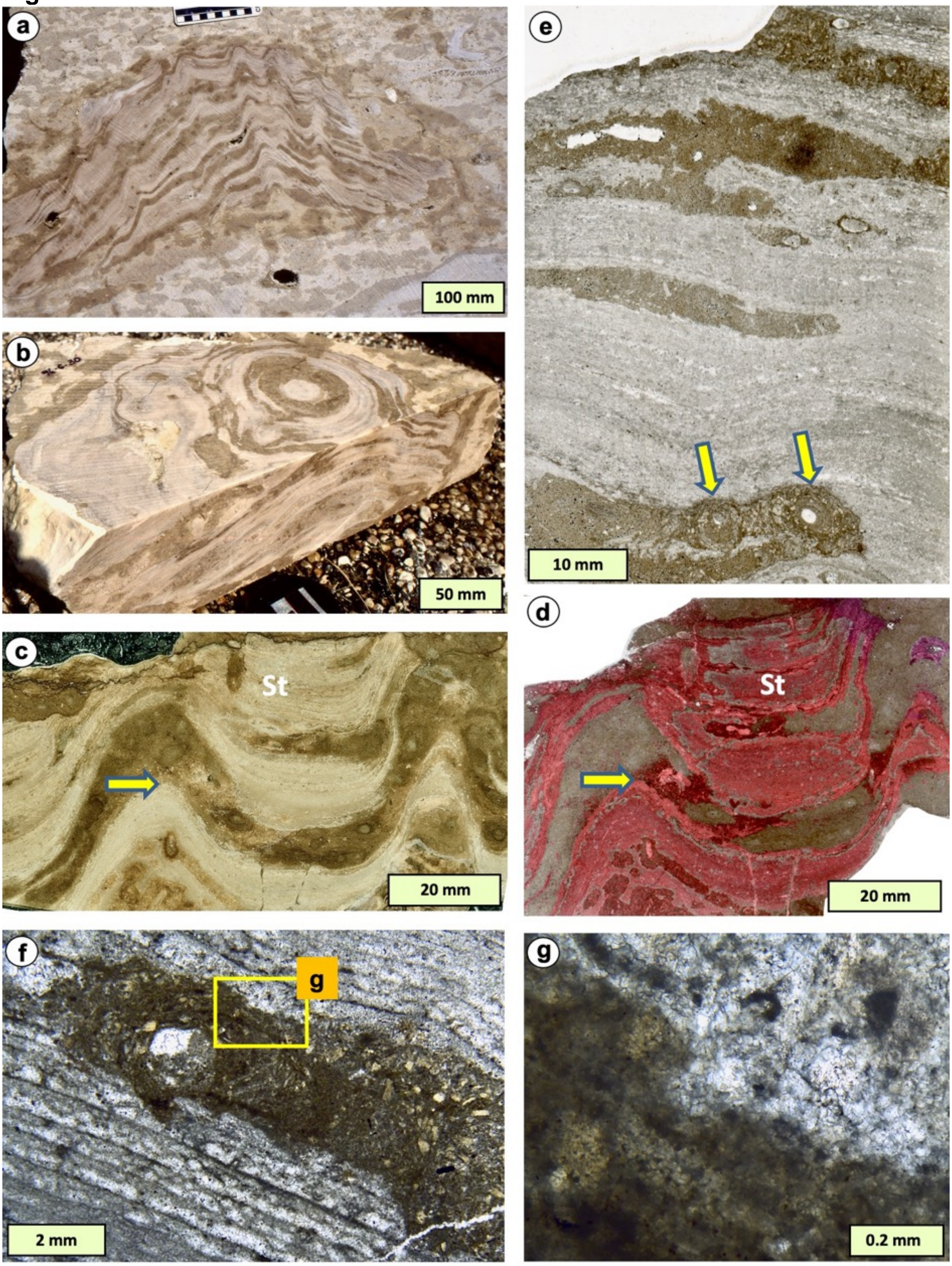

Fig. 16 Evidence of early cementation in Ordovician stromatoporoid *Cystostroma* sp. (see Bolton, 1988 for stromatoporoid taxa). **a, b** field views of sections through whole stromatoporoids cut by circular saws in the quarry factory; dark brown bands are sediment layers penetrating throughout the stromatoporoids; **c, d** Detail of VS of stromatoporoid skeleton (pale colour in **c** red-stained in **d**) and tangential dolomitised sediment layers (dark brown in **c**, unstained in **d**) that follow the undulations of the

stromatoporoid layering (red-stained). Yellow arrows mark matched points; **e-g** The sediment layers are revealed in detail as borings that are interpreted to have followed weakness lines along growth laminae in the stromatoporoid, and backfilled by lined burrows (**e**, yellow arrows). In **f** and **g** the borings are seen to truncate cement in stromatoporoid gallery space, evidence that the interior of the stromatoporoid was cemented prior to boring, and thus a very early diagenetic cement. Selkirk Member, Red River Formation, Katian Series (Upper Ordovician); Gillis Quarries, Garson, Manitoba, Canada.

Fig. 17

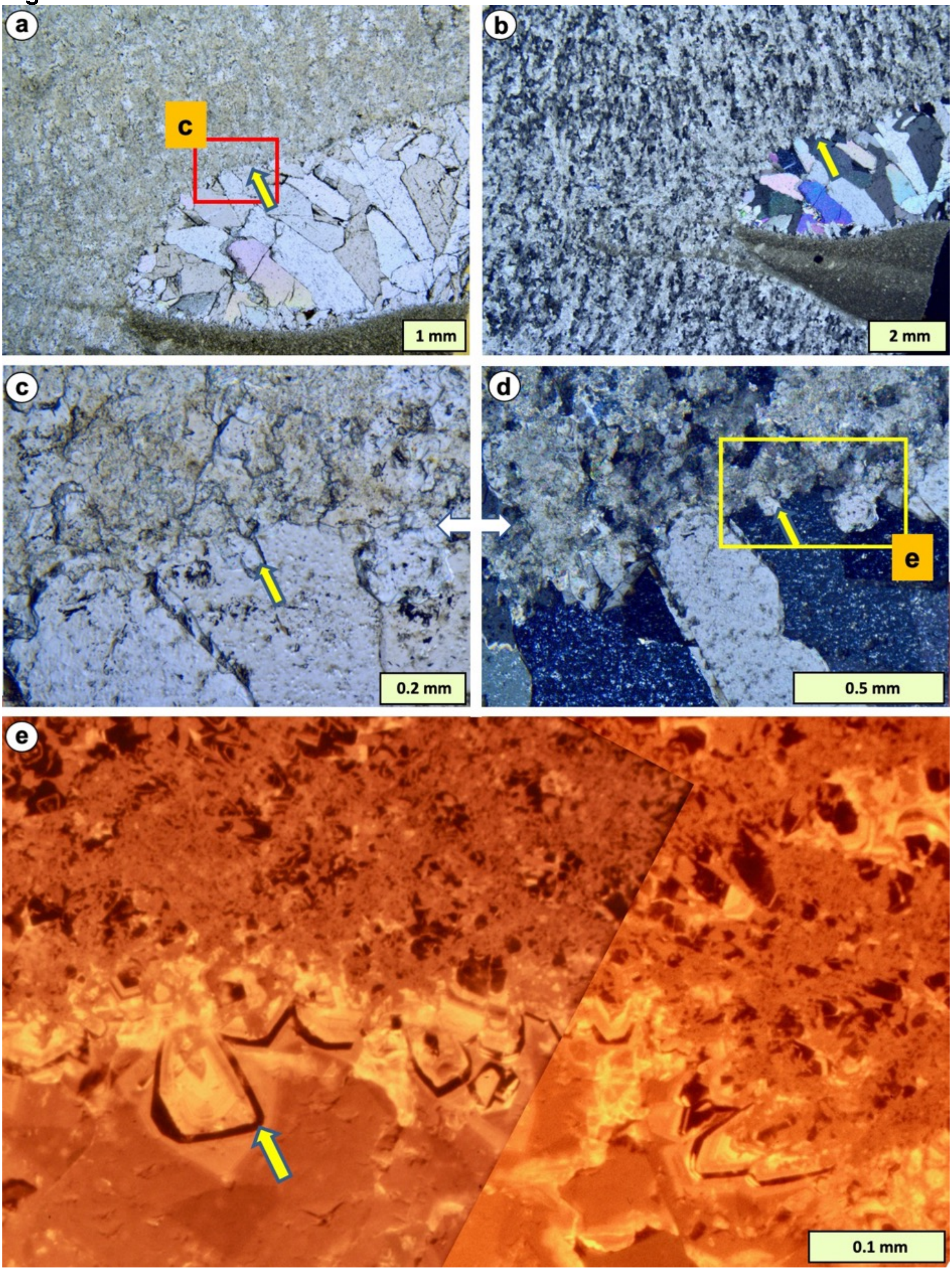

Fig. 17 Vertical section of geopetal cavity in stromatoporoid *Syringostromella borealis* showing cement filling the cavity. Yellow arrow shows matched point in all photos. **a** Plane-polarised light (PPL) general view of the geopetal structure; **b-d** XPL (**b**, **d**) and PPL (**c**) views of the upper left part of the geopetal in **a** showing FRR cement in the stromatoporoid does not pass into the cavity cement, evidence that the cavity was filled with cement prior to the stromatoporoid recrystallisation (Type 2

cavity cement, discussed in text); **e** Cathodoluminescence view of yellow box in **d**, showing the cavity cement fill began with bright cement, then a thin band of non-luminescent cement followed by dull cement in the remainder of the cavity. This sequence is different from the fill of stromatoporoid galleries, that were occupied first with non-luminescent cement, while dull cement came later. The significance of this difference is discussed in the text. Hemse Group, Ludlow (Silurian), Kuppen biostrome locality, Gotland, Sweden,

Fig. 18

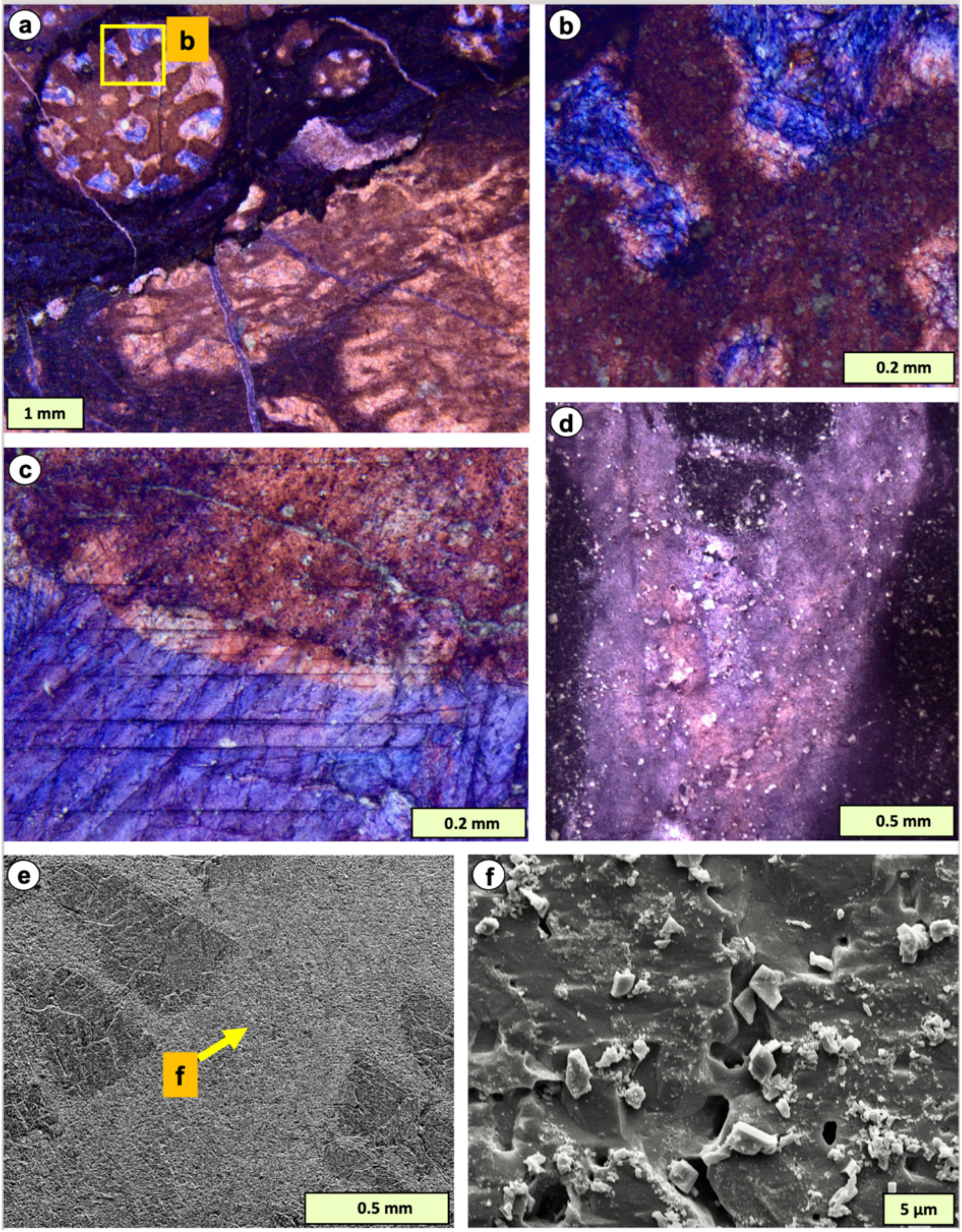

Fig. 18 Occurrence of rhombohedral carbonate, interpreted to be microdolomite (light-coloured specks in **b-d**) in stromatoporoids and associated facies in limestones stained with ARS-KFeCN. **a** Red-stained non-ferroan calcite forms the stromatoporoid skeleton and first-generation cement; **b** Enlargement of yellow box in **a** showing the two generations of cement and revealing that rhombs are abundant in the stromatoporoid skeleton but rare in the gallery cement. **a, b**: *Amphipora* in back-reef micritic limestones, Middle Devonian, Ashburton Quarry, Devon, UK; **c** Base of

a stromatoporoid over a sub-skeletal cavity, showing abundance of rhombs in the stromatoporoid but less in the ferroan cement of the cavity. *Labechia conferta* in shelf limestones of the Much Wenlock Limestone Formation, Wenlock (Silurian), Coates Quarry, Shropshire, UK; **d** From another sample in the Much Wenlock Limestone Formation (MWLF), top of a halysitid tabulate tube directly below a stromatoporoid (not shown); rhombs occur in the micritic sediment and in the tabulate walls, discussed in the text; **e, f** SEM images of vertical section of skeleton of *Labechia conferta* from the MWLF, Lea South Quarry, Wenlock Edge, Shropshire, UK, showing interpreted dolomite rhombs (f) in the stout pillars of this taxon.

Fig. 19a-f

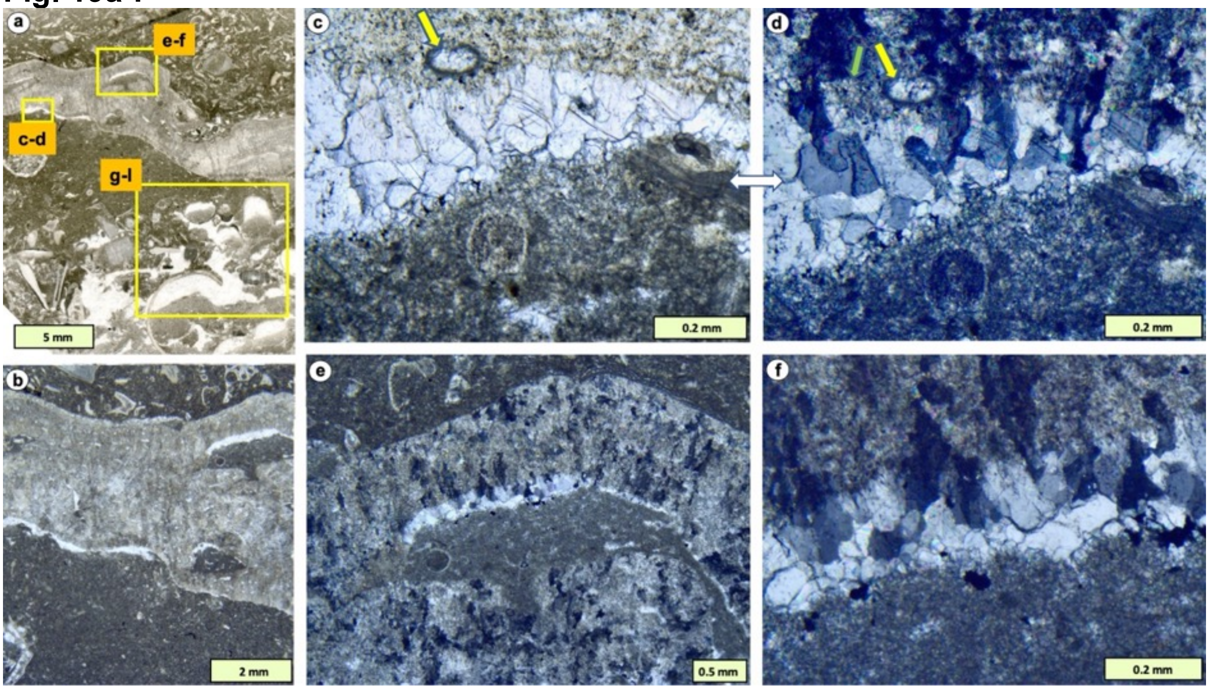

Fig. 19g-l

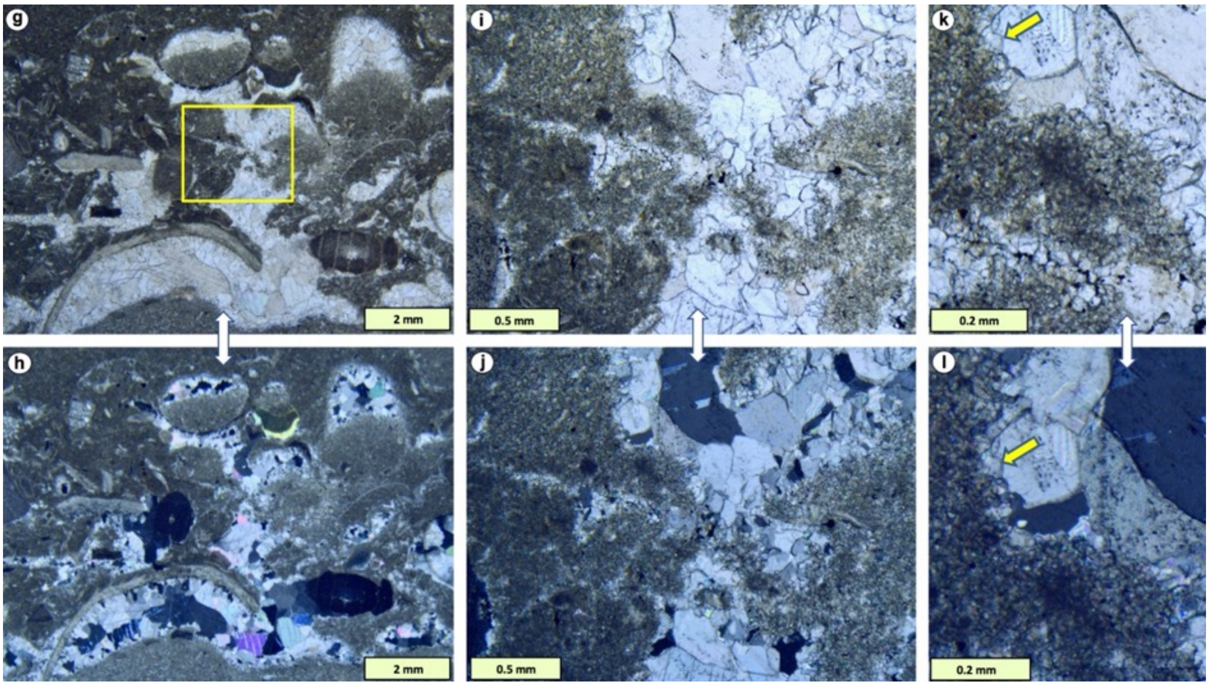

Fig. 19 Cements associated with middle Silurian (Wenlock) stromatoporoids. Low domical form of *Actinostromella vaiverensis* with underlying apparent geopetal cement and micritic sediment with an irregular surface. UK. **a, b** Vertical thin-section views in PPL showing apparent geopetals below parts of the stromatoporoid; **c, d** Details in PPL (**c**) and XPL (**d**) showing a circular bioclast (yellow arrow) directly below the stromatoporoid base with some remnant micrite adhering to the bioclast, below which is sparite cement. This may be a dissolution cavity (Scoffin 1972) or perhaps due to sediment settlement, but whichever is the cause, it occurred early in the history of the limestone. The stromatoporoid recrystallisation is seen in **d** as FRIC, that passes into the cavity with optical continuity except where the remnant sediment blocks its passage (green arrow), evidence that the cavity was open so that the FRIC developed syntaxially into the cavity; **e, f** Similar situation to **c** and **d**, but without remnant micrite in the cavity, so all the FRIC passes syntaxially into the cavity. This sample shows that if sediment removal occurred, then it happened before the stromatoporoid recrystallisation; **g, h** PPL and XPL views respectively of geopetals in shells and interpreted dissolved micrite below the stromatoporoid; **i-l** PPL and XPL enlargements of yellow box in **g** showing details of interpreted dissolved micrite, with first generation cement (yellow arrows in **k** and **l** that also mark matched points) demonstrating interpreted former open dissolution cavities filled with sparite. The process of dissolution and cement fill may have occurred at the same time as cements associated with the stromatoporoid, early in the diagenetic history. Much Wenlock Limestone Formation, Wenlock (Silurian), Lea North Quarry, Wenlock Edge, Shropshire.

Fig. 20

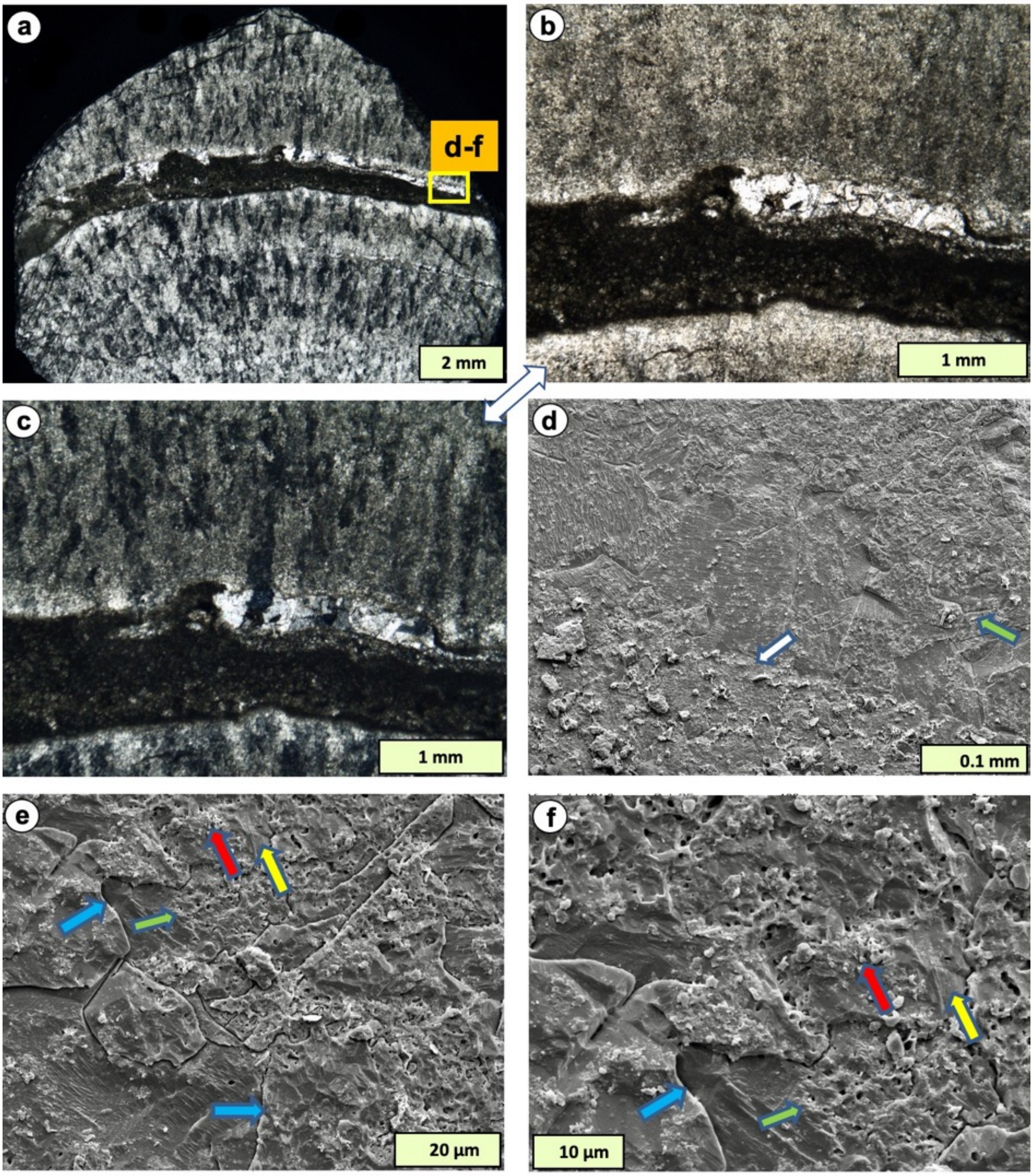

Fig. 20 Features of fabric-retentive recrystallisation and associated features in middle Silurian stromatoporoid *Densastroma pexisum*, using SEM images and a matched thin-section made from the SEM chip after SEM imaging. **a** Vertical section in XPL showing pervasive FRIC; yellow box shows location of SEM images of **d-f**. The stromatoporoid shows a minor growth interruption event, centre, with an apparent geopetal. FRIC passes from stromatoporoid syntaxially to the cavity

cement (Type 1), formed when the cavity was either empty or filled with cement of the same mineralogy as the stromatoporoid, discussed in the text; **b, c** PPL (**b**) and XPL (**c**) enlargements of centre of **a** showing detail of FRIC passing into cement below the stromatoporoid base; **d** General SEM image of part of yellow box in **a**, showing micrite with interpreted dolomite rhombs (bottom), white arrow marks top of sediment layer. Lower edge of stromatoporoid is marked by green arrow and between the white and green arrows is the cavity cement; **e, f** Enlargements in another part of yellow box in A showing detail of basal surface of stromatoporoid (green arrow), FRIC boundaries passing from stromatoporoid to cement (blue arrows), and the distinction between stromatoporoid skeleton (red arrow) and the tiny intervening gallery spaces (yellow arrow) that exist in the fine network structure which comprises *D. pexisum*. Upper four arrows in **e** are also matched points in **f**. Note: this is the lower stromatoporoid in the sample illustrated by Kershaw et al. (2006, Fig. 3A). Upper Visby Formation, Wenlock (Silurian), Ireviken 3 locality, Gotland Sweden.

Fig. 21

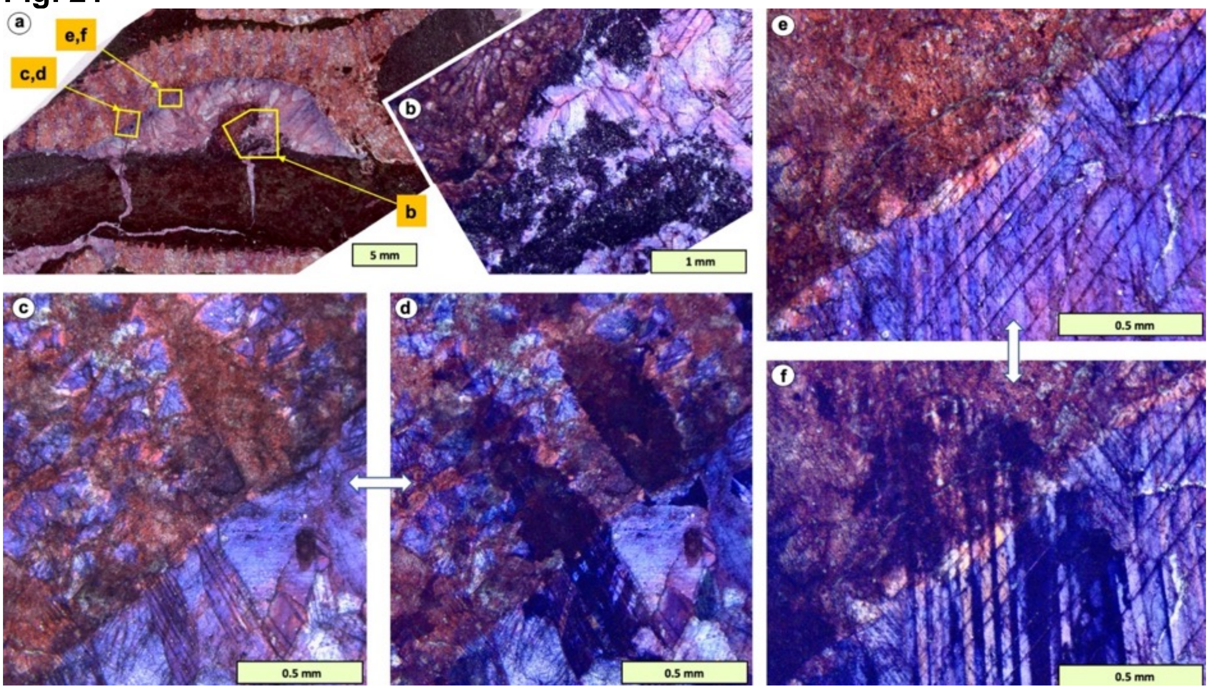

Fig. 21 Fabric-retentive recrystallisation in *Labechia conferta* in relation to discriminatory staining using ARS-KFeCN. **a** Vertical section in PPL showing curved part of laminar frame with apparent geopetal fill. Stromatoporoid is stained red, non-ferroan calcite; **b** Detail of box in A, showing interpreted dissolved sediment below stromatoporoid, including a bryozoan bioclast**; c, d** and **e, f** Paired images in PPL (**c, e**) and XPL (**d, f**) showing FRIC passing through stromatoporoid and its gallery space into the underlying cavity (Type 1 cavity cement, discussed in the text); red and blue staining shows the same sequence of changes in gallery cement and sub-skeletal cavity. The features of this sample may indicate that the gallery and cavity cements were composed of the same mineral, likely HMC as discussed in the text, and were recrystallised together by FRR. However, irregular distribution of micrite in the cavity (**a, b**) is evidence that at least the lower part of the cavity was originally filled with micrite, subsequently dissolved to create a secondary space, similar to the

process interpreted by Scoffin (1972). The sub-stromatoporoid cavity developed two generations of cement, first a thin non-ferroan layer followed by space-filling ferroan sparite, best seen in **e** prior to FRIC formation. See text for discussion. Much Wenlock Limestone Formation (Wenlock, Silurian), Coates Quarry, Wenlock Edge, UK.

Fig. 22

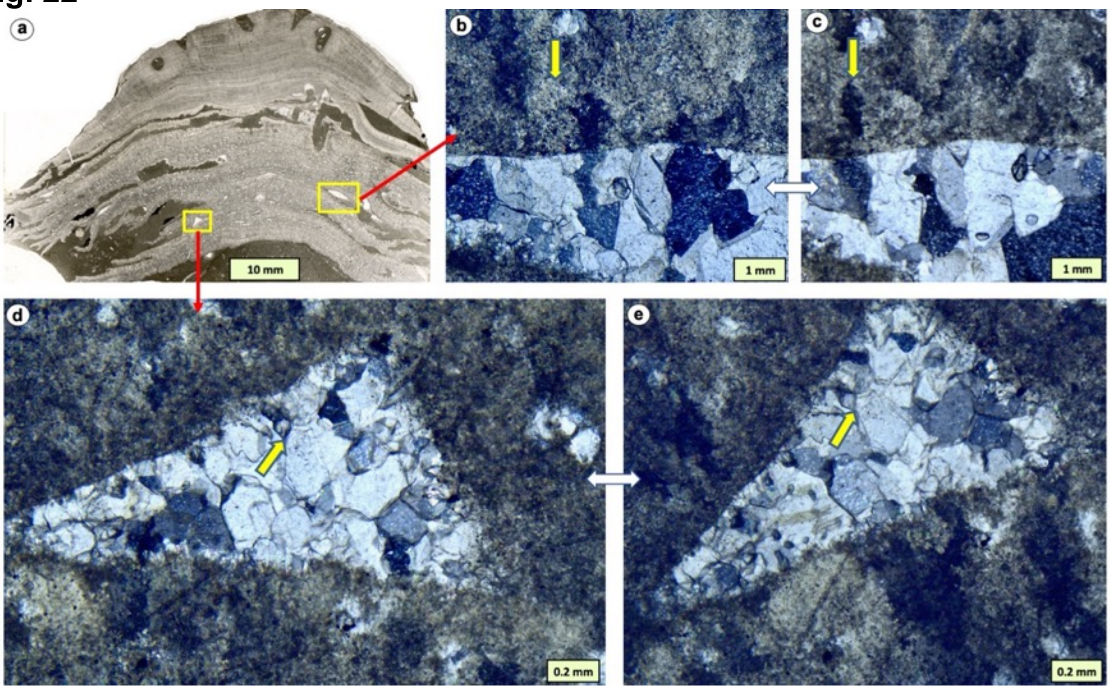

Fig. 22 Syntaxial (Type 1) and non-syntaxial (Type 2) cement fills in cavities in the same stromatoporoid specimen. **a** Vertical whole thin-section of two stromatoporoids, lower is *Eostromatopora impexa*, upper is *Densastroma pexisum*; the features illustrated here are in *E. impexa*; **b, c** XPL enlargements of right-hand box in **a** in different rotational angles, corrected to same position; yellow arrows mark matched points. FRIC is clearly seen to pass syntaxially from stromatoporoid into the underlying apparent geopetal cavity (Type 1 cavity cement); **d, e** XPL enlargements of left-hand box in **a** showing a small cavity encased in stromatoporoid and has a cement fill not in syntaxial continuation of FRIC in the stromatoporoid (Type 2 cement). Yellow arrows mark matched points. **d** and **e** are shown in different orientations to demonstrate the lack of syntaxial cement in the cavity. The two cases illustrated here are a rare example where both kinds of cavity-filling cement (syntaxial [Type 1] and non-syntaxial [Type 2]) occur in the same specimen over very short distances, with likely differences in timing. Upper Visby Formation, Wenlock (Silurian), Ireviken 3 locality, Gotland, Sweden.

Fig. 23

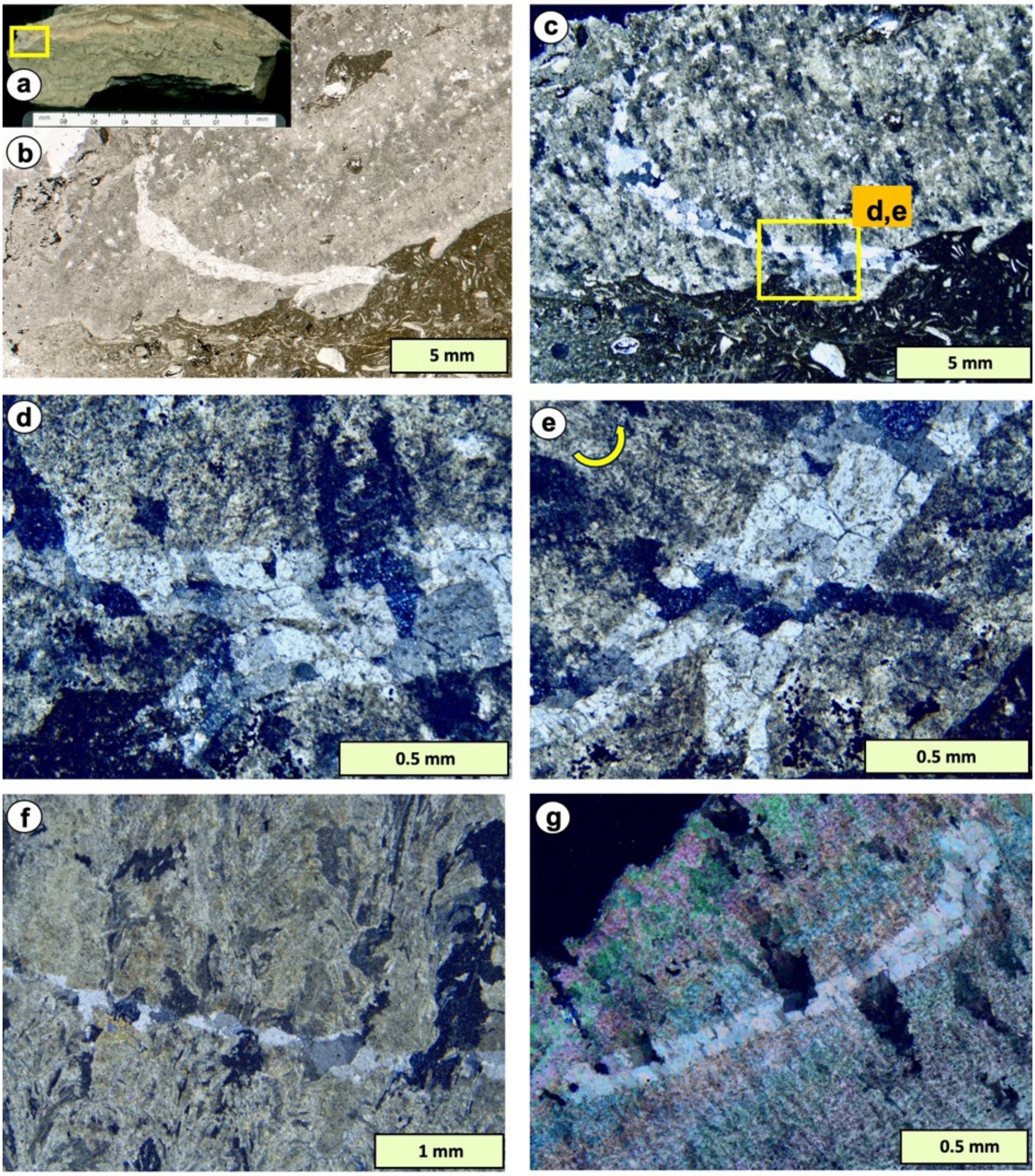

Fig. 23 Cements in three Silurian stromatoporoids, in relation to diagenetic timing. **a-e** Vertical section of *Eostromatopora impexa* showing the margin of this low domical form was broken; a small piece is detached from its base and separated about 1 mm from the base of the stromatoporoid. The cavity thus formed is filled with cement that is syntaxial with the FRIC in the stromatoporoid and is presented as evidence that FRIC developed early in the diagenetic history of the rock, filling the fracture with

cement before the sequence was compacted. Note that **e** is rotated relative to **d**, to view the FRIC; **f** Vertical thin section in XPL of *Lophiostroma schmidti* showing a fracture similar to that in **a-e**, again likely early in the diagenetic history and filled with FRIC; **g** Vertical thin section in XPL of *Densastroma pexisum*, showing a rare example of a clear cement area in the stromatoporoid structure, interpreted to be a boring that did not become filled with sediment. The resulting cavity was filled by cement syntaxial to the FRIC in the stromatoporoid. Black area upper left is the thin-section glass. **a-e** and **g** from Upper Visby Formation, Wenlock, Ireviken 3 locality; **f** from Hemse Group, Ludlow, Kuppen locality; all Silurian, from Gotland, Sweden.

Fig. 24

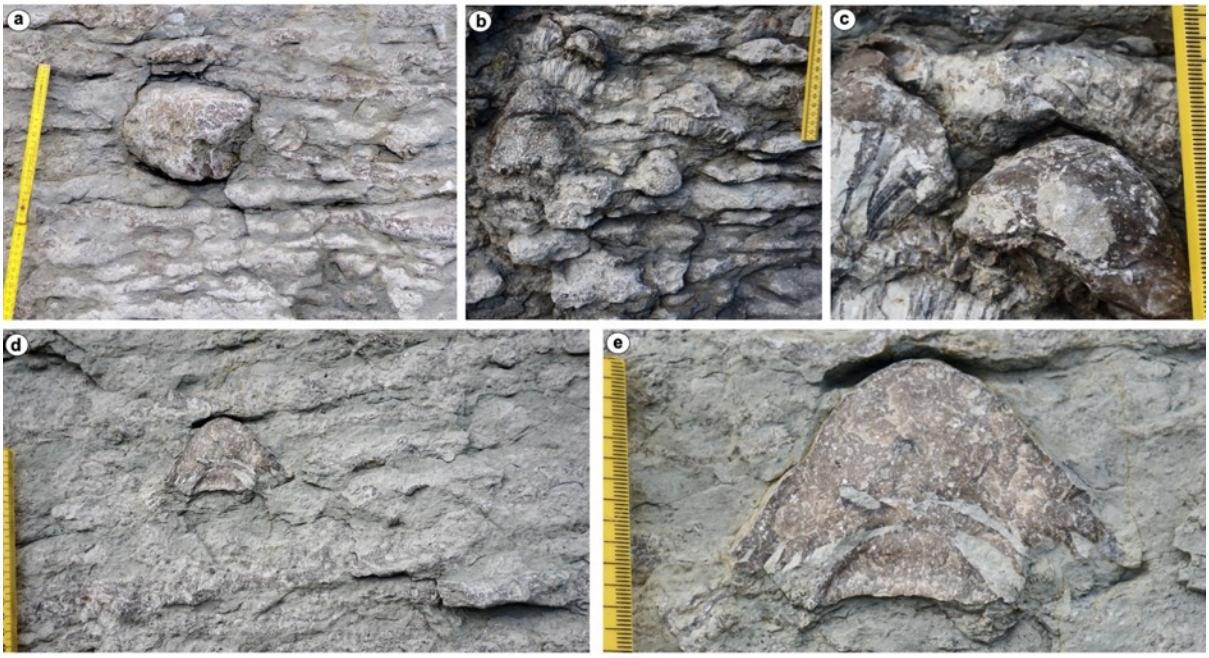

Fig. 24 Stromatoporoids in limestone-marl rhythms. **a-e** Field photographs show the partially regular limestone-marl alternations do not cement the stromatoporoids, which can be easily extracted entire from the rock face, and therefore can be displayed entirely on large thin-sections, seen in many figures in this study. The source of cements in stromatoporoid internal cavities is likely to be the adjacent sediment, as the process of sediment reorganisation progresses. Evidence in these photos supports the view that stromatoporoids had an original high-magnesium calcite mineralogy, see text for discussion. Upper Visby Formation, Wenlock (Silurian), Halls Huk locality, Gotland, Sweden.

Fig. 25

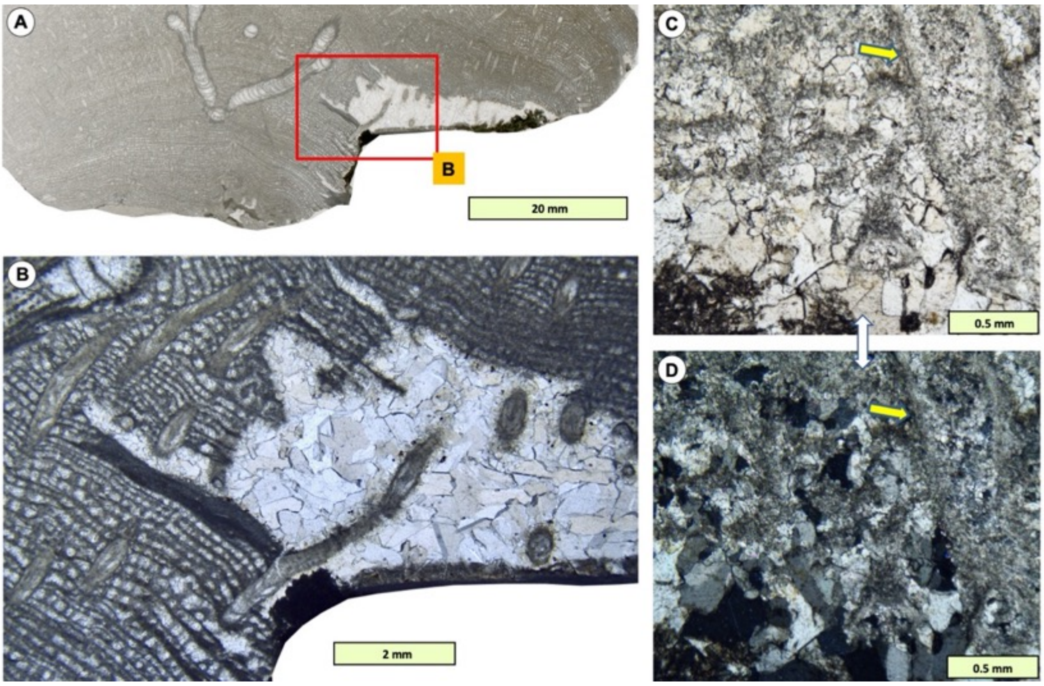

Fig. 25 Differential dissolution and cement precipitation in stromatoporoid-coral intergrowth. **a** Whole thin-section in PPL showing partial dissolution of stromatoporoid, but intergrown syringoporid tabulates resisted dissolution; **b** Enlargement of box in **a** emphasising the differential dissolution, note that long axes of rugosan and syringoporid corallites are oblique to the plane of the thin-section and therefore pass out of the plane of view, rather than being lost in diagenesis; **c, d** PPL (**c**) and XPL (**d**) views from another thin-section of the same specimen, showing stromatoporoid structure overprinted by FRIC and affected by dissolution, but the intergrown syringoporid (matched arrows) is not. Hemse Group, Ludlow (Silurian), Kuppen biostrome locality, Gotland, Sweden.

Fig. 26

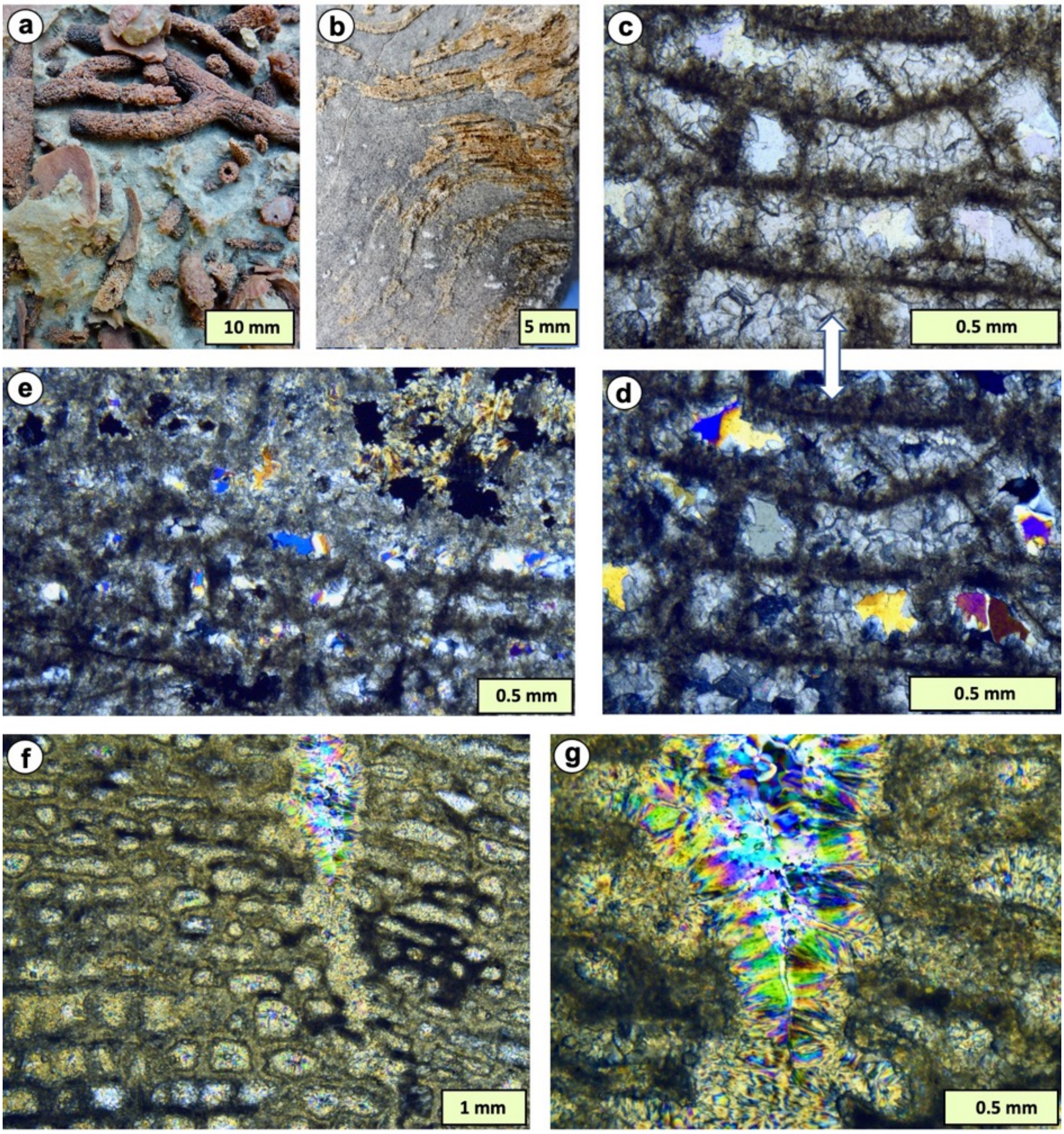

Fig. 26 Silicification of three Devonian stromatoporoids. **a** Hand-specimen of silicified branching stromatoporoids associated with silicified brachiopods. Fore-reef limestone, Sadler Limestone Formation, Frasnian (Devonian), Emmanuel Range, Canning Basin, Australia; **b-e** Partially silicified stromatoporoid (brown areas in **b**, contrasting calcitic portions in grey), the laminae were conduits for silicifying fluids as in Fig. 27; **c, d** PPL (**c**) and XPL (**d**) views of the same area showing gallery space

first generation cement is calcite and final cement is silica, evidence that silicification may have occurred earlier in diagenetic history; the stromatoporoid skeleton is not silicified in these views. However, **e** shows a case (in XPL) from a neighbouring part of the same thin-section where the lower half of the image is the same as **c** and **d**, but in the upper half, silicification invaded the stromatoporoid, and altered both skeleton and gallery fill; some opaque minerals are also present. Sample donated by Bruno Mistiaen; **f, g** Vertical sections in XPL of *Stromatopora tuberculate,* labelled as collected from the “Corniferous Limestone” unit of western Ontario, sample A7384 in Sedgwick Museum of Earth Sciences, imaged with permission; in this case, silicifying fluids entered via a fracture and passed through the stromatoporoid, altering both skeleton and gallery cement, leaving a fully silicified specimen that retains its skeletal structure, a reflection of FRR. See text for discussion.

Fig. 27

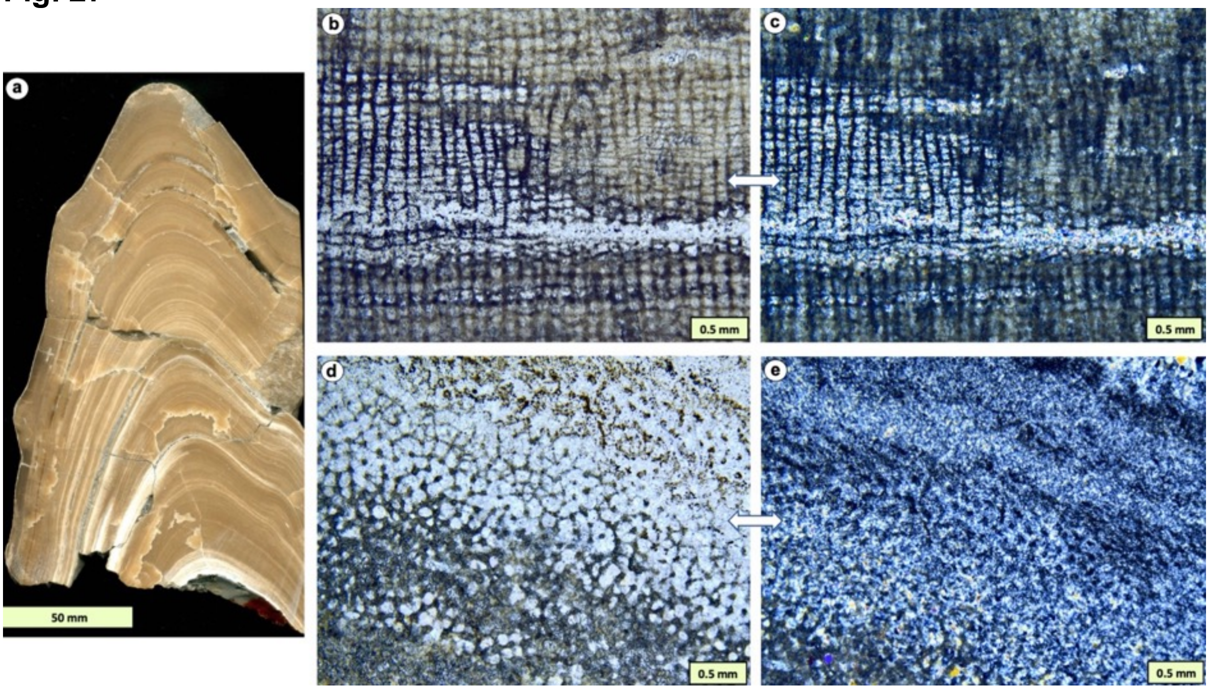

Fig. 27 Silicification of *Plectostroma scaniense*, a stromatoporoid taxon with skeleton composed of long pillars and connecting processes, with variations in silicification. **a** Hand-specimen sectioned vertically, silicified bands are white coloured near the base of the specimen. **b, c** Vertical section in PPL (**b**) and XPL in **c**; note that the irregular patch of silicification has differentially altered the structure, so the skeletal elements are still present, as silica, the intervening space is crystalline silica. **c** shows relationship between FRIC and silicification, the timing of the silicification is not clear, discussed in the text. **d, e** Transverse XPL view of *P. scaniense*, showing preservation of pillars and connecting processes, all completely silicified. Hemse Group, Ludlow (Silurian), Kuppen biostrome locality, Gotland, Sweden.

Fig. 28

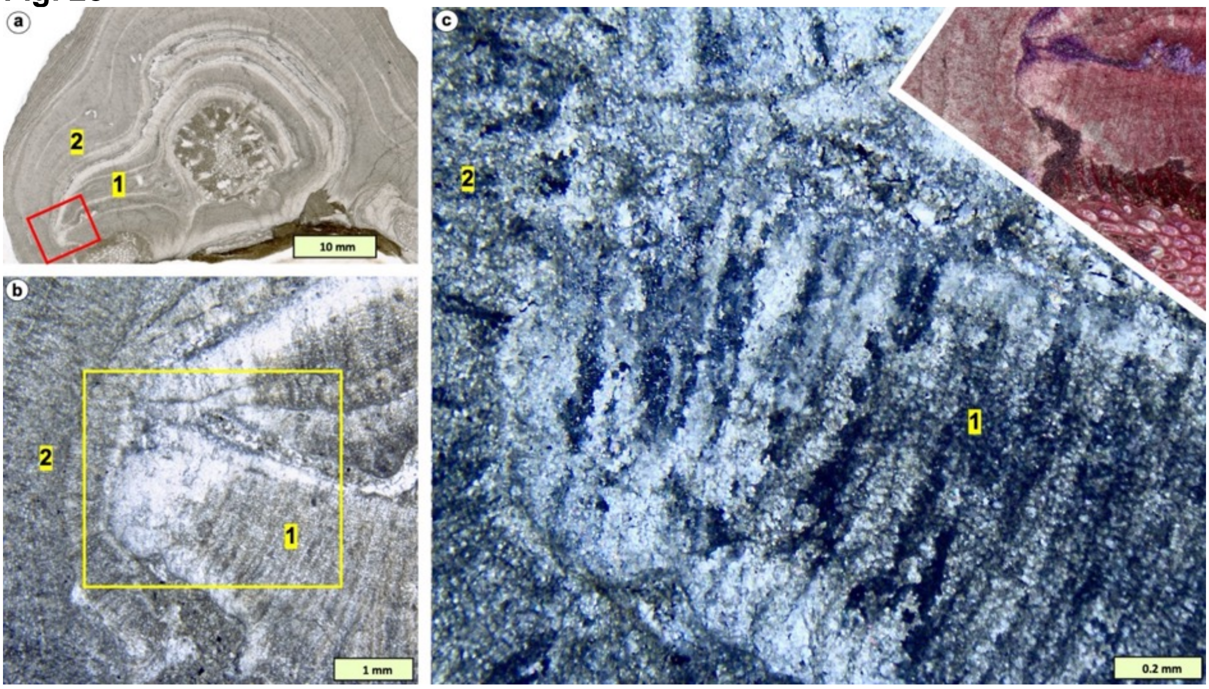

Fig. 28 Fabric-retentive recrystallisation and later alteration in a middle Silurian stromatoporoid, *Densastroma pexisum*. **a** Whole thin-section in PPL showing stromatoporoid encrusted a solitary rugose coral. The stromatoporoid shows two phases of growth, phase 1 shows marginal alteration and phase 2 shows partial alteration in its early growth, shown by lighter areas of the thin-section; **b** Enlargement in PPL of box in **a**, showing detail of contact between phases 1 and 2, emphasising the light area where the skeletal structure is not visible because of alteration. **c and inset.** Main picture is XPL detail of box in **b** showing loss of stromatoporoid skeletal fabric yet the FRIC is still visible. Inset picture (PPL) shows parts of the altered area where the fabric is sparitic and ferroan calcite, yet the FRIC is all non-ferroan calcite. Note that the different orientation of FRIC in phase 2 does not pass into phase 1 FRIC. These images show that FRIC may have undergone further diagenetic change whereby the stromatoporoid skeleton was lost yet may still be recognised as a stromatoporoid by the presence of FRIC, evidence that the stromatoporoid skeletal structure continued to play a controlling role in diagenesis even when the stromatoporoid skeletal structure is no longer visible. Alteration of this sample is interpreted to have occurred along the contact between growth phases 1 and 2 that allowed penetration of fluids, so that the interior of the sample was altered whereas other parts were not. Much Wenlock Limestone Formation, Wenlock (Silurian), Wren's Nest, west Midlands, UK.

Fig. 29

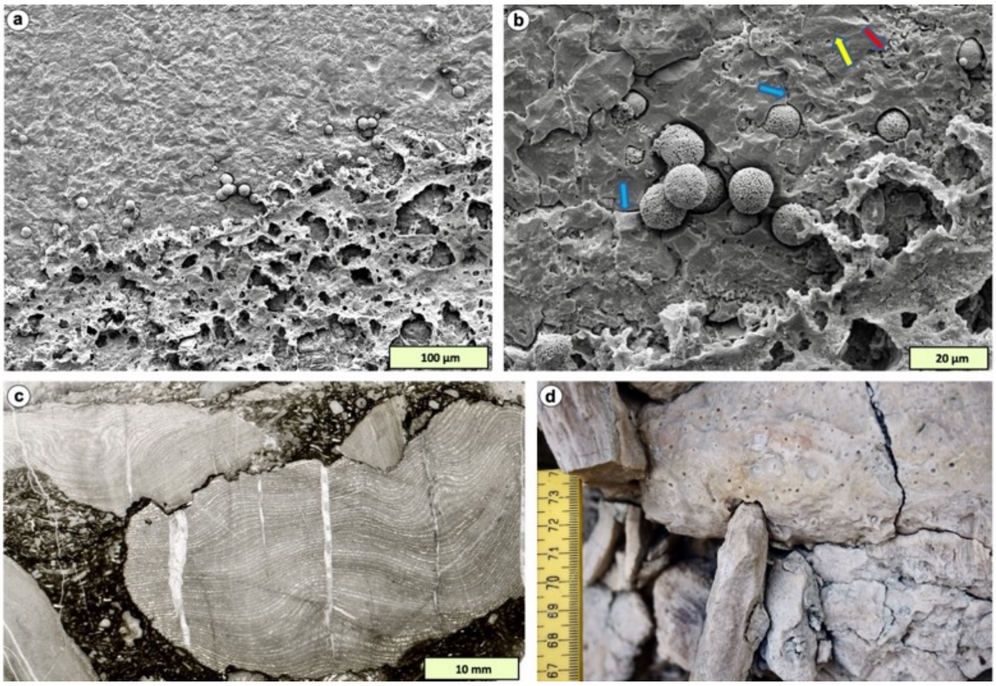

Fig. 29 Other diagenetic features in stromatoporoids. **a, b** Pyrite framboids in stromatoporoids. *Densastroma pexisum*, Upper Visby Formation, Wenlock (Silurian), Ireviken 3 locality, Gotland Sweden. **a** Base of stromatoporoid on argillaceous micritic sediment; pyrite framboids occur along the bottom of the stromatoporoid; **b** Enlargement of central part of **a** showing framboids forming across both skeletal elements (pitted areas, red arrow) and internal cement (clean crystals, yellow arrow). The timing of framboid formation in relation to FRIC is not determined; it is not clear if framboids cut across FRIC, or FRIC cement margins curve around earlier-formed framboids. However, framboids certainly formed below the redox boundary and, as is seen from stained cements in other figures, are possibly early in the diagenetic history; **c, d** Late-stage pressure dissolution. **c** Vertical thin-section of *Stictostroma* sp. impacted by pressure dissolution. Daddyhole Limestone Formation, Eifelian/Givetian (Devonian), Hope’s Nose locality, Devon, England; **d** Field view of stromatoporoids in a biostrome, Hemse Group, Ludlow (Silurian), Kuppen locality, Gotland, Sweden, showing one stromatoporoid impacted into an overlying specimen (centre); on the right side, stromatoporoids are pressed together into a fitted fabric due to pressure dissolution.

Fig. 30

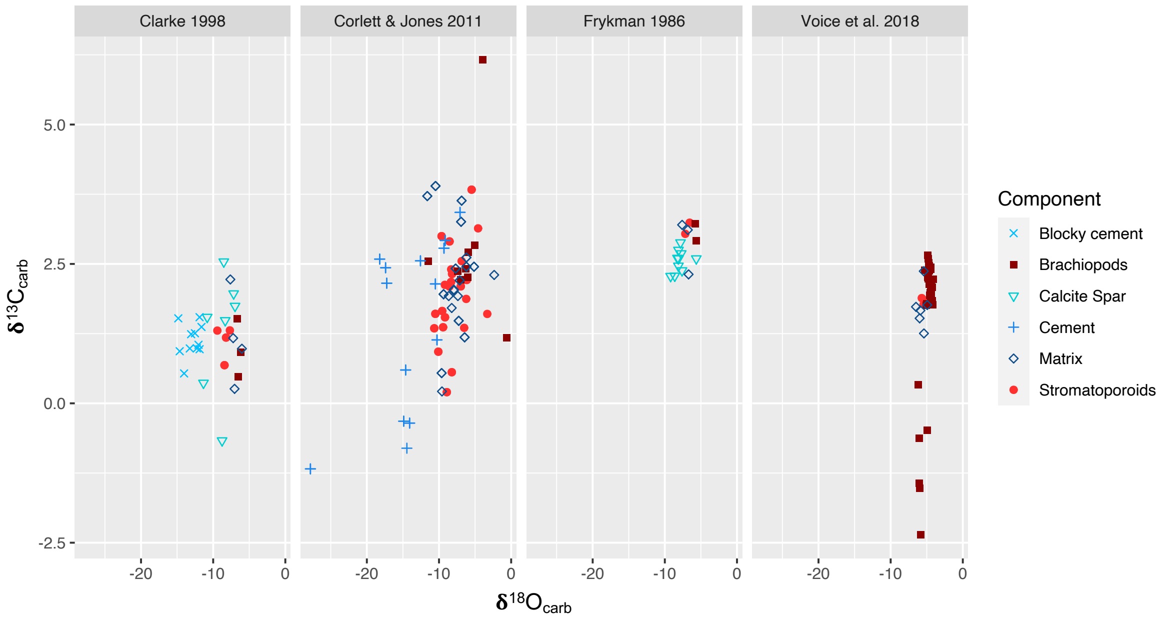

Fig. 30 Compilation of carbon and oxygen isotope data from literature, demonstrating the range of variation of their values in stromatoporoids is broadly consistent with other components in the rocks. See text for discussion, and Supplemental file (Kershaw et al. 2021), Table 1, for data sources.